Electrogeneration of hydrogen peroxide for applications in water/wastewater treatment

by

Robertson Reid

A thesis
presented to the University of Waterloo
in fulfillment of the
thesis requirement for the degree of
Master in Applied Science
in
Civil Engineering

Waterloo, Ontario, Canada, August 2017

Author's declaration

I hereby declare that I am the sole author of this thesis. This is a true copy of the thesis, including any required final revisions, as accepted by my examiners.

I understand that my thesis may be made electronically available to the public.

Abstract

Hydrogen peroxide (H_2O_2) is an effective, environmentally friendly oxidant used directly and in advanced oxidation processes for water and wastewater treatment. Although most H_2O_2 is currently manufactured offsite, concentrated, and trucked to sites where it must be safely stored and handled, it may also be generated on site electrochemically, commonly over a gas diffusion electrode (GDE). This technology has the potential to make processes more economical, feasible, available, and flexible depending on the application and the site.

H_2O_2 electrogeneration has been heavily studied but there are particular knowledge gaps around performance of commercially available, unmodified, metal-free GDEs, contradictory evidence about optimum pH and cathode potential, a lack of studies using continuous mode reactors, weak quantification mass flows inside reactors, and a lack of studies looking at *in situ* treatment that take advantage of anodic oxidation and that do not require advanced oxidation. The present work addresses these gaps in two phases of experimentation (Chapters 3 and 4) and provides a brief comment on economic viability (Chapter 5)

Firstly, effects of hydraulic retention time, cathode potential, reactor geometry, and pH in a continuous mode dual chamber reactor, including kinetic quantification and mass balance modelling are studied in Chapter 3. Performance shows a tradeoff where concentrations up to ~6500 mg L^{-1} may be generated but at a CE approaching 0% while CE near 100% can be maintained when H_2O_2 is produced at ~22 mg L^{-1}. Additionally, a microbial electrochemical cell (MEC) is demonstrated to have a comparable current density to abiotic tests.

Secondly, in Chapter 4, sulfur(IV) is demonstrated to be treated by both electrogenerated H_2O_2 and anodic oxidation in a single chamber electrolysis cell. CE is improved 3-8 times compared to H_2O_2 production alone, and near complete removal (at a low CE of 61.1%) or near 200% CE (at a low removal rate of only 27%) are achieved under various operating conditions, with intermediate values obtained by changing operating conditions.

In summary, this work is establishes the maximum performance H_2O_2 electrogeneration under realistic conditions and shows how *in situ* treatment improves system efficiency by reducing H_2O_2 loss and taking advantage of anodic oxidation. The advantages of *in situ* production (and treatment) are complemented by a predicted comparable operating cost to traditional H_2O_2 technologies, suggesting that this technology is ready for scaling up and commercialization and has to potential to help secure safe water resources for the future.

Acknowledgments

Firstly, I acknowledge the land this research was carried out on at the University of Waterloo is the traditional territory of the Anishnawbe, Haudenosaunee and Neutral peoples, and furthermore situated on the Haldimand Tract, land six miles deep on either side of the Grand River granted to Six Nations in the Haldimand Proclamation of 1784.

Many people were necessary to complete the work that made this research possible. Firstly, I must thank Mohammed Galib and Junyoung Sim, Master's students, for training and advising me in the early stages of my work. I must also thank our postdoctoral fellows Junyeoung An, Elsayed Elbeshbishy, and later Abid Hussain, and Jangho Lee for their supervision, collaboration, and expertise. To my fellow students I owe thanks for their help, advice, and encouragement on a daily basis: Ziyi Xiong, Swakshar Saha, Yaohuan Gao, Bipro Dhar, Wael Alrashed, and especially Bumkyu Kim, who devoted much time and care to discussing experimental design, mathematical modelling, and fundamental science with me.

I thank Stella Kim and Max Li for their help conducting experiments. Stella was a co-op student in Spring 2015 and Max volunteered in the lab in Winter 2017. I wish them both the best.

I owe great thanks to Mark Merlau, Mark Sobon, and Terry Ridgeway for being constantly available to help with anything I needed, from running hundreds of IC samples and recommending analytical methods to teaching me to solder. I also owe thanks to the expertise and patience of the staff in the Engineering Student Machine Shop: Phil, Grant, and Andrew, who took the time to teach and advise me on parts manufacture.

Lastly, I must thank my supervisor Dr. Hyung-Sool Lee for his direction throughout this process and for accommodating my nonlinear path to completing this thesis.

Dedication

To everyone who made themselves part of this work by supporting me along the way.

To my family - my parents, Debbie and James, who gave me life and every experience and opportunity they could. My grandmother (Nana), who has patiently waited for trimestered visits for the last 8 years. My sister Jessica who has shown endless generosity and hospitality. The Hamilton Reids: Ian, Carolyn, Tobin, and Rowan, for taking good care of me including housing me on co-op. My evil twin brother Andrew and his partner in crime Marissa. The Dargavel clan: Lorraine, Warren, Meagan, Ryan, and especially Pam and Greg, who housed me twice on co-op.

To my friends - my Victoria family: Alex, Ewelina, and Róisín for welcoming me to the best coast. My collection of roommates in Waterloo: Tall Matt, Small Matt, Mike, Zac, Jimmy, Jacob, and Anand, for sharing their lives and living spaces. To my dearest conspirators, companions, and comrades not yet mentioned: Filzah, Majd, Sylvia, Leah, Xerxes, Neill, and Casey.

I love you all.

Table of contents

Author's declaration ii
Abstract iii
Acknowledgments iv
Dedication v
Table of contents vi
List of figures x
List of tables xi
List of abbreviations xii
List of symbols xiii
1 Introduction 1
1.1 Current challenges in water and wastewater treatment 1
1.2 Innovations in water/wastewater treatment 2
1.3 Electrogeneration of hydrogen peroxide in water/wastewater treatment 3
1.4 Scope and objectives 3
2 Background 5
2.1 Industrial use and dosage 5
2.2 Conventional production and handling 6
2.3 Chemical properties 7
2.4 Electrogeneration of H_2O_2 9
2.4.1 Microbial electrochemical technologies 11
2.4.2 Non-microbial electrochemical technologies for H_2O_2 production 12
2.4.3 Cathodes 20
2.4.3.1 Gas diffusion electrodes 20
2.4.3.2 Catalyst 21
2.4.3.2.1 Materials and preparation 21
2.4.3.2.2 Function and pathway 24
2.4.3.3 Cathode potential 25
2.4.3.4 Degradation 27
2.4.4 Anodes 28
2.4.4.1 Bioanodes 28
2.4.4.2 Non-microbial anodic oxidation 28
2.4.5 pH 28
2.4.6 Mass transfer 30
2.4.6.1 Liquid phase mass transfer 30

2.4.6.2 Aeration and gas-liquid mass transfer 31
2.4.7 Electrolyte 32
2.4.8 Separation 33
2.4.9 Surface area to volume ratio 36
2.4.10 Temperature 36
2.4.11 Decomposition 37
2.5 *In situ* application of electrogenerated H_2O_2 38
2.5.1 Direct oxidation 38
2.5.2 Advanced oxidation processes 39
2.5.2.1 UV+H_2O_2 39
2.5.2.2 Electro-Fenton processes 40
2.5.2.3 Bioelectro-Fenton processes 41
2.5.2.4 Photoelectro-Fenton processes 41
2.6 Summary of research gaps 42
3 Optimization of cathodic conditions for H_2O_2 electrogeneration over gas diffusion electrode in a dual-chamber electrolysis cell 43
3.1 Overview 43
3.2 Introduction 43
3.3 Materials and methods 45
3.3.1 Apparatus 45
3.3.2 Electrolytes 47
3.3.3 Operating and sampling conditions 47
3.3.4 Analytical methods 49
3.3.5 Calculations 49
3.4 Results and discussion 51
3.4.1 Batch tests 51
3.4.1.1 Decomposition tests 51
3.4.1.2 Electrogeneration tests 53
3.4.2 Continuous tests 54
3.4.2.1 Effect of HRT 54
3.4.2.2 Effect of pH 55
3.4.2.3 Effect of cathode potential and current density 56
3.4.2.4 Bioanode 58
3.4.3 Aggregate analysis 59
3.4.4 Mass balance model 60
3.4.4.1 Batch tests 60

3.4.4.2 Continuous tests 60
3.5 Conclusions 63
4 *In situ* oxidation of S(IV) in a single chamber electrolysis cell via cathodic hydrogen peroxide electrogeneration and anodic oxidation 64
4.1 Overview 64
4.2 Introduction 64
4.3 Materials and methods 66
4.3.1 Electrolysis cell 66
4.3.2 Reactor operation, sampling, and data processing 69
4.3.3 Reagents 69
4.3.4 Analytical methods 70
4.3.4.1 Reagent validation 70
4.3.4.2 Experimental measurement 70
4.3.5 Baseline reactor performance 72
4.4 Results and discussion 73
4.4.1 Comparison of coulombic efficiency with and without *in situ* treatment 73
4.4.2 Determination of removal mechanism 74
4.4.3 Factors affecting reactor performance 75
4.4.3.1 Mixing 75
4.4.3.2 Cathode potential 76
4.4.3.3 pH 77
4.4.3.4 Surface area to volume ratio 77
4.4.3.5 Influent concentration and conductivity 78
4.5 Conclusion 79
5 Economic outlook 81
5.1 Operating costs 81
5.1.1 H_2O_2 production only 81
5.1.2 *In situ* treatment 83
5.2 Capital costs 84
5.2.1 Electrodes 84
5.2.2 Separators 84
5.2.3 Power supply and regulation 85
5.3 Conclusion 85
6 Conclusions 86
7 Recommendations 88
7.1 H_2O_2 electrogeneration 88

7.2 Model 88
7.3 *In situ* treatment 88
8 References 89
Appendix A Summary of experimental data 102
Appendix B Supplemental cyclic voltammetry 106
Appendix C Kinetic quantification of S(IV) oxidation by H_2O_2 108
C1 Materials and methods 109
C2 Results 109
Appendix D Effect of pH on S(IV) treatment reactor 110

List of figures

Figure 1 - Schematic of the anthraquinone oxidation process for hydrogen peroxide synthesis. 7

Figure 2 - Schematic of a typical electrochemical cell for H_2O_2 production. 10

Figure 3 - Summary of maximum performance attained for H_2O_2 production from reviewed literature. 19

Figure 4 - Schematic of gas diffusion electrode (GDE) 20

Figure 5 - Schematic of electrochemical cells used for experiments 46

Figure 6 -a: Effect of pH, mixing, and aeration on non-Faradaic decomposition with no electrodes or catalysts present. b: Effect of GDE on H_2O_2 decomposition 51

Figure 7 - Low scan cyclic voltammetry plots for used and new cathodes. 52

Figure 8 - Typical H_2O_2 batch test result. Reactor used was Reactor A with 0.1 M NaCl as electrolyte and -800 mV vs Ag|AgCl (-577 mV vs SHE) applied cathode potential 53

Figure 9 - Effect of HRT in Reactor B. All reactors used a cathode potential of -1000 mV vs Ag|AgCl (-778 mV vs SHE) 54

Figure 10 - a: Effect of pH in 1 M HCl, NaCl, and NaOH solutions in Reactor B. b: Effect of electrolyte in conductivity-controlled trials. 55

Figure 11 - Effect of cathode potential on current density and resulting reactor performance in Reactor B under 2 HRTs and 2 electrolytes and in Reactor C. 57

Figure 12 - Coulombic efficiency/ H_2O_2 concentration tradeoff curve for global data. 59

Figure 13 - a: Relationship between modelled (a) non-Faradaic losses and (b) Faradaic losses as a percent of total produced H_2O_2 and effluent H_2O_2 concentration 61

Figure 14 - Effect of cathode potential on model results for Faradaic and non-Faradaic losses in Reactor C 62

Figure 15 - Reactor construction and experimental setup. A, B, and C show Reactors A. B and C, respectively; D shows the experimental setup. 68

Figure 16 - Comparison of coulombic efficiency achieved in Reactor A with and without a S(IV) feed 73

Figure 17 - Coulombic efficiency and removal rate in Reactor B's half cells (first two sets of data) compared with performance in an undivided Reactor B. 74

Figure 18 - Effect of mixing on S(IV) removal and CE in Reactor A 76

Figure 19 - Effect of cathode potential on S(IV) removal, coulombic efficiency, and current density in Reactor A. 76

Figure 20 - Effect of surface area to volume ratio on S(IV) removal, coulombic efficiency, and current density in Reactor A. 78

Figure 21 - Effect of influent concentration and conductivity (K) adjustment on ratio on S(IV) removal, coulombic efficiency, and current density in Reactor A. 79

List of tables

Table 1 - H_2O_2 dosage for common industrial uses..... 6

Table 2 - Potentials of selected electrochemical half-reactions important for hydrogen peroxide production and reaction..... 8

Table 3 - Comparison of recent literature on H_2O_2 production in MECs..... 13

Table 4 - Comparison of recent literature on production of H_2O_2 in abiotic electrochemical systems..... 15

Table 5 -Summary of experimental conditions. Only potentials are against Ag | AgCl are listed for brevity..... 48

Table 6 - H_2O_2 cost comparison..... 82

List of abbreviations

AEM	Anion exchange membrane
Ag|AgCl	Silver/silver chloride reference electrode
AO	Anthraquinone oxidation
AOP	Advanced oxidation process
AS	Activated sludge
BES	Bioelectrochemical system
BOD	Biological oxygen demand
CE	Coulombic efficiency
CEC	Contaminant of emerging concern
CEM	Cation exchange membrane
COD	Chemical oxygen demand
CV	Cyclic voltammetry
DBP	Disinfection byproduct
DSA	Dimensionally stable anode
DO	Dissolved oxygen
EAOP	Electrochemical advanced oxidation process
$E_{cathode}$	Cathode potential
GDE	Gas diffusion electrode
HRT	Hydraulic residence time
MEA	Membrane-electrode assembly
MEC	Microbial electrolysis cell
MET	Microbial electrochemical technology
MFC	Microbial fuel cell
MPL	Macroporous layer
MPPC	Microbial peroxide-producing cell
NOM	Natural organic matter
ORR	Oxygen reduction reaction
PTFE	Polytetrafluoroethylene
RVC	Reticulated vitreous carbon
SHE	Standard hydrogen electrode
USD	United States dollars
UV	Ultraviolet
VUV	Vacuum ultraviolet

List of symbols

CoPc	Cobalt phthalocyanine
H_2O_2	Hydrogen peroxide
HO_2^-	Hydroperoxide anion
O_2	Diatomic oxygen
•OH	Hydroxyl radical
Pt	Platinum
Ru	Ruthenium
S(IV)	Sulfur (IV): e.g., sulfite, bisulfite, sulfur dioxide, metabisulfite
S(VI)	Sulfur (VI): e.g., sulfate
Ti	Titanium

1 Introduction

1.1 Current challenges in water and wastewater treatment

Water resources are under increasing pressure from numerous converging and interconnected factors. The UN World Water Development Report [1] discusses how increasing water use for agriculture (at least 19% by 2050) and energy (~15% by 2035), especially in developing countries, is raising aggregate demand for fresh water. At the same time, an urban population set to increase by nearly double to 6.3 billion will require intensive drinking water and wastewater treatment. About a third, or 1 billion, of present city-dwellers currently lack adequate drinking water [1].

Happening alongside these direct water issues brought on by population growth and development is the context of global climate change - as noted in UN World Water Development Report, "water is the primary medium through which climate change influences Earth's ecosystem and thus the livelihood and well-being of societies." In many areas, more efficient water use and reuse will be necessary as climates become hotter and drier. In South Asia and Southern Africa, 44 million people will be affected by water stress by 2070 [1].

Although significant concern exists about water issues in developing countries, water issues are also present in the world's wealthiest countries. In Europe, summer flows are forecasted to drop 80% by 2070 [1]. Canada is currently dealing with its own long-standing water crisis on First Nations reserves [2] and the United States is still in the midst of resolving its most recent water crisis in Flint, Michigan [3]. The factors leading to these failures are technical, managerial, political, and economical, and prove that wealthy countries are not immune to needing to adapt to the changing nature of water resources.

Compounding these water stresses are uncertainties about contaminants of emerging concern (CECs), including pharmaceutical, personal care products, hormones, disinfectants, disinfectant by-products (DBPs) and other classes[4]. As further research leads to stricter water quality regulations, new treatment technologies may be required. For sustainability of the system, it is required that treatment technologies do not create secondary problems, for example DBPs from chlorination or increased greenhouse gas emissions associated with energy-intensive treatment technologies like membrane filtration or advanced oxidation processes (AOPs).

Thus the water and wastewater field is faced with the challenge of providing more water for industrial use and human consumption, conserving freshwater resources, satisfying increasingly strict water quality guidelines, and doing so in a way that is sustainable economically and environmentally. Addressing these challenges requires consideration of existing and upcoming options in water and wastewater treatment, including biological treatment, chemical and electrochemical treatment, membrane technologies and others.

1.2 Innovations in water/wastewater treatment

In wastewater treatment, the traditional biological treatment strategy of using the activated sludge (AS) process involves directly contacting aerobic bacteria, organic substrate, and dissolved oxygen. Due to their aeration requirements, AS processes require huge energy costs: 30-60% of electricity consumption in treatment plants, and wastewater treatment as a whole costs on the order of 1-1.5% of all electricity in the US [5]. Furthermore, traditional biological processes alone are insufficient in treating non-readily biodegradable wastewaters, which are of increasing interest and imperative to address [6], [7].

Although activated sludge processes do have advantages and will continue being used, many other technologies have been adopted or are being presently researched and developed that may achieve more complete removal of a larger array of contaminants, use less energy, require less footprint, and/or recover nutrients and energy, chiefly as biogas. For removal of biodegradable organic carbon. technologies such as high rate anaerobic treatment [8], anaerobic-aerobic treatment [9], membrane filtration and membrane bioreactors [10], and microbial electrochemical technologies [11] are among those at various stages of research and application in industrial and municipal wastewater treatment for biological organic carbon removal. To address the issue of non-biodegradable wastes, numerous technologies have been researched for both pre- and post-treatment of wastewaters. These strategies all focus around oxidation with strong oxidants including free radicals (i.e., AOPs) and include cavitation, photocatalytic oxidation, Fenton reactions, and combinations of ozonation, hydrogen peroxide, ultraviolet (UV) [6], [7].

Drinking water may also treated with AOPs, where it is usually used as a polishing step to mineralize natural organic matter (NOM) before chlorination to avoid the formation of DBPs. AOPs specifically studied for drinking water treatment have been photocatalytic oxidation,

Fenton reactions (including photo-Fenton), ozonation (with H_2O_2, UV), ultraviolet (UV), vacuum ultraviolet (VUV), and ionizing radiation [12].

1.3 Electrogeneration of hydrogen peroxide in water/wastewater treatment

Hydrogen peroxide is a compelling oxidant to study specifically because it can be easily produced *in situ* in electrochemical systems using only air, water, and electrical power, over simple electrodes. So-called electrogeneration offers potential cost savings, environmental benefits, and flexibility over the current monopoly that the anthraquinone oxidation (AO) process holds in the industry. AO currently supplies 95% of the world's H_2O_2 in an energy-intensive process that uses non-aqueous solvents and produces potentially hazardous concentrates that demand special transportation, handling, and storage [13]. These potential benefits make electrogeneration of H_2O_2 the focus of the present work.

Electrogeneration was one of the earliest industrial manufacturing process for H_2O_2 [13] but it since appears to have only been widely taken up in the pulp and paper industry [14]. There is however a very active research community investigating H_2O_2 electrogeneration, be it in purely chemical systems [15]-[32], H_2O_2-producing microbial electrochemical technologies [33]–[43], in *in situ* treatments using some of the already discussed AOPs: H_2O_2/UV [23], electro-Fenton[15], [44]–[47], bioelectro-Fenton [48]–[61], photoelectro-Fenton[21], [62]–[65], or in systems that use H_2O_2 directly as an oxidant *in situ* [66], [67]. One of the most significant innovations allowing this explosion of research has been the gas diffusion electrode (GDE), which provides a three-phase boundary where liquid electrolyte and gases can meet at a conducting solid that also supports a heterogeneous catalyst. Despite this research attention, there remain gaps in understanding around optimum process pH, electrode choice and polarization, reactor performance in continuous mode operation, quantification of reaction and side reactions, and the limited number of studies that use H_2O_2 directly as an oxidant for *in situ* treatment.

1.4 Scope and objectives

The present work addresses the following questions:

1. Using a dual chamber, continuous flow electrochemical reactor equipped with a commercially-available, metal-free GDE, what are the optimum conditions to produce

high concentrations of H_2O_2 at high efficiency when considering the following variables?

   a. Hydraulic retention time
   b. Cathode potential
   c. Mixing and aeration
   d. Electrolyte strength and pH
   e. Surface area to volume ratio

2. Are the microbiological anodes used in microbial electrochemical systems compatible with the optimal cathode conditions or desirable for further development of H_2O_2 electrogeneration cells?
3. Can intrinsic limitations of electrogeneration be overcome by conducting treatment processes *in situ* using H_2O_2 directly as an oxidant using an undivided, continuous flow reactor with GDE?
4. How do operational parameters affect *in situ* treatment process with respect to the following variables?
   a. Hydraulic retention time
   b. Cathode potential
   c. Electrolyte strength and pH
   d. Surface area to volume ratio
5. How competitive is H_2O_2 electrogeneration with existing alternatives?

Chapter 3 investigates the first and second research questions while Chapter 4 investigates the third and fourth. In Chapter 4, we use sulfur(IV) as a model pollutant since it is vulnerable to oxidation by H_2O_2 and of practical importance for sulfur recovery from fugitive emissions in chemical manufacture and an important and tightly regulated atmospheric pollutant. Chapter 5 briefly discusses the fifth item.

2 Background

2.1 Industrial use and dosage

Although hydrogen peroxide may be used in addition, reduction, and substitution reactions [13], its chief industrial uses are for oxidation of organic and inorganic compounds. H_2O_2 is used in the water and wastewater industry for disinfection, in the semiconductor industry in etching processes, for bleaching in the textile and pulp and paper industries, and as a reagent in various chemical syntheses, and among other uses [13]. Peroxide has limited used when applied directly as an oxidant, being effective only for reduced sulfur compounds, cyanides, and certain organics including aldehydes, formic acid, some nitro- and sulfo-organics [68].

In the water and wastewater industry, peroxide is most often applied as a hydroxyl radical precursor in AOPs using UV for photolysis [69]. In these types of reactors, the optimal concentration of H_2O_2 is 0.5-2 mM (17-68 mg L^{-1}) [70]. These typically use concentrated H_2O_2 purchased in bulk and piped into reactors. In Fenton processes, an AOP using ferrous iron to product hydroxyl radicals, 50-250 mg L^{-1} is a useful range [44].

When used directly as a disinfectant, 0.01% H_2O_2 (10 mg L^{-1}) removes 50% of bacteria after 1 hour contact time, 0.1% solution (100 mg L^{-1}) led to 3-log reduction (99.9%) [42].

In pulp and paper, the Kraft process is the most valuable bleaching process in market share. It requires a 2-3%wt (20-30 g L^{-1}) solution of H_2O_2 [14]. Unlike the water/wastewater industry, the pulp and paper industry does sometimes use electrochemically generated H_2O_2 [13], however technologies reviewed for the industry do not include *in situ* reaction, rather concentrated solutions are generated then piped into an external reaction chamber. Because of the high concentrations generated, oxidation of membranes used to prevent anodic oxidation of H_2O_2 is a major operational concern [14]. Other applications of electrogenerated H_2O_2 are reviewed by Pletcher [71].

Another industrial use of H_2O_2 is for sulfide oxidation in wastewater systems, mainly for odour control, recommending application at 1.5-2.5 mg L^{-1} [72]. The reaction is pH-sensitive as it is the bisulfide form which is vulnerable to oxidation; the reaction rate around pH 3 is over 100-150 times slower than that at pH 7-8 [73], [74]. Gaseous sulfur can also be controlled with AOPs based on H_2O_2 for example in volatile sulfur compounds scrubbing from gaseous emissions [75].

Table 1 summarizes dosages required for the industrial processes discussed.

Table 1 - H_2O_2 dosage for common industrial uses

Application	Dosage ($mg\ L^{-1}$)	Source
UV-H_2O_2 AOP	17-68	[70]
Fenton AOP	50-250	[44]
Direct disinfection	100	[42]
Kraft process	2000-3000	[14]
Sulphide control	1.5-2.5	[72]

2.2 Conventional production and handling

Hydrogen peroxide is conventionally produced through the anthraquinone oxidation (AO) process, also known as the Riedl-Pfliederer process after its inventors [76]. The AO process has the advantage of producing relatively high concentrations of hydrogen peroxide (30%wt before distillation) but it does require several steps, and intense energy, high heat, [13] and access to hydrogen gas and non-aqueous solvents [71]. More than 95% of industrially-used H_2O_2 is produced this way [13]. Figure 1 below gives an overview of the manufacturing pathway.

Industrial concentrated peroxide is reported to cost in the range of USD 430-760 per tonne [59], [77] (100% basis, before delivery) and global production is 3 million tons [78].

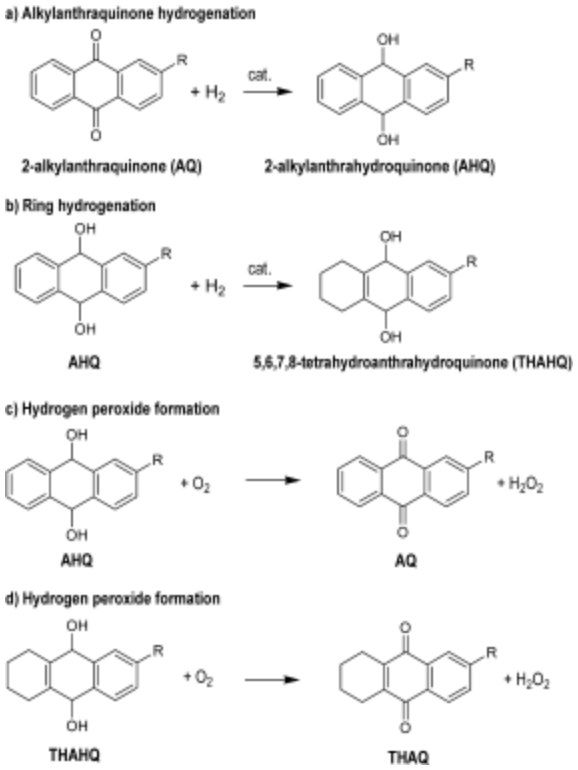

Figure 1 - Schematic of the anthraquinone oxidation process for hydrogen peroxide synthesis. Source: [13]

Concentrated hydrogen peroxide (70% w/w) must be stored and handled carefully due to its strong oxidizing nature. Material safety data sheets instruct users to use gloves and a face mask when handling and to prevent contact with combustible materials, metals, organics, reducing agents, metal oxides, bases, and dust [79]. The main hazards result from peroxide's oxidizing power, which can be used to burn combustible material, and its exothermic decomposition reaction which releases oxygen gas and 100.4 kJ mol^{-1} of energy [13]. Concentrated hydrogen peroxide is typically preferred by industrial consumers to reduce trucking requirements and storage footprint.

2.3 Chemical properties

Chiefly used as an oxidizing agent, H_2O_2 can be first understood in terms of its electrochemical thermodynamics. Table 2 below summarizes the redox potentials for half reactions relevant to discussion of H_2O_2.

Table 2 - Potentials of selected electrochemical half-reactions important for hydrogen peroxide production and reaction.

Reaction *(Acidic form, alkaline form)*	Standard Electrode Potential (E^0) (V vs SHE)	Electrode potential at environmental conditions (V vs SHE)	Equation number	Reference
$\bullet OH+e^-\leftrightarrow OH^-$	2.70	3.11	(1)	[80]
$H_2O_2+2H^++2e^-\leftrightarrow 2H_2O$	1.763	1.346	(2)	[81]
$HO_2^-+H_2O+2e^-\leftrightarrow 3OH^-$	0.867		(3)	[82]
$HClO+H^++2e^-\leftrightarrow Cl^-+H_2O$	1.49	1.28	(4)	[83]
$OCl^-+H_2O+2e^-\leftrightarrow Cl^-+2OH^-$	1.08		(5)	[84], [85][a]
$O_2+4H^++4e^-\leftrightarrow 2H_2O$	1.229	0.762	(6)	[81]
$O_2+H_2O+4e^-\leftrightarrow 4OH^-$	0.401		(7)	[82]
$O_2+2H^++2e^-\leftrightarrow H_2O_2$	0.695	0.181	(8)	[81]
$O_2+H_2O+2e^-\leftrightarrow HO_2^-+OH^-$	-0.065		(9)	[82]
$2H^++2e^-\leftrightarrow H_2$	0	-0.828	(10)	[81]

a: calculated from Gibb's free energy values from listed sources
Note: Environmental conditions refers to a pH of 7, O2 saturated at 8.74 mg L-1, and all other species kept at 1 M.

Equations 2 and 3 show the redox potentials for the reduction of H_2O_2 and its counterion HO_2^- (termed hydroperoxide anion or hydrogen peroxide anion), the half reaction that takes place when H_2O_2 is used directly as an oxidant. This report will refer to both species as H_2O_2, though at some of the more alkaline pH conditions that will be discussed, significant proportions will be present as HO_2^- as well (pK_a=11.65 [86]). Note that the hydroperoxide anion HO_2^- should not be confused with the hydroperoxyl radical $HO_2\bullet$, a species formed from interaction between hydrogen peroxide and hydroxyl radicals [87].

Equation 1 shows the potential for the reduction of the hydroxyl radical to hydroxide. This is shown both to compare its redox potential with H_2O_2 to get a sense of relative oxidizing power, but also because H_2O_2 is often used as a hydroxyl radical precursor. Advanced oxidation processes (AOPs) that make use of hydroxyl radicals may be broadly divided into those that use water as a precursor and those that use H_2O_2 [88].

Similarly, Equations 4 and 5 are included to give a sense of relative oxidizing power as hypochlorous acid and hypochlorite are commonly-used sources of active chlorine. The

reverse reaction, formation of hypochlorite from chloride is also a consideration on electrochemical cell anodes, where it can reduce H_2O_2 by oxidizing it to O_2 [19].

Equations 6-9 are oxygen reduction reactions (ORRs) which commonly occur at electrochemical cell cathodes exposed to air. In fuel cells, the water-producing, 4-electron ORR is desirable because of the higher cell voltage that can be generation, while the 2-electron H_2O_2-producing reaction is minimized. Maximization of the H_2O_2 reaction is the subject of studies interested in the electrogeneration of H_2O_2 and the focus of this thesis; this discussion is continued in detail in Section 2.4.

Lastly, Equation 10 is included to illustrate the limit of water stability. In an anaerobic water, the reverse H_2 formation reaction may occur at an electrochemical cell cathode when there is no O_2 available to reduce via Equations 6-9. Additionally, H2 is commonly used to feed fuel cell anodes, most often with cathodic water generation in mind for maximum cell voltage but occasionally with H_2O_2 generation in mind [16], [20], [22], [24] .

It should be noted that the potentials discussed are only thermodynamic, open circuit potentials; the actual ability to perform a reaction depends on the specific substrate, matrix, and presence of catalysts. These factors will be further explored in the remainder of the review which focusses on specific applications. Milner et al. [89] investigated H_2O_2 formation at electrochemical cells cathodes and present some empirical open circuit potentials which may be compared with the theoretical values presented in Table 2.

2.4 Electrogeneration of H_2O_2

A corollary of the redox reactions presented in Equations 8 and 9 is the possibility, over the right catalyst, to generate H_2O_2 cathodically in an electrochemical system where O_2 and H^+ or H_2O are available. This electrogeneration (also termed electrosynthesis or electrochemical generation) or H_2O_2 offers the advantages of using inexpensive reagents, providing on-demand convenience, reducing plant footprint from storage and handling, and availing H_2O_2-based treatment in distributed and remote systems [23]. There is presently a general demand for more decentralized chemical synthesis technologies [78] and H_2O_2 electrogeneration has the potential to address various needs in the growing clean tech industry. Electrochemical production of H_2O_2 predates the now-dominant anthraquinone oxidation method [13], and has been of great interest recently as will be reviewed in the following sections.

The essential components of an electrochemical cell are an anode, where an oxidation reaction takes place to supply electrons, an external circuit, which may either add or remove energy from the system, and a cathode, where a reduction reaction takes place, in this case the 2-electron ORR. Most of the systems reviewed use liquid electrolyte and a separator to prevent bulk mixing of anolyte and catholyte, although a huge variety is possible and will be discussed. A basic system is pictured below in Figure 2.

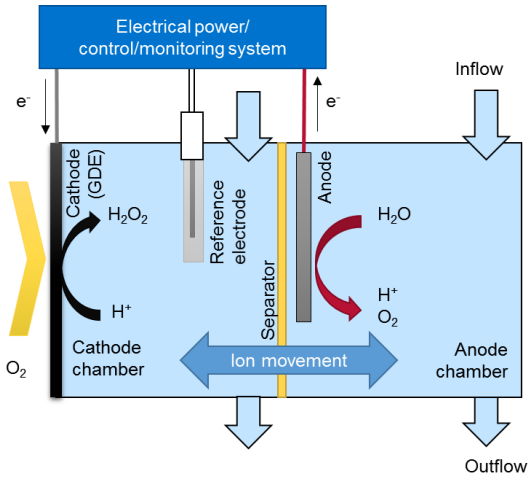

Figure 2 - Schematic of a typical electrochemical cell for H_2O_2 production.

Systems for H_2O_2 electrogeneration may be compared on a few criteria. One is the maximum concentration of H_2O_2 the system is capable of producing. A second is the coulombic efficiency (CE) at which the system generates H_2O_2, that is the proportion of electrons that travel through the external circuit that end up in H_2O_2 molecules. This may be calculated via generally via Equation 11:

$$CE = \frac{n \cdot F \cdot V \cdot C}{Q} \tag{11}$$

where n is the number of electrons transferred (per molecule counted in C; 2 per mole H_2O_2) and C is the concentration change of the target chemical (H_2O_2), F is Faraday's number (96485 C mol e^{-1}), V is the volume of fluid used (reactor volume for a batch or effluent volume for a continuous reactor), and Q is the charged passed through the external circuit during operation (C). Though Equation 11 has a charge term it does not have a voltage term, so an

additional energy efficiency metric may be useful; this report will use kWh kg^{-1} H_2O_2 using an 100% H_2O_2 basis. Lastly the net speed of the reaction can also be characterized via the apparent H_2O_2 formation rate (in concentration per time, mg L^{-1} h^{-1} to be used in this report) or via the current density (mA cm^{-2}), normalized against the cathode surface area.

2.4.1 Microbial electrochemical technologies

One area of innovation in the water space is the development of microbial electrochemical technologies (METs, also referred to as microbial electrochemical systems, MESs, or bioelectrochemical systems, BES), as mentioned in Section 1.2. These systems exploit exoelectrogenic bacteria that can metabolize electrons from solid electrodes directly [90]. Most commonly, these bacteria are used for oxidation of organic carbon at an anode (therefore a bioanode) and are thus termed anode respiring bacteria (ARB). METs may be configured to provide diverse treatment processes at their anodes and/or cathodes, to name a few: organic carbon oxidation, denitrification, production of hydrogen peroxide, hydrogen gas, and organic compounds including fatty acids, amino acids, and alcohols. At the same time, they may produce electricity (a microbial fuel cell; MFC) or accept electrical energy directly for use to drive electrochemical reactions (a microbial electrolysis cell, MEC) [11]. The broad diversity of arrangements and applications possible based on this technology has led to it being regarded as a platform technology, and over fifty genres of METs have been documented [91], to mention a few: plant microbial fuel cells, benthic microbial fuel cells, solar-powered microbial fuel cells, microbial desalination cells, and microbial carbon capture cells.

METs provide the opportunity to harness some of the energy contained in wastewater and use it to offset electricity requirements or even generate surplus electricity, as well as providing an opportunity to carry out various valuable chemical production or treatment processes. Foley et al. [92] conducted life cycle assessments of high rate anaerobic treatment, MFCs, and MECs intended to produce H_2O_2 for on-site use. Their review concluded that the H_2O_2-MEC (also termed a microbial peroxide producing cell, MPPC in some literature) had the greatest potential of the three when considering criteria for human health, ecosystem quality, climate change, and resource sustainability. The principle reason is not so much the absolute performance of the H_2O_2 MEC but its relative advantage of displacing the AO process.

Recognizing that H_2O_2-MECs are one of the most promising platforms for deployment of METs, several studies to date have researched them in detail. A number of studies have focus directly on producing H_2O_2 directly [33]–[41], [43] at MEC cathodes. These are summarized in Table 3. Specific aspects of performance are discussed in greater detail in subsequent subsections of Section 2.4.

2.4.2 Non-microbial electrochemical technologies for H_2O_2 production

Although METs provide one avenue toward producing H_2O_2 for water/wastewater treatment, H_2O_2 may also be produced in abiotic, chemical electrolysis cells. Biotic systems offer advantages such as energy recovery and organic carbon removal but abiotic systems are simpler to start up and operate, tolerate harsher conditions of temperature, pH, and chemical concentrations, and current densities. Arends et al. [42] operate both microbial and non-microbial systems and suggest that the non-microbial system may be more economical and feasible overall. A number of abiotic systems for H_2O_2 production are compared in Table 4. These are compared graphically with microbial technologies from Table 3 in Figure 3. Figure 3 shows that the highest performing systems in terms of maximum achievable concentrations and coulombic efficiencies are indeed abiotic, but that technologies overlap heavily. The highest performing systems [16], [22] both use a hydrogen fuel cell style membrane electrode assemble (MEA) and pure hydrogen gas anodic feed, which is not possible in a biotic system, but many of the others use two aqueous electrodes very similar to MECs and MFCs. The costs of the systems are also comparable: an electrolysis cell using a 2.5 V DC input and achieving 100% CE would cost 3.9 kWh kg^{-1} while real studies show costs as low as 2.5 kWh kg^{-1}[42], while real data from studies with MECs cost 3-8.3 kWh kg^{-1}, depending whether the wastewater is synthetic or real [35]. Costs are discussed in greater detail in Chapter 5.

Table 3 - Comparison of recent literature on H_2O_2 production in MECs.
Note: Unless specified, all studies use a dual chamber construction. Potential conversions assume $E_{Ag|AgCl}$=222 mV vs SHE and SCE = 144mV vs SHE unless an alternate value is given by the study being referenced.

Ref.	Configuration	Cathode construction	Bioanode construction	Performance highlights
[33]	MFC	Spectrographically pure graphite (SPG) rod, pure O_2 sparged, 100 mM Na_2SO_4 electrolyte (theoretical pH=7.5), 70 mL	SPG rod embedded in granular carbon, synthetic wastewater, 50 mL	78.85 mg L^{-1} at 12.26% CE; 6.57 mg L^{-1} h^{-1}
[34]	MEC	GDE made with PTFE and carbon nanoparticles, 50 mM NaCl catholyte electrolyte (theoretical pH=7.0), 9 mL	Graphite rod with carbon felt, synthetic or real wastewater, 9 mL, potentiostated at -110 mV vs NHE	2284 mg L^{-1} at 95.1% CE, 1.01 kWh kg^{-1} (9 h batch) 4589 mg L^{-1} at 59% CE (21 h batch)
[35]	MEC	GDE made with PTFE, graphite powder, and carbon nanoparticles, 50 mM NaCl (theoretical pH=7.0), 5 mL,	Graphite rod with carbon felt, synthetic or real wastewater, 23 mL, potentiostated to -100 mV vs SHE	Real wastewater: 2260 mg L^{-1} at 66% CE, 8.3 kWh kg^{-1} Synthetic wastewater: 9670 mg L^{-1} at 78% CE, 3.0 kWh kg^{-1}
[43] (Ch. 3)	MEC	GDE (AvCarb GDS 2230 as in the present work), DI water (pH=6.5-7), 10 L	Carbon fibre, synthetic wastewater (real wastewater also tested), 100 L, potentiostated to -400 mV vs Ag|AgCl (-177 mV vs SHE)	Synthetic wastewater: 843.50 mg L^{-1} at 37% CE
[36]	MEC	Serpentine aqueous flow over GDE made with PTFE, Nafion, and carbon black (Vulcan XC72), active air feeding to gas side, 200 mM NaCl (theoretical pH=7.0), 18 mL	Carbon fibre, synthetic medium, 200 mL, potentiostated to -300 mV vs Ag|AgCl (-30 mV vs SHE)	3100 mg L^{-1} at ~37% CE, 1.1 kWh kg^{-1}

Ref.	Configuration	Cathode construction	Bioanode construction	Performance highlights
[37]	MEC	Specially made GDE for hydrogen peroxide production (ETEK ELAT), 50 mM NaCl (theoretical pH=7.0), 336 mL,	Graphite rod embedded in granular graphite, synthetic wastewater, 182 mL, potentiostated to -200 mV vs NHE	1300 mg L^{-1} at 83.1% CE, 1.9 79 mg L^{-1} h^{-1}, 0.93 kWh kg^{-1}
[38]	Microbial reverse electrodialysis electrolysis cell (MREC)	Graphite plate, air sparged, 600 mM NaCl (theoretical pH=7.0), 40 mL. ~-375 to ~-475 mV vs Ag|AgCl (~-178 to ~-278 mV vs SHE) cathode potential generated from reverse electrodialysis stack and anode	Carbon fibre brush, real wastewater with acetate amendment, 100 mL,	778 mg L^{-1} at 53.26%, 11.5 mg L^{-1} h^{-1}, 0.45 kWh kg^{-1}
[39] (Biotic)	MEC	GDE (AvCarb GDS 2230 as in the present work), tap water (circumneutral pH), 70 mL, -5.3 to -12.7 V vs Ag|AgCl (-5.1 to -12.5 vs SHE)	Carbon fibre, synthetic and real wastewater, 289 mL, potentiostated to -400 mV vs Ag|AgCl (-177 mV vs SHE)	Highest production rate: ~140 mg L^{-1} at ~30%, 6 mg L^{-1} h^{-1} (6 h HRT) Highest concentration: 1447 mg L^{-1} at ~25% CE (24 h HRT)
[40]	MFC	Submerged three-dimensional cathode made with graphite particles and PTFE binder on a graphite rod, aerated, 50 mM Na_2SO_4 (pH=7), 169 mL, ~-200 mV vs SCE (-56 mV vs SHE) with 20 Ω resistor	Carbon felt, synthetic wastewater, 84.5 mL, ~-200 mV vs SCE (-56 mV vs SHE) with 20 Ω resistor	196.5 mg L^{-1} at 70% CE; 10.15 mg L^{-1} h^{-1}
[41]	MEC	GDE prepared with PTFE and carbon black (Vulcan), 100 mM NaOH (theoretical pH=13), ~-500 mV vs Ag|AgCl (-277 mV vs SHE)	Carbon fibre on Ti current collection, fed diluted primary sludge (pH=7 via NaOH), potentiostated to -300 mV vs Ag|AgCl (-77 mV vs SHE)	230 mg L^{-1} at ~35% CE; 0.87 kWh kg^{-1}

Table 4 - Comparison of recent literature on production of H_2O_2 in abiotic electrochemical systems.
Note: Potential conversions assume $E_{Ag|AgCl}$=222 mV vs SHE and SCE = 144mV vs SHE unless an alternate value is given by the study being referenced.

Ref.	Configuration	Cathode	Anode	Performance highlights
[39] (Abiotic)	Dual chamber aqueous electrolysis cell	GDE (AvCarb GDS 2230 as in the present work), tap water (circumneutral pH), 25 mL, -800 mV vs Ag|AgCl (-577 mV vs SHE)	Graphite plate, tap water, 35 mL	~1400 mg L^{-1} at ~25% CE, 141 mg L^{-1} h^{-1}
[15]	Single chamber electrolysis cell, acidic sulfate buffer (0.1 M H_2SO_4, 0.1 M K_2SO_4, theoretical pH=1.12), 450 mL	GDE based on carbon black (Printex 6L), with and without modification with cobalt(II) phthalocyanine, potentiostated optimally at -700 mV vs Ag|AgCl (-477 vs SHE) for the best modified electrode and -800 mV vs Ag|AgCl (-577 mV vs SHE) for the unmodified electrode	Platinum	Unmodified: 176 mg L^{-1} at 69.7% CE Modified: 331 mg L^{-1} at 81.5% CE (CE and concentration from separate experiments)
[16]	Dual chamber electrolysis cell, two GDEs each own gas supply, both using 2 M NaOH (theoretical pH 14.3), 1.19 mL per chamber, galvanostated to 70 mA cm^{-2}	GDE made from vapour-grown carbon fibre (VGCF), carbon black, and PTFE, fed air, potential of -1520 mV vs Ag|AgCl (-1297 mV vs SHE)	GDE made from VGCF, PTFE, and platinum black, fed H_2	61 180 mg L^{-1} at 88%CE
[17] (3.1-3.3)	Single chamber electrolysis cell, sulfate buffer (40 mM Na_2SO_4, 50 mM $NaHSO_4$; theoretical pH= 2.06), 100 mL	Carbon/PTFE GDE, fed with O_2 to gas side, potentiostated to -900 mV vs SCE (-656 mV vs SHE)	Platinum	~750 mg L^{-1} at ~90% CE
[18]	Rotating ring-disk electrode (RRDE) experiment ins single chamber, 1 M $HClO_4$ (theoretical pH=0.0)	Partial carbon deposition over platinum/carbon electrode, O_2 sparged, potentiostated to ~50 mV vs RHE	Platinum	H_2O_2 concentration unreported, 41% CE

Ref.	Configuration	Cathode	Anode	Performance highlights
[19]	Single chamber electrolysis cell, 10 mM sulfate buffer (Na_2SO_4 + $NaHSO_4$; pH=3), 3mm separation between electrodes, galvanostated to 70 mA cm^{-2} (resulting cell voltage 9.25 V)	GDE made from PTFE and carbon black (Black Pearls 2000), fed pure O_2 to gas side	Dimensionally stable anode (DSA)	2593 mg L^{-1} at 58.39% CE, 24.97 kWh kg^{-1}
[19]	Dual chamber electrolysis cell (MK 40 PEM), 10 mM sulfate buffer (Na_2SO_4 + $NaHSO_4$; pH=3), 3mm separation between electrodes galvanostated to 50 mA cm^{-2} (resulting cell voltage 5.85 V)	GDE made from PTFE and carbon black (Black Pearls 2000), fed pure O_2 to gas side	Ti-IrO_2-SnO_2 mesh	1000 mg L^{-1} at ~80% CE, 7.45 kWh kg^{-1}
[20]	Fuel cell with aqueous cathode, gas anode	Graphite+PTFE+Au mesh on Nafion membrane, 0.1 M HCl catholyte (pH=1.1), O_2 sparged	Platinum dispersion on other side of Nafion membrane, fed H_2 gas	59.5 mg L^{-1} at ~25% CE
[22]	Fuel cell, dual chamber, two GDEs each with own gas supply, both using 2 M NaOH (theoretical pH 14.3), 1.18 mL per chamber	GDE made from VGCF and PTFE, fed O_2 to gas side, potential of -500 mV vs Ag|AgCl (-303 mV vs SHE)	GDE made with Pt, carbon black, and VGCF, fed H_2 to gas side, potential of -850 mV, (-653 mV vs SHE)	~68 000 mg L^{-1} at ~85%
[24]	Fuel cell with bipolar membrane, no electrolyte, H_2O_2 recovered from vapour by condensing on	Carbon cloth modified with anthraquinone derivatives and PTFE, fed O_2	Carbon cloth modified with Pt and carbon black, fed H_2	H_2O_2 concentration unreported, 1% CE

	PTFE tubes, 10 cm_2 electrodes			
Ref.	**Configuration**	**Cathode**	**Anode**	**Performance highlights**
[25]	Single chamber electrolysis cell, 1 M KOH (theoretical pH= 14), 400 mL	GDE based on carbon black (Printex 6L), PTFE, potentiostated to -1100 mV vs Ag | AgCl (-877 mV vs SHE)	Pt mesh	3370 mg L^{-1} at 33.3% CE, 59.7 mg L^{-1} min^{-1}, 8.0 kWh kg^{-1} Max of 6424 mg L^{-1} generated (CE unspecified)
[26]	Dual chamber electrolysis cell, 50 mM Na_2SO_4 pH adjusted to neutral used in both chambers	Carbon-PTFE GDE (Gaskatel), 250 mL, galvanostated to 30 mA cm^{-2}	Pt wire, 10 mL	330 mg L^{-1} at 53% CE
[27]	Dual chamber electrolysis cell, 0.05 M $NaClO_4$ used as electrolyte in both chambers (pH=2)	Graphite plate, sparged with O_2 or air, 4000 mL, potentiostated to -500 mV vs SCE (-356 mV vs SHE)	Graphite plate, 3000 mL	O_2: ~75 mg L^{-1} at 81% CE Air: ~30 mg L^{-1} at 90% CE
[28]	Single chamber electrolysis cell, 100 mM H_2SO_4 with 100 mM K_2SO_4 (pH=1) used as electrolyte, 250 mL	GDE prepared with Printex 6L carbon black, PTFE, and 2-ethylanthraquinone, fed pure O_2 to gas side of GDE, potentiostated to -600 mV vs Ag | AgCl (-378 mV vs SHE).	Pt foil	~725 mg L^{-1}, CE unreported; 660 mg L^{-1} h^{-1}
[23]	Dual chamber electrolysis cell, 122 mL each chamber, 12.5 mM NaCl electrolyte (theoretical pH=7), galvanostated to 3 mA/m2	GDE prepared with PTFE and carbon black (Black Pearls 2000)	Ti mesh with Ir mixed metal oxide coating	68 mg L^{-1} at 99% CE, 900 mg L^{-1} h^{-1}
[29]	Single chamber electrolysis cell, 2 mm spacing between electrodes, 100 mM K_2SO_4 with 100 mM H_2SO_4 electrolyte (pH=1),	GDE prepared with PTFE and carbon black (Printex 6L), potentiostated to of -2250 mV vs Pt/Ag/AgCl pseudoreference electrode (mV vs SHE unknown), supplied with pressurized O_2	DSA	414 mg L^{-1}, CE unreported; ~17 kWh kg^{-1}

	constant recirculation in laminar flow			
Ref.	**Configuration**	**Cathode**	**Anode**	**Performance highlights**
[31]	Single chamber electrolysis cell, 100 mM K_2SO_4 with 100 mM H_2SO_4 (pH=1 based on other studies), 400 mL,	GDE prepared with PTFE and carbon black modified with *tert*-butyl-anthraquinone, supplied with pressurized O_2	Unspecified	301 mg L^{-1} at ~89.6% CE (CE measured during separate test); 354 mg L^{-1} h^{-1}, 6.0 kWh kg^{-1}
[30]	Single chamber electrolysis cell, 50 mM Na_2SO_4 (pH=3), galvanostated to 20 mA cm^{-2}, 200 mL	PTFE and carbon black (acetylene black) modified with hydrophobic organic groups and PTFE film on steel mesh, sparged air	Pt	~590 mg L^{-1} at 92.7%CE; 235.6 mg L^{-1} h^{-1}
[42] 3.2	Dual chamber electrolysis cell, galvanostated to 1 mA cm^{-2},	Carbon felt with embedded, cemented carbon rods, 100 mM NaCl (theoretical pH=7) or treatment wetland effluent, sparged O_2 to maintain 8 mg L^{-1} DO, maintainted near -230 mV vs SHE, 500 mL	DSA (Ir coated Ti mesh), treatment wetland effluent, 500 mL	H_2O_2 concentration unreported, 40% CE; 54 mg L^{-1} h^{-1}, 2.5 kWh kg^{-1}
[32]	Triple chamber electrolysis cell (third chamber is between anode and cathode chambers containing 0.1 M H_2SO_4, theoretical pH=1.01)	Porous graphite/carbon felt, 1 M KOH (theoretical pH=14), sparged with O_2	DSA (IrO_2 coated Ti), 1 M H_2SO_4 (theoretical pH<0)	6500 mg L^{-1}
[21]	Single chamber electrolysis cell, 100 mL, thermostated to 10°C, 300mM K_2SO_4 (pH=10)	Rotating reticulated vitreous carbon (RVC, a type of glassy carbon foam) electrode, potentiostated to -1600 mV vs SCE (1456 mV vs SHE), DO maintained at 25 mg L^{-1}	Pt foil	~275 mg L^{-1} at 7.8% CE; 50 kWh kg^{-1}

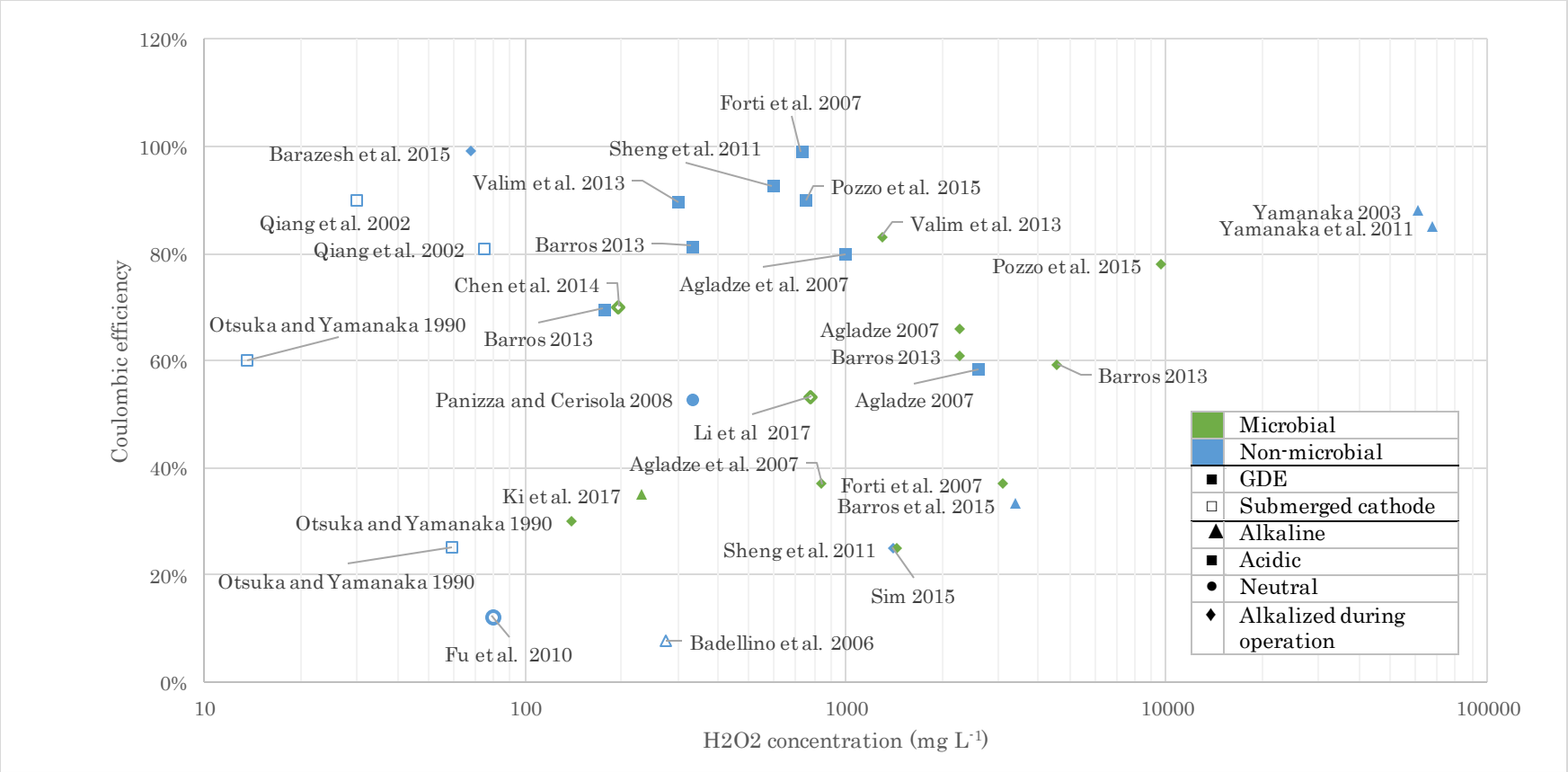

Figure 3 - Summary of maximum performance attained for H_2O_2 production from reviewed literature.

2.4.3 Cathodes

At the heart of H_2O_2 electrogeneration systems is the cathode, the electrode over which the 2-electron ORR produces H_2O_2. The cathode has two chief functions: to conduct electrons from the external circuit to the electrogeneration site and to provide the site for electrogeneration, i.e., to catalyze the reaction. The first function is easily fulfilled in electrochemical cells reviewed as the use of conductive materials such as graphite and metal causes negligible losses compared to other kinetic limitations [93].

Several types of cathodes have been reviewed: graphite, carbon cloth, carbon felt, and various gas diffusion electrodes (GDEs), which are for the most part based on carbon paper but sometimes use carbon cloth or metallic mesh as support. Carbon is an ideal cathode choice because it conducts electricity and exhibits catalytic activity for H_2O_2 production. Additionally, carbon-based catalyst layers can be adhered to carbon supports to increase surface area and provide better kinetics.

2.4.3.1 Gas diffusion electrodes

GDEs were used by a majority of the studies reviewed because they provide simultaneous access to aqueous electrolyte, gaseous oxygen, and electrons in a solid conductor by providing a three-phase reaction boundary. A simple schematic of a GDE in cross-section is provided in Figure 4.

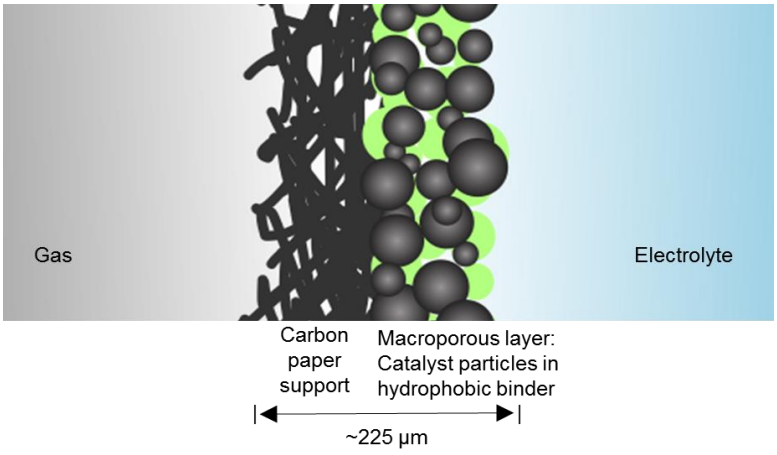

Figure 4 - Schematic of gas diffusion electrode (GDE)

The basic components of a GDE are a support layer, usually carbon paper, which provides mechanical support and a conductive surface to build off, and a macroporous layer (MPL) containing catalyst particles and binder which provides waterproofing and high surface area

for catalysis. Some GDEs have additional current collection via a metallic mesh on the air-facing side or additional layers of waterproofing on the air-facing side.

A number of studies compared the performance of submerged graphite plates relying on dissolved oxygen with GDEs and found GDEs had better overall performance and additionally did not require active aeration [17], [39], [67].

GDEs are also widely used in fuel cells, often with a GDE for each electrode connected by a non-conducting solid electrolyte in a membrane electrode assembly (MEA).

2.4.3.2 Catalyst

Since the 4-electron ORR is thermodynamically favourable to the 2-electron ORR, producing H_2O_2 instead of water requires a catalyst that provides the 2-electron pathway an advantage. The following two sections review the properties of catalysts being used and the pathways in which they work.

2.4.3.2.1 Materials and preparation

Both organic and inorganic catalysts have been applied as solid catalysts used for heterogenous catalysis of the 2-electron ORR. The literature from chemical engineering fields tends to examine metallic and metal oxide catalysts while environmental engineering literature has a strong focus on graphite-based catalysts, arising from research around developing economical electrolysis cells.

From the chemical engineering literature, Siahrostomi et al. [78] report that palladium-modified gold (Pd-Au) is effective both for synthesis from H_2 and O_2 gas as well as from electrolysis, the latter achieving 90% selectivity[1]. Less expensive gold nanoparticles were found to have comparable 80% selectivity, while on the organic side, porphyrins doped with 3-d transition metals such as cobalt were effective but degraded with use. Choi et al. [18] used Pt particles as catalyst, but partially covered particles with carbon via chemical vapour deposition to promote adsorption of O_2 at orientations advantageous for the 2-electron ORR, they achieved 41% selectivity. On the other hand, work by Yamanaka et al. [16], [22] reported production of concentrated hydrogen peroxide at 85-93% selectivity over a non-metallic catalyst, vapour-grown carbon fibre.

[1] Selectivity is equivalent to coulombic efficiency in the context of an electrochemical cell

As shown in Table 3 and Table 4, the majority of catalysts used employ carbon based material: carbon black, graphite, carbon nanoparticles, vapour-grown carbon fibre particles, and carbon cloth. As visible in Figure 3, these carbon-based electrodes have been shown to outperform the few metallic ones used and prove the metal-free catalysts, which are less expensive, are perform competitively this justifying the heavy focus on them.

Structurally, the carbon-based materials present all share similarities in their common featuring of sp2-bonded carbon, which exists in flat planar sheets with hexagonal subunits that bond at 120° to each other. A perfect sheet is graphene, graphite is composed of many layers of graphene in imperfect orientation. Pyrolytic graphite is structurally distinct from normal graphite because of turbostratic, misaligned nature of its graphene sheets, while glassy carbon is another turbostratic material that also has a quasi-crystalline structure, causing it to cleave like glass [94]. Carbon nanoparticles use the same sp2 sheets as graphitic materials but may distort them into 3D shell shapes such as tubes (nanotubes) and polyhedra; although they are three-dimensional they do not use sp3 hybridized bonds as a diamond does [95]. Carbon fibres (by themselves, woven into cloth) are composed of the same subunits as graphite, but oriented in circular layers in a filament instead of parallel layers in a sheet flat [96]. Carbon felt is an anisotropic, amorphously arranged network of carbon fibres [97]. Carbon black, made through burning a hydrocarbon substrate, is a fine powder with particles consisting of small stacks of graphite layers agglomerated in random orientations; increasing the layer size eventually causes clusters to orient themselves more orderly and resemble graphite [98].

Graphite-based catalysts' delocalized pi bonds provide good electrical conductivity which helps reduce ohmic losses in the system, but the planar sp2-hybridized carbon-carbon bonds do not provide catalytic function. Graphite is not automatically a good catalyst for H_2O_2 production, in fact, much research has focused on using graphite-based catalysts in fuel cell cathodes to reduce oxygen to water [99], an unwanted side reaction for hydrogen peroxide electrogeneration. It was suggested early on that the edges of graphene sheets rather than the flat cleavage plane provide the catalytic activity in graphite catalysts [100]. Further study has proposed that functional groups such as quinones, the key group in the AO process, that form on the surface are the likely catalysts [101]. Other surface groups that exhibit catalytic activity for ORR are oxygen-containing groups such as carboxylic acids, anhydrides, phenols, and carbonyls, which subsequently lower hydrophobicity and anchor metals and metallic

precursors that provide catalytic function [102]. Assumpcao et al. [103] conducted a comparison of different carbon blacks and found that Printex 6L, the more hydrophilic option containing twice as many oxygenated acids, outperformed Vulcan XC72R in terms of coulombic efficiency and number of electrons transferred per oxygen (closer to 2 when the 2-electron ORR is targeted). A Pt-containing option they compared was highly selective for the 4-electron ORR producing water. On the other hand, it has been noted that a hydrophobic surface chemistry is good for O_2 transfer because it of the airflow channels created by unwetted pores [104]. Although they did not speculate on mechanisms, Yamanaka et al. [22] tested a variety of brands of carbon black, each with a slightly different surface chemistry, and found performance differences. Both catalytic activity and oxygen mass transfer must both be considered and balanced in order to select an ideal cathode for H_2O_2 electrogeneration.

Formation of functional groups on a catalyst surface happens automatically as a result of normal use in electrochemical systems due to exposure to electrical and chemical redox potentials. Several authors also do surface modification intentionally, either by polarizing the electrode alone or by also doping it with organic or metallic agents, which is facilitated by carbon black's amenability to modification [104]. Guinea et al. [105] activated their GDE by electrolyzing sodium sulfate at low pH and high current density for several hours while Spalek and Balej [106] prepared PTFE/carbon black GDEs via three different methods, as well as pretreating them by polarizing them in electrolytes for different times, measuring porosity, hydrophobicity selectivity, and conductivity. Other studies [107], [108] use H_2O_2 instead of an applied potential to modify the surface electrochemically.

Other authors pretreat electrodes with specific chemicals. A review by Martinez-Huitle et al. [109] concluded that carbon black/PTFE GDEs were the best options for H_2O_2 catalysis, and they could be best be improved by surface modification with quinones, although Co and Cu phthalocyanates, metal oxide nanoparticles, Ag, and anodized carbon also were effective. Similarly, Forti et al. [28] modified their cathode with 2-ethylanthraquinone to improve performance. Similarly, Valim et al. [31] used another anthraquinone, *tert*-butyl-antrthaquinone, to modify their GDE and achieved a 17% CE improvement and decrease of number of electrons transferred from 2.3 to 2.2 over unmodified carbon black.

Although we have been discussing catalysis in the context of forming H_2O_2, catalysts can also decompose H_2O_2 by various pathways. The principle of microscopic reversibility [110] predicts that a catalyst that can hold adsorbed H_2O_2 as a reaction product can similarly use the same site to bind H_2O_2 for a reverse reaction. The kinetics of the reverse reaction is dependent on the catalyst itself and the pathway it uses. Work by Choi et al. [18] tested decomposition over different catalysts they had also used for generation and characterized decomposition rates; they were able to engineer their catalyst such that their best performing catalyst for H_2O_2 also minimized H_2O_2 decomposition.

Due to its important for application in hydrogen fuel cells, significantly more research has been done on engineering catalysts for the 4-electron ORR [111]. Success in this area suggests that similar advancements for in 2-electron ORR may be made with continued research and development.

2.4.3.2.2 Function and pathway

Reaction pathways are specific to catalysts and a plethora have been proposed in the literature covering 2-electron ORR catalysis. The intermediates and pathways used depend on the catalyst's chemical structure as well as its nano-scale morphology [18]. Some examples of catalysis pathways over common carbon materials are included in the present section.

Carbon black is used as a catalyst over half of the studies reviewed in Table 3 and Table 4. The following pathways have been proposed for 2-electron ORR over carbon black [112]:

$$O_2 + e^- + * \leftrightarrow O_2^- * \quad (12)$$

$$O_2^- * + e^- + H_2O \leftrightarrow HO_2^- + OH^- + * \quad (13)$$

or alternately

$$O_2 + H_2O + e^- + * \leftrightarrow HO_2^- * + OH^- \quad (14)$$

$$HO_2^- * + e^- \leftrightarrow HO_2^- + * \quad (15)$$

where * denotes an adsorption site on the catalyst. Note that hydroperoxide anion is the product in both reactions proposed. The kinetics of the 2-electron ORR over carbon black based GDEs have been suggested to be zero order [29], [31].

Over glassy carbon, the following mechanism is proposed - again for hydroperoxide anion production [113]:

$$O_2 + * \rightarrow O_2 * \quad (16)$$

$$O_2 * + e^- \rightarrow O_2^- * \quad (17)$$

$$O_2^- * + \dagger \rightarrow O_2^- \dagger + * \quad (18)$$

$$O_2^- \dagger + H_2O \rightarrow HO_2 \dagger + OH^- \quad (19)$$

$$HO_2 \dagger + e^- \rightarrow HO_2^- \dagger \quad (20)$$

$$HO_2^- \dagger \rightarrow HO_2^- + \dagger \quad (21)$$

where * and † refer to two different active sites on the catalyst surface. Equation 17 was determined to be the rate-limiting step.

Over pyrolytic graphite the proposed pathway [82] follows the first two steps as glassy carbon (Equation 16 and 17) with Equation 16 being rate-limiting and the final step being:

$$O_2 * + \frac{1}{2} H_2O \rightarrow \frac{1}{2} O_2 + \frac{1}{2} HO_2^- + \frac{1}{2} OH^- + * \quad (22)$$

Lastly, over single-walled nanotubes, a system of 2-electron transfers is proposed [114]. The authors also detail H_2O_2 reduction and 4-electron ORR pathways in their work.

$$O_2 + * \rightarrow O_2 * \quad (23)$$

$$O_2 * + 2e^- \rightarrow H_2O_2^- * \ (or\ HO_2^- *) \quad (24)$$

$$H_2O_2^- * \ (or\ HO_2^- *) \rightarrow H_2O_2^- \ (or\ HO_2^-) + * \quad (25)$$

Although pyrolytic graphite and single walled nanotubes are not reviewed in Table 3 and Table 4, they have been included anyway to give an idea of what has been proposed to occur over various graphitic materials, which may be the route on some of the catalysts tested depending on what surface chemistry they have developed. Further catalyst innovation could be informed by this mechanistic understanding of the 2-electron ORR.

2.4.3.3 Cathode potential

Different electrodes will have different surface chemistries, different kinetics, and different open circuit potentials for 2-electron ORR. However a brief survey of optimum reported cathode potentials does offer some general insights. When considering cathode potential, it is not only the overpotential for ORR that should be considered, but also the overpotentials for side reactions (most notably Equations 2, 3, 6, and 7) and the potential of the onset of mass-transfer losses, which begin to reduce efficiency under high potential. Mass transfer is discussed separately in Section 2.4.6.

The majority of studies that tested multiple cathode potentials did find optima; those that did not find optima found that the highest overpotentials produced the best results, indicating that they may have not yet tested found optima, except for Choi et al. [18] who observed over Pt/carbon catalyst, that there was no optimum, only diminishing performance as overpotential increased.

In terms of absolute values, of studies that did test a range of values [15], [17], [27]-[29], [31], [39], optima generally ranged between -50 to -2000 mV vs SHE, although a few tests would be much higher after applying potentials up to 9250 V across the cell [19] in optimal conditions. The remainder of this section will look more relatively at cathode potentials, discussing how optimum cathode potential has been demonstrated to change based on reaction conditions.

Reis et al. [29] saw an optimum at -2250 mV vs Pt//Ag/AgCl in laminar flow-through reaction, but at just -1750 mV vs Pt//Ag/AgCl under turbulent conditions corresponding to maximum concentrations of 414 and 294 mg L^{-1}, respectively, at the end of their batch experiments. Although the better mixing afforded in the higher flow, turbulent conditions lowered the optimum overpotential, it also prevented H_2O_2 accumulation. The authors did not speculate on a mechanism.

Sim et al. [39] tested cathode potential from -400 to -800 mV vs AgAgCl (-177 to -577 mV vs SHE). Over an electrode aerated by sparging, (either GDE or graphite plate) the lowest cathode potential (and thus lowest current density) resulted in the best CE by far, but the highest concentrations of H_2O_2 happened at different potentials (-600 mV and -800 mV for GDE and graphite plate, respectively), most likely due to different catalyst kinetics. When the same GDE was used under normal, passive aeration, -800 mV was most effective for both CE and H_2O_2 concentration as well as resulting in a much smaller current (<5% of the aerated GDE), indicating that proportionally more current was used for side reactions in the aerated reactor even though it operated best under less overpotential. It was also shown that in anodically potentiostated trials, resulting very low cathode potentials (-5.3 to -12 V vs Ag|AgCl) resulted in poor CE as water was the main product under those potentials.

A number of studies show how the optimal cathode potential shifts by modifying their electrode. Forti et al [28] shows a clear optimum at -600 mV vs Ag|AgCl over a carbon black/ 2-ethylanthraquinone GDE while unmodified carbon black GDE performed best at -1000

mV. Similarly Barros et al. [15] clearly demonstrate shifting global optima based on catalyst: testing from -400 to -1400 mV vs Ag|AgCl, they found optima over pure Printex carbon black at -1000 mV, with 3% CoPc catalyst loading: -800 mV, with 5%: -700 mV, and with 10%: -800 mV. They demonstrate that catalyst loading can also be optimized using optimal cathode potential as dependent variable.

Other studies use Koutecký-Levich analysis to determine how the number of electrons transferred per oxygen reduced is affected by cathode potential. Young et al. [36] demonstrate a divergence from constant values around 2.2 electrons at potentials above -400 mV vs Ag|AgCl for most loadings of Vulcan carbon black. Conversely, Barros et al. [15] demonstrated how at a constant cathode potential, number of electrons could be changed: in a cathode modified with cobalt(II) phthalocyanate (CoPc), the number of electrons drops from 2.6 to 2.3 over the control, carbon black catalyst. Valim et al. [31] were similarly able to quantify the effect of changing the catalyst on the optimal cathode potential, achieving 65.4% more H_2O_2 produced at 200 mV less potential than the control carbon black electrode through modification with optimal loading of *tert*-butyl-ethylanthraquinone.

2.4.3.4 Degradation

Although cathodes are initially improved by being functionalized through polarization and exposure to oxidizing species, over time their function can degrade. Choi et al. [18] performed accelerated degradation tests by subjecting their cathodes to thousands of cyclic voltammetry (CV) cycles, and observed that current density fell by 15-45% in a subsequent tests due to dissolution of their catalyst from the electrode surface. Sheng et al. [30] similarly noted an oxidation and loss of their catalyst, as well as excessive wetting of pores and decrease of surface area decreased cathode life, with the latter being determined as most significant. They modified their electrode with hydrophobic organic groups as well as applying PTFE film over the whole electrode to stabilize their cathode and were able to maintain performance over more reaction cycles as a result. They also found that scraping the cathode surface off and reapplying PTFE restored performance.

Another mode of degradation is contamination: Agladze [19] noted that acid penetration had caused metals to leach into their GDE and make it less efficient for H_2O_2 production, but they could reverse polarity on the electrode to corrode them away anodically and restore 75-80% of CE.

2.4.4 Anodes

In systems focussed purely on cathodic H_2O_2 production, anodes serve only as an electron source and are not of interest - these are described as "minimum interference" counterelectrodes by Pletcher [71]. For this reasons, about half of abiotic systems reviewed in Table 4 use a platinum electrode for O_2 evolution and others use other inert electrodes such as graphite, DSA, and titanium for the same purpose. However, in other systems anodes can be leveraged to perform oxidation reactions that complement or augment cathodic treatment processes, either by performing microbial or non-microbial anodic oxidation.

2.4.4.1 Bioanodes

In MECs and MFCs, anodes oxidize organic carbon biologically. Studies use a wide variety of anodes for ARB attachment (e.g., carbon felt, granular carbon, carbon fibre), but all are based on graphitic materials that are both conductive and biocompatible. These systems are all divided cells in order to protect ARB from oxidation by H_2O_2. In the reviewed studies, anolyte and catholyte are always separated, with reactors run as two parallel streams to better control anodic conditions to make them suitable for bacterial growth. Non-microbial anodes on the other hand are more flexible.

2.4.4.2 Non-microbial anodic oxidation

Although Barazesh et al. [23] was the only study to use direct anodic oxidation out of those reviewed in Table 4, the possibility of combining anodic and cathodic reactions on a single treatment stream has been well-established. The dearth of these systems in the present review is partly due to the fact the review so far has focussed on reactors that produce H_2O_2, and not reactors that perform treatment processes as well. Pletcher [71] and Martinez-Huitle [109] each describe a number of systems that have successfully combined anodic and cathodic processes and the use of electrogenerated H_2O_2 alongside anodic oxidation for *in situ* treatment processes specifically will be discussed in detail in Section 2.5.

2.4.5 pH

In non-microbial electrochemical systems, the studies reviewed disagree as to whether acidic or alkaline pH is optimal. Moving pH to either side of H_2O_2's pK_a at 11.65 affects speciation of H_2O_2 between its non-ionized and ionized HO_2^- form as introduced in Section 2.3, while neutral pH is optimal for ORR catalytic activity of quinone groups [33], which were discussed in detail in Section 2.4.3.2.1.

The highest performing abiotic systems seen to date [16], [22], as well as others [25], [32] use a strongly alkaline electrolyte, but the majority of studies reviewed use an acidic electrolyte [15], [17], [18], [28]-[31]. A number of studies have tested multiple pH to find optima and variously concluded that acidic [19], [20], [27] or neutral [26], [33] is preferred, while others noted that electrolyte pH had no effect and was alkalized in a divided cell anyway [38]. This alkalization was noted in microbial electrochemical systems, which all used divided cells and circumneutral electrolytes [34], [35], [37], [39], [40]. As groups, abiotic systems using acidic electrolyte and microbial systems that used neutral electrolyte that became alkaline with operation showed the best performance aside from the outlying studies by Yamanaka et al. [16], [22] (as visualized in Figure 3). This comparability suggests that allowing catholyte to alkalize is a feasible option, especially at larger scales where adjusting pH would make processes uneconomical.

A few studies took more novel approaches with engineering around pH considerations. To avoid discharging alkaline effluent, Barazesh et al. [23] controlled pH with no chemical addition by circulating feed through cathode and anode chambers sequentially. Akse et al. [32] took advantage of good H_2O_2 generation in alkaline environments and better stability in acid environments by using a three-chamber system with an alkaline cathode but an acidic intermediate chamber between anode and cathode, isolated with an AEM on the cathode side and CEM on the anode side to retain counterions.

A limited number of works analyzed pH effects mechanistically. Young et al. [36] discuss how pH change contributes to thermodynamic overpotential and requires additional electrical energy input. This can be modelled via the Nernst equation [115]:

$$E = E^0 - \frac{RT}{nF}\ln(Q) \tag{26}$$

where E is the real potential, E^0 is the standard electrode potential, R is the gas constant, T is temperature, n is the number of electrons transferred in a unit reaction, and Q is the reaction quotient, using exponents also corresponding to a unit reaction. Because the reaction quotient for the 2-electron ORR has H^+ in the numerator:

$$Q_{2e^-ORR} = \frac{[H^+]^2[O_2]}{[H_2O_2]} \tag{27}$$

increasing pH increases Q which decreases E, thus requiring a higher overpotential to make thermodynamically favourable. Thus, improving proton conduction between anode and

cathode is an important way to reduce overpotentials in systems. Modin and Fukushi [34] quantified the effect of the dominant H_2O_2 species, showing that at pH>pKa, CE was greater than 50.3% while at pH<pKa, CE dropped to less than 28.1%.

pH differences are further aggravated by poor mass transfer inside 3D electrodes and at electrode surfaces. Although studies measure solution pH, pH close to or inside an electrode can be substantially different [109]. Since effective catalysts have a high surface area, the electrodes studied are generally all vulnerable to strong pH changes around the ORR site. Mass transfer is discussed in detail in the following section, Section 2.4.6. Additionally, the effect of pH on H_2O_2 decomposition is discussed in Section 2.4.11.

2.4.6 Mass transfer

Mass transfer considerations at GDEs concern dissolution and diffusion of O_2 to the reaction site, the removal of H_2O_2 from the cathode surface before being further reduced to water, and the pH gradient that gets established between the bulk liquid and the reaction site on or within an electrode.

2.4.6.1 Liquid phase mass transfer

At the micro scale, material such as carbon felt or carbon paper provides a much greater surface area to react on and tortuous pathways for reaction products to travel through. This results in a longer residence time on the electrode and greater opportunity for accumulated hydrogen peroxide to be reduced to water. At the nano-scale, intermolecular hydrophobic and hydrophilic interactions, electric field interactions, solvation, and other microfluid dynamics govern the strength of interactions between molecules and surfaces and thus the residence time on the electrode.

Yamanaka et al. [16] exploit these nano-scale considerations who use an alkaline electrolyte to push the acid/base equilibrium of hydrogen peroxide to form more hydroperoxide anions which are electrically repelled from negatively-charged cathodes.

Tuning these surface interactions while maintaining good catalyst surface area is important. Virtually all the studies reviewed used PTFE as a binder and waterproofing agent in cathodes, which provides a hydrophobic surface but also reduces the exposed catalyst. Giorgi et al. [116] experimented with PTFE concentration in their formulation and found their best

result with the lowest loading, while others found that coating their whole electrode in PTFE did not negatively affect performance [30].

At the macro scale, mixing and diffusion are the principal mass transfer mechanisms. The majority of studies reviewed do so in batch reactors, which must be stirred or recirculated to achieve mixing, while continuous flow reactors [16], [22], [23], [35], [36], [39] are inherently mixed to some degree. In the parallel plate designs adopted by some studies [19], [23], [29], this results in high rates of shear across the electrode surface. Reis et al. [29] studied flow regime explicitly and found that laminar flow across the electrode surface was more favourable that turbulent flow; increasing the recirculation rate 6 times led to a 29% decrease in H_2O_2 concentrations yielded. However they determined that this was due to effect of liquid mixing on gas-liquid mass transfer not on liquid phase mass transfer *per se*. Thus liquid/liquid mass transfer and gas-liquid mass transfer may be coupled.

2.4.6.2 Aeration and gas-liquid mass transfer

Limitations in mass transfer of O_2 to reaction sites were largely solved by the advent of the GDE. Sim et al. [39] compared both GDEs and a submerged graphite electrode and found GDEs were theoretically more attractive due the lack of a power requirement for pumping air or purifying oxygen and that in practice they work better than aerated systems anyway.

Earlier studies which use submerged electrodes and supply dissolved oxygen (DO) by sparging with air or purified gas tended to find profound importance in O_2 supply. For example, Otsuka and Yamanaka [20] determined this to be the rate-limiting step of their system and determined that increasing mixing was more effective than increasing cathode surface area. Qiang et al. and Li et al. [27], [38] independently reported the best performance was associated with the highest DO, but that additional sparging past the minimum required deteriorated performance, but neither speculated on a mechanism.

A number of studies investigated difference in supplying O_2 versus air. Qiang et al. [27] found that switching to air this lowered the current but slightly raised CE. GDEs also sometimes use pressurized air or oxygen (on the air side of the cathode) to increase mass transfer. Panizza and Cerisola [26] observed that thermodynamically, O_2 and air supply were identical (same open circuit potential) but that using O_2 did lead to greater currents. They did not find that the increased current density led to losses in CE. Sim et al. aerated a GDE by sparging the liquid side and found this increased the current but had much lower CE. Since the

conditions in all these studies vary, it is difficult to draw general conclusions other than more rapid mass transfer facilitates greater current densities, but CE may not be maintained.

Lastly, when considering gas-liquid mass transfer in a GDE, one must consider not just the flux but the surface area available. As alluded to previously in Section 2.4.6.1, Reis et al. [29] suggest that the balance of pressure between the liquid and gas sides of a GDE influences the penetration of water into MPL pores and changes the surface area available for O_2 diffusion.

The question of the economics of using active aeration on the gas side of a GDE is not analyzed specifically by any of the studies reviewed, but based on the comparable performance of systems using active and passive aeration on the gas side of GDEs as summarized in Table 3 and Table 4, it is likely that at scale, passive aeration of GDE is probably more economical.

2.4.7 Electrolyte

The supporting electrolytes in electrochemical cells work as charge carriers and determine the resistance of the solution between electrodes. Solution resistance may be chiefly overcome by two strategies: minimizing the spacing between electrodes and increasing the ionic strength of the electrolyte [93]; Ki et al. [41] attribute the excellent energy performance for their MFC to the low internal resistance they achieved by paying attention to these in their design.

Theoretically, in potentiostatic operation, having a more conductive solution can result in higher current densities and in galvanostatic operation more conductivity means less voltage is required across the cell. Qiang et al. [27] confirmed experimentally that, in galvanostatic mode, increasing $NaClO_4$ electrolyte strength affects voltage but not net current density or H_2O_2 generation rate. On the other hand, Fu et al. [33] operated their system galvanostatically and found an optimum electrolyte strength at 100 mM (200 mEq) Na_2SO_4, though they did not speculate on a mechanistic cause.

In MFC operation, conductivity is even more critical because there is limited energy available to spend and solution losses decrease the potential available for ORR. Modin and Fukushi [34] operated an MFC on both synthetic and real wastewaters and saw a decrease in conductivity from 777 to 127 mS m^{-1} between feeds, causing an internal resistance rise that

made the MFC less productive. Conversely, Li et al. [38] experimented with increasing conductivity in the catholyte of their microbial reverse electrodialysis electrolysis cell (a fuel cell) and observed H_2O_2 concentration and current increase as catholyte conductivity was increased. A plateau was reached around 360 mM NaCl.

Though less important than in an MFC, conductivity in MECs is also important. In work by Sim (Ch 3 of [43]), who used just tap water as catholyte, conductivity rose during operation because of diffusion of ions from the relatively rich anolyte to values around 2 mS cm^{-1} using an anion exchange membrane (AEM) but as high as 10 mS cm^{-1} with cation exchange membrane (CEM). The CEM reactor had better production and efficiency too: 98 mg L^{-1} at 4.1-7.2% versus 9 mg L^{-1} at 0.2-0.35% with the AEM, although current densities were similar, varying greatly and below 1 mA cm^{-2}. Rozendal et al. [37] similarly saw catholyte conductivity rise from 5.5 mS cm to 12.3 mS cm^{-1} through a CEM. Membranes are discussed in detail in Section 2.4.8.

In all studies reviewed, inert electrolytes were selected and the choice of the electrolyte itself did not seem to matter. Yamanaka et al. [22] tested K, Li, and NaOH electrolytes and found that differences in performance could be attributed to current densities linked to conductivity differences. On the other hand, there is some evidence that halides can promote H_2O_2 formation over Pd/Pt/Au catalysts, reported by two patents originally by DuPont [117], [118]. One ion to be careful of is carbonate, which is ubiquitous in natural waters but is a scavenger for H_2O_2, acting as an oxidant and forming carbonate radicals, $CO_3^{-}\bullet$ [41] and has been shown to also lower the process efficiency of peroxide bleaching [119]. Additionally, carbonates can be detrimental because metal-hydrogen-carbonate complexes may catalyze decomposition [36]. Decomposition will be discussed in detail in Section 2.4.11.

An additional factor that should be considered when selecting the electrolyte itself are conductivity through a separator, if one is being used, which is discussed in the following Section 2.4.8.

2.4.8 Separation

Separators are used to split an electrolysis cell into isolated half cells while maintaining ion conductivity between electrodes. They may be ion exchange membranes (e.g., AEM, CEM, or proton exchange membrane (PEM)) that do not allow bulk mixing of anolyte and catholyte or simple size-exclusion membranes such as water filtration membranes or even textiles [120].

Separation is done for a few reasons. In microbial systems, the anolyte is typically rich in organics and possibly pathogens and should not be mixed with a potential treatment stream in the catholyte; while conversely the ARB are vulnerable to damage by H_2O_2. In chemical systems, the greater concern is anodic oxidation of H_2O_2 via Equations 8 and 9. This is a second electrochemical route to H_2O_2 destruction in addition to the already discussed cathodic reduction, and has been quantified to occur at a greater rate [19] or at least cause the performance reduction seen between undivided and divided systems [26]. Leng et al. [121] even found that in an undivided system, H_2O_2 was so quickly destroyed anodically that it could not be measured at all. However, a number of the studies reviewed in Table 4 use single chamber designs and have good performance [15], [17], [19], [25], [28]-[31] despite not taking precautions against anodic oxidation. These studies for the most part use platinum anodes that have been demonstrated elsewhere to be active for H_2O_2 oxidation [26]. The requirement for separation is unclear given the mixed results from different researchers.

Ion exchange membranes are the most commonly used separator. These do not allow solvent to pass through them, but contain functional groups of opposite charge to the molecules to be transmitted that can bind and pass the molecule through the membrane [122]. Aside from keeping H_2O_2 away from the anode, if an ion exchange membrane is used as a separator, it is possible isolate either cations or anions selectively. Carbonate, an anion has been discussed in Section 2.4.7. For the chloride component of NaCl, a commonly used and inexpensive electrolyte, it may be recommended to use an CEM to isolate electrolytes as chloride anions may be anodically oxidized to active chlorine species [23], [42]. Although in some applications this may be attractive as source of more dissolved oxidizing power, active chlorine can also oxidize H_2O_2 as it has a higher redox potential, shown previously in Table 2. An AEM may be preferred to keep metal cations out of catholyte where they can catalyze H_2O_2 decomposition (discussed in Section 2.4.11) and better control pH (due to their polyvalent charge) [41]. AEMs in H_2O_2 system though may allow migration of HO_2^- ions; Arends et al. [42] saw 2.6% of the H_2O_2 they produced migrate across their AEM due to alkalization of the catholyte.

PEMs like Nafion, which allow only conductance of protons and not of other ions, are widely used, but they are also more expensive than CEMs and AEMs, amounting up to 40% of system cost [123]. In tests where they are directly compared, Nafion did show better

performance [36], although other researchers suggest AEMs are still preferred over Nafion especially when economics are considered [124].

Membranes provide more design opportunities than just choosing between undivided or divided, dual chamber systems. For example one design intended for use in spacecraft [32] uses a three-chamber system to generate and store H_2O_2 in different pH environments by using an AEM to bound the strongly alkaline cathode chamber, a CEM to bound the strongly acidic anode chamber, leaving a weakly acidic concentration chamber. The centre stream is then pervaporated through an external fourth membrane into the treatment stream.

Although the separation functions can be valuable to engineering the chemistry of half cells, the cost of membranes is also felt in the internal resistance they add. For an idea of the relative burden imposed, the conductivity of Nafion 117 is on the order of 250 mS cm^{-1} (depending on how it is prepared) [125] and a commonly used AEMs and CEMs by Membranes International have a conductivity of >1.35 mS cm^{-1} [126], [127]. For comparison, tap water has a conductivity of just 0.05 to 5 mS cm^{-1} [128]).

A risk of using membranes in any application is the occurrence of fouling, especially on long term performance [129]. Although not many studies mentioned fouling directly, Modin and Fukushi [34] did observe fouling as white deposits on the cathode side of the Nafion PEM they used in their system. Fouling increases internal resistance in the cell by impeding mass transfer of ions and inhibiting charge neutrality. Although methods to address fouling have been addressed in other membrane science fields such an anaerobic membrane bioreactors [10], work specific to H_2O_2 electrogeneration systems is not available, probably because it is a more operational concern that will receive attention as the technology is scaled up.

Another operational issue that may arise is the degradation of membranes over time, both decreasing membrane function and contaminating electrolytes. Young et al [36] tested a variety of membranes and found that all membranes exposed to H_2O_2 or high pH released organic carbon into the water. This is of increased concern in reactors for H_2O_2 generation for the Kraft process where membranes must be sufficiently resistant to oxidation in relatively concentrated H_2O_2 streams [14].

H_2O_2 decomposition may be catalyzed over reactor walls, which is elaborated upon in Section 2.4.11, and membranes provide possible reaction sites that may decrease H_2O_2

concentrations. Young et al [36] tested a number of membranes for catalytic activity for H_2O_2 decomposition and found that none did.

Lastly, it should be mentioned that although membranes provide important functions that have been discussed in this section, separating anolyte and catholyte in the electrochemical reaction itself does not preclude more creative reactor configurations. Fluid may be circulated between half-cells at different stages of treatment as explored for wetland-coupled MFCs [42] and a UV-H_2O_2 system [23].

2.4.9 Surface area to volume ratio

In an electrochemical reactor, the surface of the electrode is where the primary chemical reaction happens and basic modelling will emphasize that increasing the surface area of the electrode relative to the volume of the reactor provides the best use of space. Additionally, since excess reaction chamber volume dilutes any electrogenerated chemicals, reactors with larger surface area to volume ratios can more easily concentrate H_2O_2 to concentrations which may be required. Arends et al. [42] specifically note that they should have used a 5 ml rather than 500 ml cathode to easily improve performance of their system.

One common approach to maximizing surface area in electrochemical systems, where catalyst needs to be in contact with liquid as well as the external circuit, is to use parallel plates a few mm [19] to a few hundred µm apart [130]. These designs can be scaled up by rolling into a tube [130], a strategy used in filtration membrane modules [131].

An alternate approach to maximizing surface area it to use finned cathodes, however this limits use to submerged cathodes only. This approach was used to linearly increase current and H_2O_2 generation while sustaining the same CE on a potentiostated cathode [27]. Submerged electrodes using granular or porous material (like graphite granules or carbon felt) were adopted by a few studies [32], [40] and had comparable performance to other work despite the poor mass transfer inherent to a 3D electrode, this may have been supplemented by factors such as mixing induced by aeration or electrostatic repulsion.

2.4.10 Temperature

Not many studies discuss temperature at all, as most are carried out at ambient temperature which is well-suited to low-cost scale up. Badellino et al. [21] tested 10 and 18°C electrogeneration batches and found that roughly 3 times as much H_2O_2 could be

accumulated at the lower temperature, regardless of whether an acidic or basic pH was used. Qiang et al. [27] tested three temperatures from 13-33°C and found that the lowest temperature trial had better CE and H_2O_2 production under galvanostatic conditions. This was due to the increased O_2 solubility and decreased H_2O_2 decomposition, despite the mass transfer coefficient for O_2 dissolution being smaller. Decomposition specifically is discussed in the following Section 2.4.11.

2.4.11 Decomposition

One can note from Table 2 that the peroxide reduction to water (Equations 2 and 3) may be coupled to the 2-electron ORR (Equations 8 and 9) to yield a thermodynamically favourable decomposition reaction:

$$2H_2O_2 \leftrightarrow 2H_2O + O_2, \qquad (E^0 = +1.06\,V) \tag{28}$$

Though this reaction is favourable, it is suggested that it is either facilitated by catalysis [27] or interaction with HO_2^- in an alkaline environment rather than H_2O_2 [27], [132], [133]. H_2O_2 decomposition catalysts including enzymes (e.g., catalase [13]), polyvalent metal ions of manganese [134], iron [135](the basis for Fenton processes), and copper [136], metal oxides[137], and container walls [27]. Commercial peroxide is stabilized using sodium pyrophosphate, sodium stannate [13], ethylenediaminetetraacetic acid (EDTA) [133], magnesium sulfate, sodium silicate, and diethylenetriaminepentaacetic acid (DTPA) [119] to chelate any impurities and thus inhibit catalysis. In addition to catalysis by homogenous catalysts and container walls, catalysts for H_2O_2 generation, even when not polarized, can also catalyze decomposition. However, fortunately catalyst design allows for catalytic selectivity such that the best catalysts for electrogeneration on a polarized electrode do not also exhibit the highest activities for decomposition [18].

pH is important to stability not only because it governs the amount of HO_2^- present, but also because pH controls speciation of trace metals which may act as catalysts [27]. Optimal pH in the context of decomposition (i.e., not in an electrochemical cell with polarized electrodes) was examined by a number of studies. Qiang et al. [27] found inflection point around pH 9, more than 2.5 units below the pK_a for H_2O_2, above which decomposition rates sharply increased across all temperatures they tested. They also found a small peak at 3, the Fenton reaction optimum, suggesting some trace metal contamination. Similarly, Young et al. [36] found the lowest decomposition rates were associated with the lowest pH they tested (pH=4.5

out of a range going to pH=12). They also noted that the electrolyte itself had a strong effect that rivalled the influence of pH; phosphate buffer solution at pH=7.5 performed better than NaCl at pH=6.5 and NaCl at pH=12 performed better than Na_2CO_3 at pH=11.5.

Temperature has been examined for its effect on decomposition rates as well. Lee et al. [119] saw ~10 fold increases in first order rate constant for decomposition when temperature was changed from 30 to 50°C in alkaline medium.

An addition path for H_2O_2 decomposition is photolysis under visible or UV light, the basis of H_2O_2 AOPs [21]:

$$H_2O_2 \xrightarrow[h\nu]{} 2 \bullet OH \tag{29}$$

The reactive hydroxyl radical is rapidly reduced to water, thus providing another pathway to decompose hydrogen peroxide. This reaction is undesirable for storage, where it may be avoided easily by storing in a dark container.

Although decomposition is a well-known operational concern, not many studies quantify the relative importance of these reactions to overall reactor productivity. Agladze [19] identifies five modes of H_2O_2 loss in a working electrochemical cell: bulk decomposition, direct anodic oxidation, direct cathodic reduction, oxidation mediated by hypochlorite at the anode, and reduction mediated by superoxide, hydroxyl, or hydroperoxyl radicals at the cathode. They state that bulk decomposition is relatively slow, and that anodic oxidation is the chief mechanism for H_2O_2 loss in their undivided reactor at pH=3. One way to avoid the problem of H_2O_2 loss, either through decomposition in the bulk or through reactions on electrodes, is to react H_2O_2 *in situ* for a treatment process, which is discussed in the following section Section 2.5.

2.5 *In situ* application of electrogenerated H_2O_2

In situ application of electrogenerated H_2O_2 is as heavily studied as *in situ* electrogeneration alone. However, due to the wide variety of matrices, mechanisms, and target compounds, this section is organized to highlight some key, generalizable findings of specific works rather than compare performance directly as done in Section 2.4.

2.5.1 Direct oxidation

Despite the limited applicability of H_2O_2 as a direct oxidant outlined in Section 2.1, a small number of studies do use H_2O_2 as-is as an oxidant, and by doing so, avoiding incurring

additional costs for things like UV lamps, catalysts, and pH control required by other methods of *in situ* treatment. Do and Yeh [138] cleverly used an aerated pretreated graphite cathode and SnO_2-PdO-RuO_2-TiO_2/Ti anode to treat phenol by simultaneous anodic oxidation mediated by active chlorine and cathodic oxidation mediated by H_2O_2 in a dual-chamber batch reactor and saw similar CEs in each half-cell which diminished as batch life progressed and phenol concentration dropped. They also tested adding ferrous iron to start a Fenton process (discussed in detail in Section 2.5.2.2) but found only about a 1.5 percentage point improvement in degradation fraction by adding an optimal dose of ferrous iron. Shen et al. [67] similarly designed a dual chamber system to treat dye by oxidation at both their graphite anode and platinized carbon GDE cathode. They found their system performed much better at acid-neutral pH than in alkaline, with their pH 10 trial showing almost no COD removal, and that greater removal occurred at the H_2O_2-producing cathode than the anode. They also did testing with ferrous iron in an electro-Fenton system and found that the addition improved the cathodic COD removal about up to around 10 percentage points maximum but did not affect anodic removal due to the H_2O_2 gradient in the cell.

One other study that uses H_2O_2 directly is a patent for organosulfur compound oxidation in hydrocarbon processing, i.e., in non-aqueous media [66]. The process uses a dual chamber system with a GDE cathode and suggest a number of possible inert anodes as well as those known to be active for anodic oxidation, for example, boron-doped diamond.

2.5.2 Advanced oxidation processes

The majority of studies employing electrogenerated H_2O_2 for *in situ* treatment use some technique to generate hydroxyl radicals (•OH) to increase the oxidizing power and versatility of their system However there are a number of arrangements possible.

2.5.2.1 UV+H_2O_2

As recently discussed in Equation 29 in Section 2.4.11, H_2O_2 can be photolysed by UV light to yield two •OH radicals.

In one study applying this technique, Barazesh et al. [23] pass an organic carbon-containing treatment stream (surface water, groundwater, or final effluent) over a dual chamber system's GDE cathode for H_2O_2 generation, then through a UV reactor for •OH generation, then back through the anode chamber for pH readjustment and residual H_2O_2 removal. They found that the process exhibits diminishing returns as H_2O_2 concentration rises because of

H_2O_2 scavenging •OH and screening UV light from directly photolysing organics. They also found that depending on catholyte pH, carbonate scavenging could also affect performance, but nitrite would not be an issue for the treatment streams tested. Though Barazesh et al. allowed pH to change in response to electrode processes, Badellino et al. [21] tested UV+H_2O_2 at pH 3 and 10 as part of a larger work and noted that at alkaline pH, H_2O_2+UV was less effective than at acidic pH despite higher amounts of HO_2^-.

2.5.2.2 Electro-Fenton processes

Electro-Fenton systems innovate on the classic Fenton system by using electrogeneration as the H_2O_2 source. Fenton systems rely on the following chemical reactions, which together consume then regenerate ferric ions while producing hydroxyl, hydroperoxyl, and superoxide radicals [68]:

$$H_2O_2 + Fe^{2+} \rightarrow Fe^{3+} + \cdot OH + OH^- \quad (30)$$

$$H_2O_2 + Fe^{3+} \rightarrow Fe^{2+} + HO_2 \cdot + H^+ \quad (31)$$

$$Fe^{3+} + HO_2 \cdot \rightarrow Fe^{2+} + O_2 + H^+ \quad (32)$$

$$H_2O_2 + \cdot OH \rightarrow H_2O + HO_2 \cdot \quad (33)$$

$$HO_2 \cdot \leftrightarrow H^+ + O_2^- \cdot \quad (34)$$

$$Fe^{3+} + O_2^- \cdot \rightarrow Fe^{2+} + O_2 + H^+ \quad (35)$$

$$Fe^{3+} + O_2^- \cdot + 2H_2O \rightarrow Fe^{2+} + 2H_2O \quad (36)$$

The first study [44] using electrogenerated H_2O_2 (using the same reactor as a previous study [19] including a carbon black/PTFE GDE) for an electro-Fenton process compares the performance of treatment *in situ* and *ex situ* processes. Two comparable experiments both used an undivided cell with external reservoir recirculation but the *ex situ* process used the raw feed is used as electrolyte but did not dose it with iron until moved to a second, stirred reactor, unlike the *in situ* process which applied iron inside the electrolysis cell. The feed used was a partially-treated construction plant wastewater. They found faster COD reduction and more complete COD removal in the *ex situ* process, where they achieved 76% COD removal using 5 minutes of electrogeneration (yielding 250 mg L^{-1} H_2O_2) and 1 hour of contacting in the Fenton reactor. They point out that in the *in situ* process, the pH gradients in electrode pores discussed in Section 2.4.5 can cause iron to precipitate as iron hydroxide in the alkaline environment close to the electrode, a drawback to putting both processes in the same reactor. Another evident drawback is the vastly different retention times required

for the two stages of treatment: 5 minutes versus 1 hour. This work brings attention to important operational issues for conducting *in situ* treatment over a GDE.

A number of studies using undivided cells, GDE cathodes, and platinum anodes were subsequently published for *in situ* treatment of organics such as dyes [45], [104] and dimethyl phthalate [46] as well as a two-chamber systems for phenol [47]. These studies did effectively sustain Fenton reactions with electrogenerated H_2O_2, but did not take advantage of anodic oxidation processes. Additionally, electro-Fenton studies frequently point out the operational cost of treating effluents to acceptable pH and iron levels [47], [104].

2.5.2.3 Bioelectro-Fenton processes

Bioelectro-Fenton systems are a variation that use a bioanode to supply electrons to a cathode producing H_2O_2 and maintaining acidic and iron-containing conditions needed for the Fenton reaction. This is benefificial as a power and electron source as well as providing the cobenefit of organiz carbon removal. These systems have been studied widely for dye treatment [48]–[52], emerging contaminants [53], arsenite [54], [55] , Cr(VI) [56], [57], triphenyltin chloride [58], phenol [59], tetracycline [60], and enhanced glucose removal [61].

2.5.2.4 Photoelectro-Fenton processes

A fourth advanced oxidation process applying *in situ* electrogenerated H_2O_2 combines elements of UV with Fenton to create a photoelectro-Fenton process where both UV photolysis and Fenton reactions create radicals and regenerate ferrous iron. Photo-Fenton systems introduce two additional reactions [68] to those presented in Section 2.5.2.2, firstly photolysis of Fe(III) hydroxide, the dominant Fe(III) species:

$$Fe(OH)^{2+} \underset{h\nu}{\rightarrow} Fe^{2+} + \bullet \mathrm{OH} \tag{37}$$

as well as the photodecarboxylation of Fe(III) complexes, for which the general formula is:

$$Fe(OOCR)^{2+} \underset{h\nu}{\rightarrow} Fe^{2+} + CO_2 + \bullet \mathrm{R} \tag{38}$$

where R represents an arbitrary organic compound.

Badellino et al. [21] demonstrated that the photolectro-Fenton process was an improvement upon UV+H_2O_2 treating the pesticide 2,4-dichlorobenzene, relying on cathodic processes only. Other studies have innovated at both anode and cathode reactions. Wang et al. [62] use an active anode (RuO_2/Ti) that produces radicals to increase anodic oxidizing power for

treatment of the antibiotic sulfamethoxazole while Xie and Li [63] use a photoanode that uses the same UV light as the photo-Fenton process to create oxidizing species on the anode to treat orange-G dye. Isarain-Chavez et al. [64] use two cathodes, one specialized for iron regeneration and the other for H_2O_2 production, in treating the drug atenolol. Casado et al. [65] innovate by using sunlight as a UV source, addressing one of the principles costs of UV AOPs. None of these treatment innovations are specific to the model compounds being studied, and all represent manners in which the performance of electrochemical treatment systems may be increased through efficient, creative design, as we attempt in the present work.

2.6 Summary of research gaps

Chapter 2 has discussed extensively researched carried out around H2O2 electrogeneration both for systems that produce H_2O_2 and those that produce and react it *in situ*. The following are the main research gaps identified in through this review which are addressed by the objectives set forth in Section 1.4.

1. Performance and operational considerations for continuous-flow reactors
2. Maximum performance achievable from commercially-available, metal-free catalyst
3. Ambiguity about optimal pH, especially with operational considerations
4. Relative magnitudes of mass flows for different reactions on electrogeneration reactor
5. Treatability of sulphur(IV) specifically and quantification of performance improvement

3 Optimization of cathodic conditions for H_2O_2 electrogeneration over gas diffusion electrode in a dual-chamber electrolysis cell

3.1 Overview

H_2O_2 is electrogenerated in a dual-chamber electrochemical cell over a commercially-available, metal-free gas diffusion electrode and optimized for hydraulic residence time (HRT), cathode potential, and pH. Kinetic testing of H_2O_2 decomposition in the reactor is used to build a mass balance model to quantify mass flows in the reactor. During continuous testing, it is shown that moderate CE of 60-70% is maintained up to 11 h HRT, that decreasing cathode potential and concomitant currently density ride result in modest CE losses, and that alkaline pH is optimal for H_2O_2, though under operation with neutral influent pH becomes alkaline without other pH adjustment. Modelling shows that as H_2O_2 concentrations increase, non-Faradaic decomposition becomes the dominant route for H_2O_2 loss and a tradeoff curve is established for the GDE use between CE and effluent H_2O_2. Lastly a microbial electrochemical cell (MEC) is run with a cathode for H_2O_2 electrogeneration to demonstrate suitability of current densities obtained in abiotic experiments to biological systems.

3.2 Introduction

Hydrogen peroxide (H_2O_2) is a widely used, oxidizing agent across many industrial sectors, including manufacturing of chemicals, paper products, and metal products, drinking water and wastewater treatment, pollution control, and site remediation [139]. It is also an important hydroxyl radical precursor (·OH) in some advanced oxidation processes (AOPs), which are increasingly being applied for pre-treatment or post-treatment in hard-to-treat wastewaters [140]. The majority of industrially used H_2O_2 is synthesized and concentrated offsite and transported to its point of use, incurring costs for delivery and storage, but promising options exist for H_2O_2 production via electrogeneration in fuel or electrolysis cells [13]. Electrogenerated H_2O_2 has been currently applied for some of the pulp and paper industry [13] and there remains a huge and growing market for H_2O_2 [141] that electrogeneration may be able to meet the needs of for certain users and applications.

Electrogeneration of H_2O_2 has been studied heavily in recent years, both in abiotic, chemical electrolysis systems [15]-[32] and, with energy efficiency and sustainability, in H_2O_2-producing microbial electrochemical cells (MECs) and microbial fuel cells (MFCs) [33]-[42].

Fundamental and engineering aspects of microbiologically catalyzed anode reactions have been intensively investigated for over 10 years, but studies focussing on cathodic conditions for H_2O_2 production, such as design and modification of electrodes, pH, feeding and mixing conditions, and cathode potentials are limited.

A key innovation in electrode design has been the gas diffusion electrode (GDEs), which has the advantages as a cathode of being able to use water and atmospheric oxygen as reagents, overcoming costs and mass transfer limitations for dissolving oxygen, being commercially-available, and operating well under mild conditions of temperature, pH, and electrolyte strength. As visible in Figure 3, studies using GDEs outperformed studies using submerged electrodes fed dissolved O_2. However, nearly all of the studies reviewed (except [26], [39]) used custom-fabricated GDEs and almost no information is available about the performance of commercially-available unmodified electrodes that could be most feasibly supplied for use in scaled-up systems.

With respect to pH, there remains disagreement as to whether acidic or alkaline pH is optimal for H_2O_2 generation. The highest performing systems seen to date [16], [22], as well as others [25], [32] use a strongly alkaline electrolyte, but the majority of studies reviewed use an acidic electrolyte [15], [17], [18], [28]-[31]. A number of studies have tested multiple pH to find optima and variously concluded that acidic [19], [20], [27] or neutral [26], [33] is preferred, while others noted that electrolyte pH had no effect and was alkalized in a divided cell anyway [38]. Similarly, a number of works did not investigate pH as a variable directly but noted the alkalization of catholyte in dual chamber systems [34], [35], [37], [39], [40], suggesting this outcome to be more feasible at scale than adjusting pH. Barazesh et al. [23] controlled pH with no chemical addition by circulating feed through anode and cathode chambers sequentially. As groups, abiotic systems using acidic electrolyte and microbial systems that used neutral electrolyte that became alkaline with operation showed the best performance aside the outlying studies by Yamanaka et al. [16], [22], as visible in Figure 3.

Like pH, there exists a wide range of cathode potentials being studied. Most studies use cathode potentials between -50 to -2000 mV vs SHE, but some would be much higher after applying potentials up to 9250 mV across the cell [19] in optimal conditions. Many studies test multiple cathode potentials and do find clear optima [15], [17], [27]-[29], [31], [39], but did not identify the mechanism responsible. Fortunately, tools like cyclic voltammetry

provide easy ways to analyze electrochemical kinetics and predict performance with specific cathode kinetics and under specific thermodynamic conditions. The chief contribution of this study will be to characterize the effect of cathode potential on the selected, commercially-available GDE.

Although, the majority of studies to date use batch systems, which are sometimes preferred for kinetic analyses, only a few do a quantitative analysis [19] to explain the recurrent trend in concurrent H_2O_2 concentration rise and coulombic efficiency (the portion of current used to reduce oxygen to H_2O_2 at the cathode) drop over time, i.e. explain how much H_2O_2 loss happens via different routes. A lesser number of studies use continuous mode cathodes [16], [22], [23], [35], [36], [39], which are more feasible for scaled-up industrial processes. Compared to batch systems, continuous systems differ in that concentration in the reactor is governed strongly by hydraulic retention time (HRT) in addition to electrode processes and transport across separators. Additionally, mixing regimes are different between continuously fed and batch (stirred or unstirred) reactors, which may strongly influence processes in the diffusion boundary layer on an electrode. Yamanaka at al. [22] also point to the role of a continuous electrolyte supply in maintaining charge balance in a divided reactor, finding that without continuous flow, current density would drop due to depletion of charge carriers. Some studies do use recirculation that may help inform continuous mode reactor development [29]. On the whole, there does not presently exist a thorough body of knowledge on electrogeneration in continuous systems, especially when considering the lack of quantification of reaction routes in the system.

The present work addresses the existing knowledge gaps by conducting testing using continuous mode operation and a commercially-available, unmodified GDE and resolving mixed results about optimum pH and cathode potential. Addressing these questions facilitates further development of H_2O_2 producing cathodes in chemical or microbial systems.

3.3 Materials and methods

3.3.1 Apparatus

Dual chamber electrolysis cells were constructed by sandwiching together cylindrical reactor chambers and flat end plates made of acrylic, rubber gaskets, electrodes, and an ion exchange membrane, as shown in Figure 5. Reaction chambers and end plates were machined from acrylic blocks (Clear cast acrylic, McMaster-Carr, USA). The bored-out half cell chambers

had an internal diameter of 38.3 mm, with the anodic block having a thickness of 23.0 mm (working volume of 25 mL). Three reactors having different sizes of a cathode chamber were used for the experiments. Reactor A used the same size cathode chamber as the anode chamber (working volume of 25 mL), Reactor B used a smaller cathode chamber (working volume of 10 mL), and Reactor C used a 3.0 mm Neoprene gasket (working volume of 3.5 mL) instead of an acrylic chamber. The cathode chambers in Reactor A and B were drilled and fitted with an Ag | AgCl reference electrode (MF 2052, BASI, USA) and influent and effluent line fittings. In Reactor C, a fitting for the reference electrode was made on the effluent line using a T-junction, and hypodermic needles were used to provide influent and effluent fittings as shown in Figure 5.

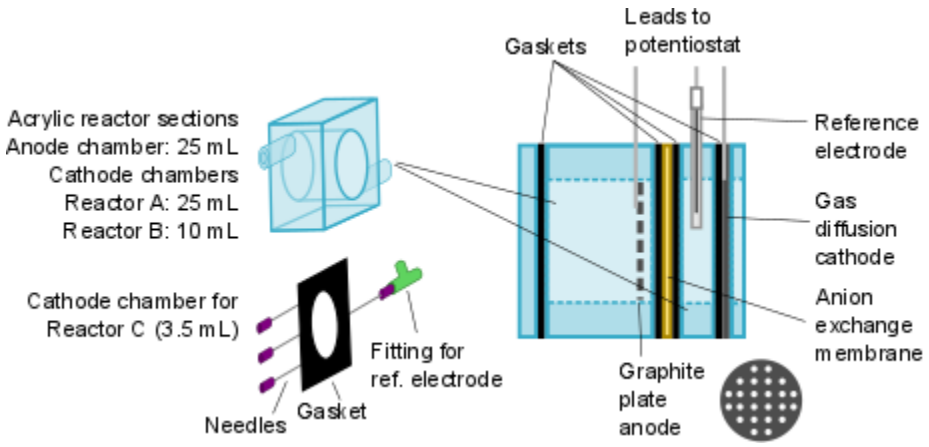

Figure 5 - Schematic of electrochemical cells used for experiments

A gas diffusion electrode (GDE; GDS 2230, AvCarb, USA) was used as the cathode, consisting of a carbon paper base (~225 µm thick) with a polytetrafluoroethene (PTFE) and carbon black macroporous layer (MPL). The anode was a flat graphite disc (Isomolded Graphite Plate 203101, Fuel Cell Earth, USA), with regularly-spaced holes drilled to maximize surface area and allow diffusion to either side of the electrode and a stainless steel wire sewn through to provide an electrical lead out of the reactor. Ion exchange membranes were either anion exchange membranes (AEM; AMI-7001, Membranes International, USA) or cation exchange membrane (CEM; CMI-7000, Membranes International, USA), as specified.

For preliminary experiments requiring simply a vessel for liquid, Reactor A components were used to control for potential catalysis due to container walls [27]. Reactor A_2 is Reactor A's cathode chamber capped with two solid end plates with no electrodes and Reactor A_3 is

Reactor A's cathode chamber capped with a solid end plate on one side, a GDE and solid end plate on the other.

3.3.2 Electrolytes

Electrolytes were prepared by dissolving food-grade sodium chloride (Iodized table salt, Windsor Salt Company, Canada), sodium hydroxide (technical grade, Anachemia, Canada), or hydrochloric acid (37%wt, ACS grade, Sigma-Aldrich, USA) in in deionized water (>1 µS cm^{-1}). For H_2O_2 decomposition tests, either 35%wt H_2O_2 (technical grade, BDH, USA) or electrogenerated H_2O_2 was used as H_2O_2 source.

3.3.3 Operating and sampling conditions

Three rounds of experiments were conducted to investigate performance of the reactor under various operating conditions as summarized in Table 1: decompositions tests, batch mode operation, and continuous mode operation.

Two sets of decomposition tests were undertaken. For decomposition tests for pH, mixing, and aeration, unreplicated tests were run in acrylic reactor chambers as in Reactor A_2. The stirred test used a magnetic stir bar at ~450 rpm, the aerated test used compressed air fed at ~25 L min^{-1}ute, and the pH-adjusted trials used NaOH and HCl for pH adjustment as described above. 850 mg L^{-1} solutions of commercial H_2O_2 were used as feed. All reactions were run simultaneously to control environmental conditions like temperature and light. For decomposition tests examining the effects of GDE catalyst, tests were performed in triplicate and standard deviation is shown as error bars. The mean R^2 between the three tests is shown, consistently presenting accurate first order kinetics despite variation between trials. The initial H_2O_2 concentrations in the tests were 207 mg L^{-1}, 65 mg L^{-1}, and 39 mg L^{-1}, but no clear correlation between initial concentration and first order rate constant is evident.

For batch mode tests, samples were withdrawn from the reactor with a pipette after plunging at least 3 times (0.5 mL each) and analyzed immediately. New electrolyte was added to make up the volume loss.

Table 5 -Summary of experimental conditions. Only potentials are against Ag|AgCl are listed for brevity.

	Variable studied	Reactor	Electrolyte	Cathode potential	HRT
Batch	Decomposition; pH, mixing, aeration	A_2	Commercial H_2O_2	NA (No electrode)	NA (Batch)
	Decomposition; catalyst	A_3	Electrogenerated H_2O_2	NA (Open circuit)	
	Electrogeneration; potential, separator, GDE orientation, mixing, surface area to volume ratio	A, B	100 mM NaCl	-600 to -1200 mV	
Continuous	pH	B	1 M NaOH, NaCl, HCl	-1000 mV	~0.46
			NaOH, NaCl, HCl diluted to 9.23 mS cm^{-1}		~13
	HRT	B	100 mM NaCl	-1000 mV	0.4 to 13
			1 M NaOH		0.48 to 2.1
	$E_{cathode}$	B	100 mM NaCl	-800 to -1200 mV	~11.2
					~0.6
		C	100 mM NaCl	-400 to -1000 mV	1
	Bioande	B	100 mM $KHCO_3$	~1300 mV (Potentio-stated anode)	35

For continuous tests, electrolysis cells were fed using a digital pump (Masterflex 7523-80, Cole-Parmer, USA) on the influent line. Effluent drained from the effluent line fitting at the top of the reactor and was collected in a sampling vial kept on ice and out of direct light.

Tygon tubing (size 16, Masterflex, Cole-Parmer, USA) was used for influent and effluent. Only the catholyte was run with continuous feeding, anolyte has no continuous flow. Flow rates were quantified by measuring total effluent volume in a graduated cylinder and recording sampling time. Reactors were sampled regularly (for longer HRTs >10 minutes, every 2-5 HRTs; for shorter HRTs <1 minute, every 200-500 HRTs) and samples were analyzed immediately. An exhaustive electrolysis [25] was performed: once effluent H_2O_2 concentration stopped rising consistently (for at least 3 consecutive samples), the experiment was stopped. Chemical analyses were at least conducted in duplicate, and average data was reported.

3.3.4 Analytical methods

H_2O_2 concentration was determined spectrophotometrically (Genesys 10S UV-Vis, Thermo Scientific, USA) using a vanadate method developed by Nogueira et al. [142] but with a 10 times higher sulfuric acid concentration to ensure that strongly alkaline samples were fully acidified. Nominal 35%wt H_2O_2 (technical grade, BDH, USA) standardized against oven-dried potassium permanganate (ACS grade, EMD, Germany) was used as a standard. The calibration curve had an R^2 of 0.98. All electrical signals (current and electrode potential) were measured using EC-Lab software in a BioLogic VSP potentiostat connected to a personal computer. Measurements were logged at 30 second intervals. Sample pH was measured using a benchtop pH meter (Orion Star A111, Thermo Scientific, USA) after calibration with pH 4, 7, and 10 buffers. Conductivity was measured with an Oakton Con 11 Series conductivity/TDS/thermometer (USA). Volumes were measured using a graduated cylinder with 1 mL increments.

3.3.5 Calculations

Coulombic efficiency (CE) for H_2O_2 synthesis was calculated using Equation 39.

$$CE = \frac{n \cdot F \cdot V \cdot C}{Q} \tag{39}$$

where n is the number of electrons transferred per mole H_2O_2 generated (2 mol e^- mol $H_2O_2^{-1}$), F is Faraday's number (96485 C mol e^{-1}), V is the catholyte volume (25 mL for Reactor A, 10 mL for Reactor B, and 3.5 mL for Reactor C), C is the concentration of H_2O_2 measured, and Q is the cumulative charges in reaction time (C).

A mass balance on batch and continuous mode reactors can be derived from an exact model for instantaneous performance:

$$\frac{dC}{dt} = \frac{I_{formation}}{Vn_{formation}F} - \frac{I_{reduction}}{Vn_{reduction}F} - k_{decomposition}C - \frac{C\dot{V}}{V} - \frac{\dot{M_{other}}}{V} \quad (40)$$

$$I_{total} = I_{formation} + I_{reduction} \quad (41)$$

Where C is the concentration of H_2O_2 in the reactor (mol L^{-1}) which is assumed equal to the concentration in the reactor (i.e., fully mixed during batch sampling or continuous flow), dC/dt is the instantaneous rate of concentration change, $I_{formation}$ is the current being used for H_2O_2 formation (A), $n_{formation}$ is 2 moles electrons per mol O_2 reduced to H_2O_2, F is Faraday's number, $I_{reduction}$ is the portion of the current used to reduce H_2O_2 to water (A), $n_{reduction}$ is 2 moles electrons per mole H_2O_2 reduced to H2O, $k_{decomposition}$ is the first order rate constant for non-Faradaic decomposition (i.e. using something other than an electrode as an electron source/donor, s^{-1}), V is the catholyte volume (L), and $\dot{V}$ is flow rate (L s^{-1}; neglected in batch systems), and $\dot{M}$ is the mass flow for all other losses, for example permeation of the membrane, which will be neglected here due to its small importance as shown in past work [42]. $I_{reduction} + I_{formation}$ would be equal to I_{total}, the current measured running through the cell. This model assumes that the only Faradaic reactions possible on the electrode surface are O_2 reduction to H_2O_2 and subsequent reduction to H_2O. This assumption is supported arguments about the mechanism made by others [20], [114] as well as by the present batch data showing near 100% CE at low concentration (Figure 8).

This balance may be approximated as the following for discrete sampling data for batch systems:

$$\frac{dC}{dt} \approx \frac{\Delta C}{\Delta t} = \frac{C_2 - C_1}{t_2 - t_1} = \frac{I_{formation}}{Vn_{formation}F} - \frac{I_{reduction}}{Vn_{reduction}F} - \frac{k_{decomposition}(C_1 + C_2)}{2} \quad (42)$$

$$I_{total} = \frac{Q_2 - Q_1}{t_2 - t_1} \quad (43)$$

In Equations 42 and 43, Q refers to charge (i.e., cumulative current, C) and subscripted variables refer to the beginning (1) and ending (2) of an interval between two measurements. Concentrations are assumed to be fully mixed due to plunging before sampling.

A similar mass balance for the continuous mode reactor can be created assuming that the reactor has reached a pseudo-steady state:

$$C\dot{V} = \frac{I_{formation}}{n_{formation}F} - \frac{I_{reduction}}{n_{reduction}F} - k_{decomposition}CV \quad (44)$$

Equation 44 may again be used to give the average current throughout the sampling interval.

3.4 Results and discussion

3.4.1 Batch tests

3.4.1.1 Decomposition tests

In an electrochemical cell, H_2O_2 may be destroyed by Faradaic processes at electrodes as well as non-Faradaic processes catalyzed by trace metals in solution, container walls, hydroperoxide anions [27], light [143], or, as shown here, electrodes themselves (alongside Faradaic reactions). In order to quantify losses due to non-Faradaic decomposition and test factors affecting decomposition, the effects of pH, stirring, aeration, and catalyst presence were collected and used to estimate first order rate laws under each condition ($d[H_2O_2]/dt=k[H_2O_2]$; t being time, k being first order rate constant) are shown in Figure 6.

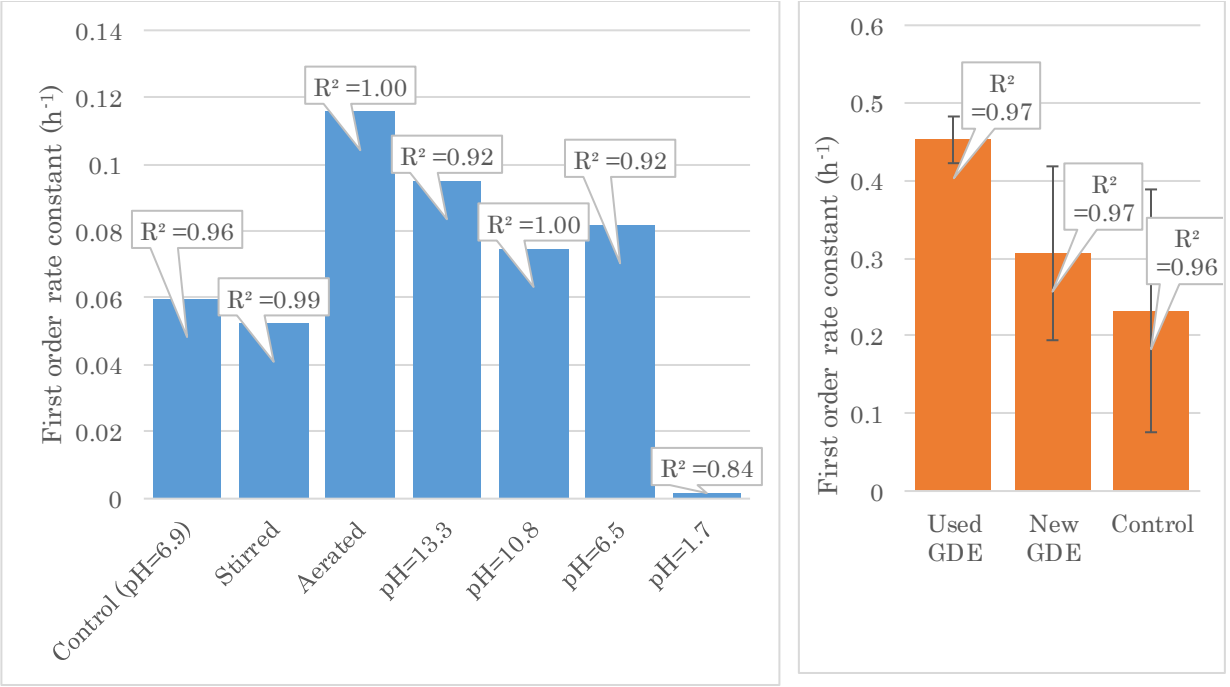

a b

Figure 6 -a: Effect of pH, mixing, and aeration on non-Faradaic decomposition with no electrodes or catalysts present.
b: Effect of GDE on H_2O_2 decomposition.

Figure 6a shows results for tests using no catalyst and a feed of commercially-available H_2O_2. It can be seen that stirring does not significantly affect decomposition, though aeration seems

to have a great effect despite the vapour pressure of H_2O_2 being much smaller than water (0.67 Pa [144] versus 4.24 Pa at 303 K [83]). Excessive aeration has also been shown to decrease H_2O_2 concentration by others [27], [38]. pH appears to have little effect through neutral and alkaline pH but at low pH decomposition is sharply reduced. This is due to the ability of H_2O_2's deprotonated ion, HO_2^- (pK_a=11.65 [86]), to catalyze decomposition at alkaline pH [121]. Young et al. [36] had similar results showing greater stability at acidic pH in their H_2O_2 stability testing.

Figure 6b shows results for tests using electrogenerated H_2O_2 free of additives that might hinder catalysis of decomposition. Since the GDE is functionalized by use and exposure to H_2O_2, new and used GDEs were compared with a control with no catalyst present. It can be seen that the used GDE has the fastest kinetics for H_2O_2 decomposition, while the new GDE and control have similar results. The difference between new and used GDEs is visible in low scan rate cyclic voltammetry shown below.

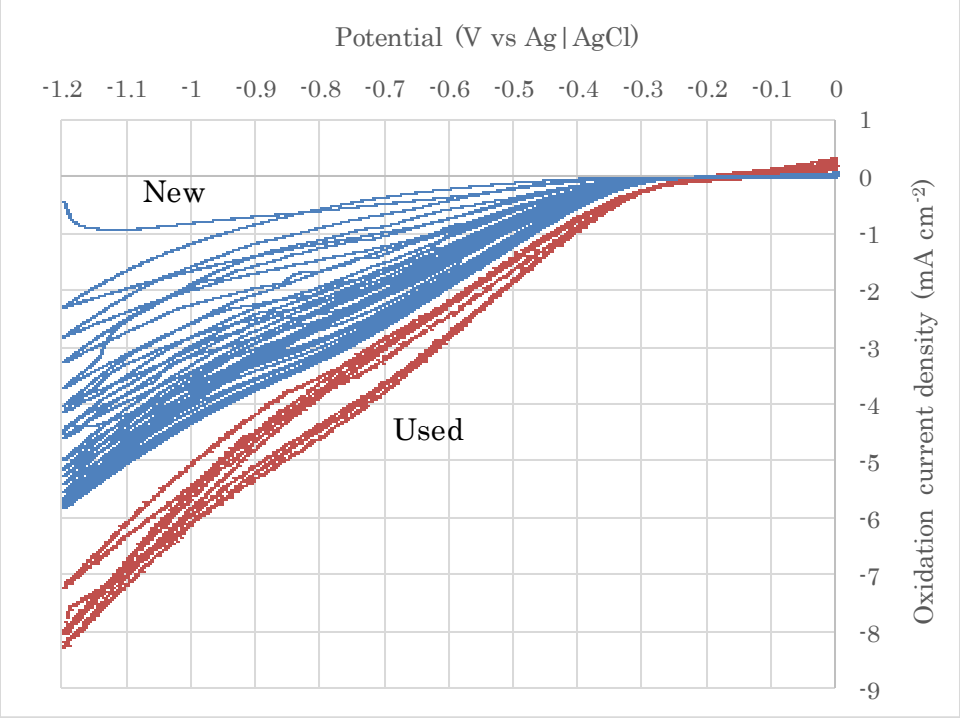

Figure 7 - Low scan cyclic voltammetry plots for used and new cathodes.
Note: New cathodes are as-received from the supplier with no pretreatment; the used cathode had been used for electrolysis of continuously flowing (HRT=1 minute) 100 mM NaCl at -1000 mV vs Ag|AgCl (-777 mV vs SHE) until current density stabilized, about 12 hours and 400 C cm^{-2}. For both tests, scan rate was 10 mV s^{-1}, scans started at 0 mV, measurements were logged during the last 50% of a voltage step. 10 cycles the used cathode are shown and 20 are used for the new cathode (the new cathode had not reached stable performance by the end of testing). Tests were performed in Reactor A.

3.4.1.2 Electrogeneration tests

Batch tests were initially performed to easily assess kinetics of the H_2O_2 production reaction. A typical batch test has characteristics as shown in Figure 8. Typically, CE is close to 100% at the beginning while H_2O_2 concentration is low, and it declines to approach 0% as H_2O_2 accumulates. pH changes in the first few minutes of the reaction to values usually <3 on the anode and >11 on the cathode, then remains relatively stable - these are close to values reported in other dual-chamber studies [35].

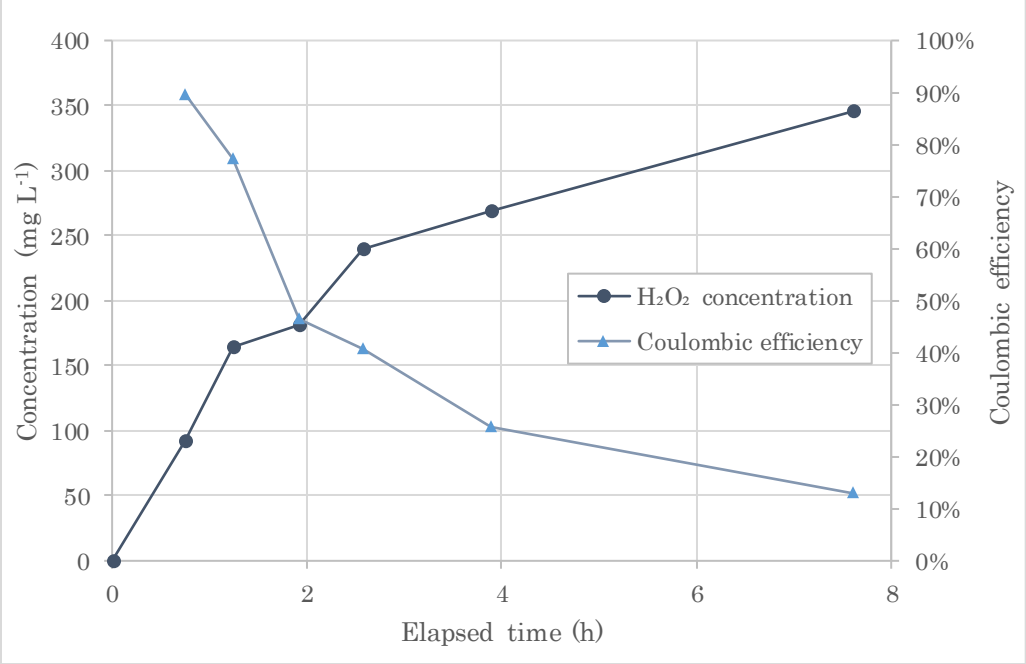

Figure 8 - Typical H_2O_2 batch test result. Reactor used was Reactor A with 0.1 M NaCl as electrolyte and -800 mV vs Ag|AgCl (-577 mV vs SHE) applied cathode potential.

Although many conditions were tested, only the highest performing batch results are discussed in the present work; these are plotted alongside continuous test results in Figure 7 and were obtained using high cathode polarization (-1200 mV vs Ag|AgCl, -977 vs SHE) and a high surface area to volume ratio (Reactor B). Over the batch, non-Faradaic losses become more important and dominate as the principle mechanism leading to low CE based on modelling, further examined in Section 3.4.4. Moving forward to continuous mode testing, it was theorized that if H_2O_2 concentration is the largest factor affecting CE, performance attained during batch tests could be attained continuously by maintaining conditions of that point in the batch trajectory by choosing optimum HRT and cathode potential.

3.4.2 Continuous tests

Full summaries of continuous test results are included in Appendix A.

3.4.2.1 Effect of HRT

Different HRTs were tested in alkaline and neutral medium, all under a cathode potential of -1000 mV vs Ag|AgCl (-778 mV vs SHE) in Reactor B. Results are summarized in Figure 9.

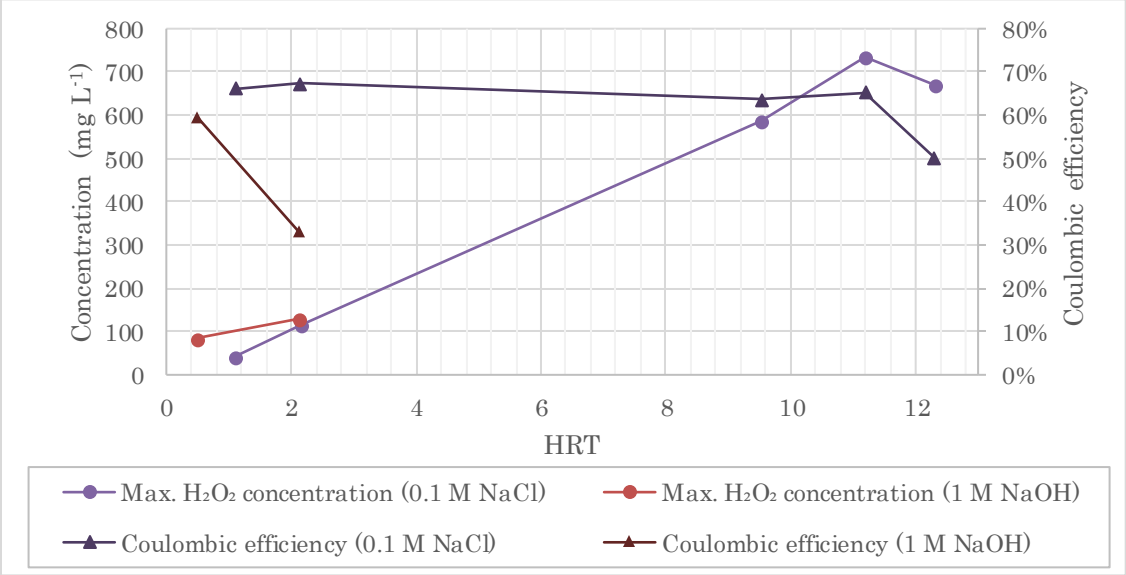

Figure 9 - Effect of HRT in Reactor B. All reactors used a cathode potential of -1000 mV vs Ag|AgCl (-778 mV vs SHE).

Firstly, a few trends are immediately visible in the NaCl series: the fairly constant coulombic efficiency until the higher HRT trials, the positive linear correlation between HRT and H_2O_2 concentration, and the positive linear correlation between HRT, current density, and H_2O_2 concentration. Current density across HRTs also rose linearly across HRTs, from 1.55-2.89 mA cm^{-2}. These trials show that under the conditions tested, higher HRTs drew more current and produced more H_2O_2 without sacrificing CE.

These trends contrast what can be observed from the NaOH series; which shows a negative correlation between CE and HRT. Current density increased from 4.71 and 6.39 mA cm^{-2}. An additional NaOH trial (data not plotted) under the same conditions but at -1200 mV vs Ag|AgCl (-977 mV vs SHE) and 2.0 min HRT, attained a similar CE (37%) with a much higher H_2O_2 concentration (274.27 mg L^{-1} vs 129.28 mg L^{-1}).

These results show that although concentration increases as HRT is prolonged, this does not always result in the CE reduction that might be expected from batch tests. In this case, the

increased current in the NaOH trials is associated with 13% more Faradaic H_2O_2 reduction compared to the NaCl trials. This decreased CE with increased current density is discussed further in Section 3.4.2.3.

3.4.2.2 Effect of pH

In order to further investigate pH effects without having major differences in electrolyte strength, tests were performed in equal concentrations acidic, neutral, and alkaline media, and then in lower concentrations of alkaline and neutral media that were adjusted to have equal conductivity empirically.

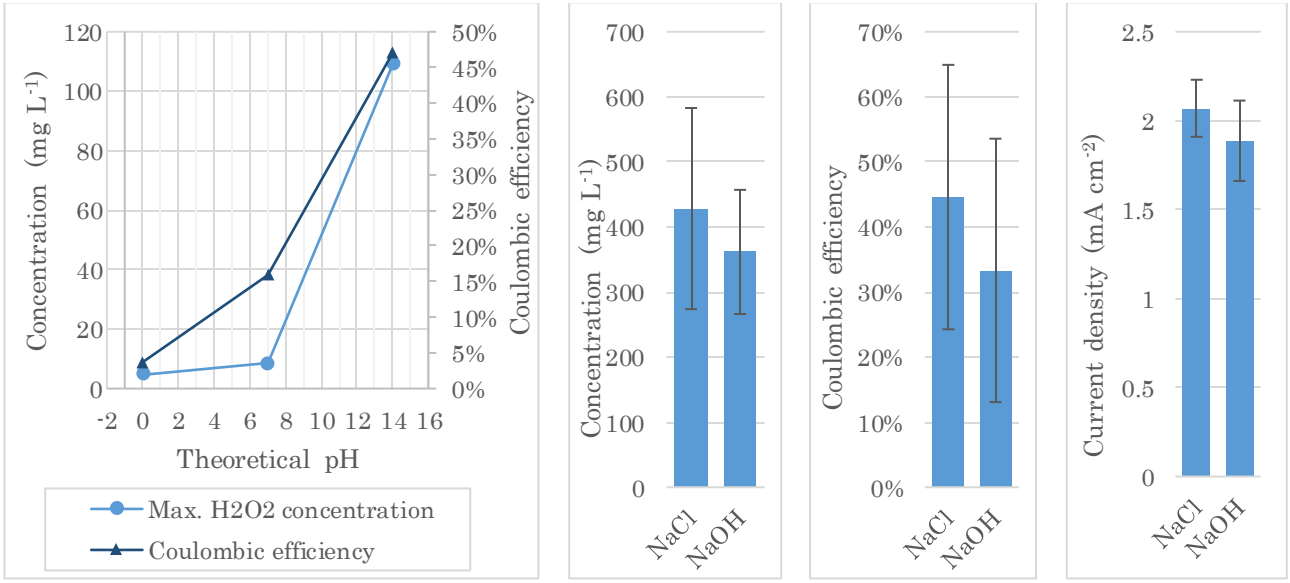

Figure 10 - a: Effect of pH in 1 M HCl, NaCl, and NaOH solutions in Reactor B.
b: Effect of electrolyte in conductivity-controlled trials.
Note: In *a*, All reactors used a cathode potential of -1000 mV vs Ag|AgCl (-778 mV vs SHE) and those in the connected series use a nominal HRT of 0.48 (+/=0.1 minutes). In *b*, For all trials, a 13 minute HRT was used (+/- 1.5 minutes) along with a cathode potential of -1000 mV vs Ag|AgCl (-777 mV vs SHE). Error bars show the standard deviations.

In the first set of trials (Figure 10a), concentration and CE rise together, unlike what was observed in batch results where high concentration led to increased cathodic reduction and lowered CE. Either the pH or the counterions in the electrolyte change the nature of the reaction. Results here agree with the many studies that report alkaline media is preferred for H_2O_2 production [15], [16], [22], [32]. The current densities from acidic to neutral across the 1 M, 0.48 minute HRT trials are -8.47, -3.24, and -10.54 mA cm^{-2}, indicating that at least the most extreme pH trials are comparable.

Additionally, a weaker acid, 0.1 M HCl, trial showed considerable improvement over the 1 M trial for both H_2O_2 concentration and CE. The current density in these trials was 2.72 mA cm^{-2}, one third of that in the 1 M HCl trial. This lower current density may explain part of the difference, with the pH difference and associated reaction kinetics explaining part as well.

In a second set of trials looking at pH (Figure 10b), electrolytes were adjusted to have equal conductivities on order to be considered more comparably. Two trials using NaCl and four repetitions using NaOH were used, the latter being more frequent due to higher variability. In all of the trials, NaCl slightly outperformed NaOH, despite alkaline medium having been widely reputed as more favourable for H_2O_2 electrogeneration. However, due to the high variability of the data it can only be concluded that neither is significantly preferable to the other. Slightly lower CE to previous results using 1 M electrolytes was seen, while H_2O_2 concentration was increased fourfold by prolonging HRT; this agrees with what was previously studied for HRT effect. Operationally, this suggests that pH adjustment from circumneutral may not be required in dilute wastewaters, despite the stronger trends seen using stronger electrolytes.

3.4.2.3 Effect of cathode potential and current density

The effect of cathode potential was tested under various other conditions. The effect of cathode potential on current density is shown Figure 11b while Figure 11a uses current density as an x-axis and summarizes reactor performance.

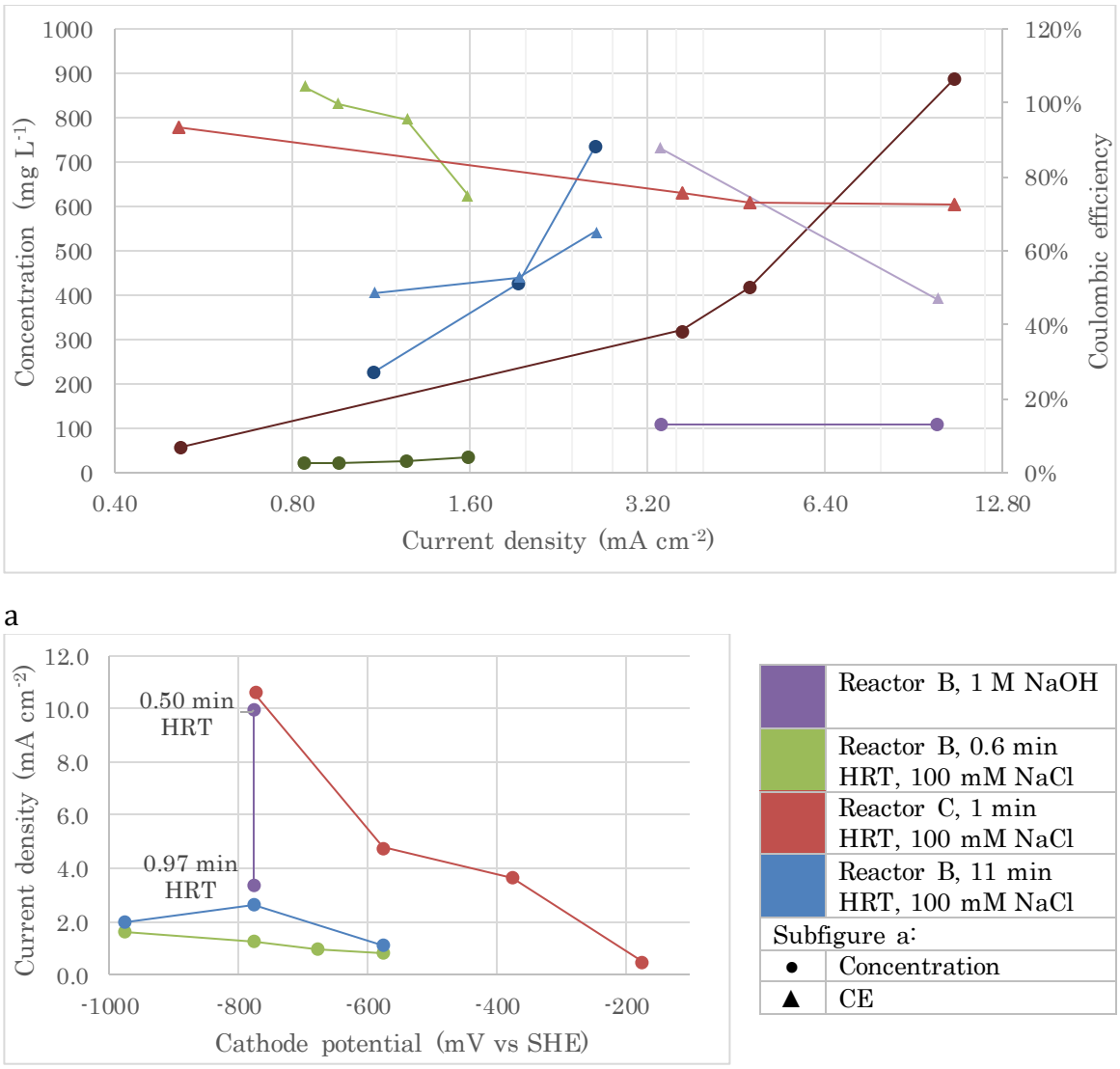

Figure 11 - Effect of cathode potential on current density and resulting reactor performance in Reactor B under 2 HRTs and 2 electrolytes and in Reactor C.

First, HRT was varied while other conditions were held constant at 100 mM NaCl in Reactor B. An obvious difference between curves is the difference between concentration values, with longer HRT trials resulting in more H_2O_2 accumulation over all cathode potentials, as has been seen previously. Conversely, the 11 minute HRT trial has CE values that are under all the CE values for the 0.6 minute trial. These general trends of HRT raising concentration and lowering CE were previously observed in Figure 9.

For both HRTs, maximum H_2O_2 concentration can be seen to generally increase with current density (cathode potential decrease) in both trials. The trend in CE however is that it rises as cathode potential rises during the 11 minute HRT trial while it falls during the 0.6 minute

HRT trial. Thus current density has been demonstrated to have opposite effects at low HRT, when mixing would be increased, than at high HRT in an H_2O_2-rich boundary layer.

In other testing using 1 M NaOH at a constant cathode potential of -777 mV vs SHE (-1000 mV vs Ag|AgCl), current density was modulated by changing HRT from 0.5 to 0.97 minutes. Resulting current densities of 3.38 and 9.97 mA cm^{-2} resulted in a nearly constant H_2O_2 concentration at 109-110 mg L^{-1} but CE was negatively correlated to current density, dropping from 88% to 47%. Again, in lower concentrations of H_2O_2, CE is seen to correlate negatively with current density.

Lastly, several cathode potentials were tested in Reactor C (surface area to volume ratio = 10.4 cm^{-1} versus 3.6 cm^{-1} in Reactor B) using 100 mM NaCl again and an HRT of 1 minute. Looking first at the current density data, this trial achieved much higher current densities at the same potential as other trials using the same electrolyte and similar HRT. This could be partly due to better kinetics due to improved fluid shear across the GDE surface. Because the cathode is potentiostated, this difference is not due to lower internal resistance in the smaller reactor, in fact since the T-junction fitting moves the reference electrode further from the cathode and increases uncompensated resistance, the actual working electrode potential is slightly less than in trials using Reactor B. The increased current density leads to increased H_2O_2 production leading to highest H_2O_2 concentration attained in the present work; 887.4 mg L^{-1} at 1 minute HRT and -1000 mV vs Ag|AgCl (-777 mV vs SHE) cathode potential. Current density and H_2O_2 concentration are correlated perfectly, with an R^2 of 1.000 ($p=7.02x10^{-6}$). CE increases as cathode potential is increased, however, less elastically than observed during other trials. Model results clearly show that Faradaic losses relate strongly to cathode potential in Section 3.4.4.2.

3.4.2.4 Bioanode

One trial was run using a bioanode consisting of a carbon felt, already colonized with anode respiring bacteria (ARB) from an existing reactor. In this trial, the anode was potentiostated to -400 mV vs Ag|Agcl (-177 mV vs SHE) to maintain a slight overpotential for acetate oxidation at the anode. The cathode potential was allowed to vary to satisfy the current demanded by the anode; the average cathode potential applied was around -1300 mV vs Ag|AgCl. The reactor used was Reactor B. A long HRT of 35.59 minutes was used. 302.65 mg L^{-1} H_2O_2 were produced continuously at a current density was 1.26 mA cm^{-2} with a

coulombic efficiency of 19.5%, higher than the 0.25 mA cm^{-2} said to be biologically relevant in other work [42]. Although the results are worse than other trials, this result shows that the current density from the bioanode is compatible with what has been being produced by the GDE, and with some adjustment of relative sizes, a bioanode could feasibly be used to supply electrons for any of the cathode setups examined.

3.4.3 Aggregate analysis

In addition to the individual experiments analyzed in detail in the preceding sections, it is also useful to examine the data in aggregate. These analyses compare trials conducted under different reaction conditions but offer some insights nonetheless. Firstly Figure 12 plots the global data using coulombic efficiency and H_2O_2 concentration as axes, thus illustrating the tradeoff curve frequently seen in individual trials. This tradeoff has also been noted explicitly as the principle challenge in peroxide electrogeneration over a planar cathode such a GDE in reviews [106]. It should be noted that although many points do not lie along the curve defining the maximum performance, even they produce H_2O_2 at concentrations that would be useful for applications such advanced oxidation via UV $h^{-1}{}_2O_2$ (20-70 mg L^{-1}) [70], Fenton processes (50-250 mg L^{-1}) [19] or water treatment membrane cleansing (~2000 mg L^{-1}) [35]. The inclusion of selected batch performance data indicates that in both the batch and continuous reactors, the same limitations were present.

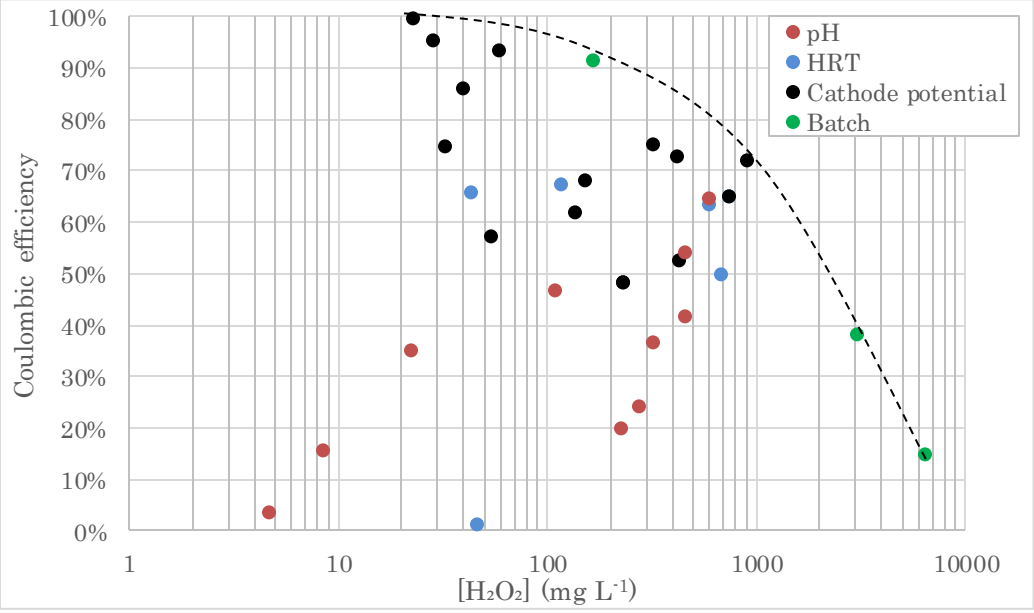

Figure 12 - Coulombic efficiency/ H_2O_2 concentration tradeoff curve for global data.
Note: Abbreviated section headings indicate which continuous mode experiments plotted data is taken from as well as the top-performing batch data.

3.4.4 Mass balance model

The mass balance model described in Section 3.3.5 was applied to both batch and continuous data to elucidate the importance of reaction pathways inside the reactor and inform reactor design. To our knowledge, this is the first time a mass balance model has been applied quantify mass flows in an H_2O_2 electrogeneration reactor. Aside from the direct measurements of concentrations, volumes, and current, the model requires the input of a first order rate constant for non-Faradaic processes. There exists uncertainty toward the kinetics of the reduction of an H_2O_2 molecule close to the surface of a polarized election; whether an appreciable portion could be catalyzed to decompose non-Faradaically, as found in Section 3.4.1.1, or whether the thermodynamic advantage of using the polarized electrode would divert the majority of H_2O_2 to Faradaic reduction to water. Thus the true figure for non-Faradaic decomposition is most likely between 0.23 h^{-1} measured for a reactor with no electrodes present and 0.45 h^{-1} measured for a reactor with a used GDE present. Both of these extremes have been modelled.

3.4.4.1 Batch tests

As already introduced, unless otherwise indicated, all batch testing was done in unstirred reactors that were only mixed before sampling. In Reactor A batches, Faradaic reduction dominates at the beginning of batches, but non-Faradaic processes become more important as concentrations accumulate. In models using the higher $k_{decomposition}$, it becomes dominant around 150-350 mg L^{-1} and reach as high as 40 times greater rates, while in those using the lower $k_{decomposition}$ Faradaic processes remain dominant, but non-Faradaic processes still take up to a third of H_2O_2 out. In Reactor B, which has a higher surface area to volume ratio and more quickly accumulates H_2O_2, the model broke down because non-Faradaic processes were being over-estimated using either of the two $k_{decomposition}$ values. This output suggests that non-Faradaic processes actually reduce H_2O_2 before Faradaic processes can, at least in a reactor with a relatively low amount of bulk fluid (surface area to volume ratio of 3.6 cm^{-1}). Thought more work is required to validate the model, these results inform both the development of validation tests and design of improved reactors.

3.4.4.2 Continuous tests

Most of the continuous reactor experiments continued to use Reactor B, but with better mixing induced by feeding. In most of the continuous mode experiments, non-Faradaic

decomposition was very low; below 1% when using either $k_{decomposition,}$ and losses generally scaled nearly linearly with concentration increase. Figure 13 plots both Faradaic and non-Faradaic decomposition against effluent H_2O_2 concentration from the model using the lower $k_{decomposition}$. When using the higher $k_{decomposition}$ value, Figure 13a shares the same shape but average losses are 95% greater, which corresponds closely to its 96% higher $k_{decomposition}$ value, while Figure 13b is visually indistinguishable.

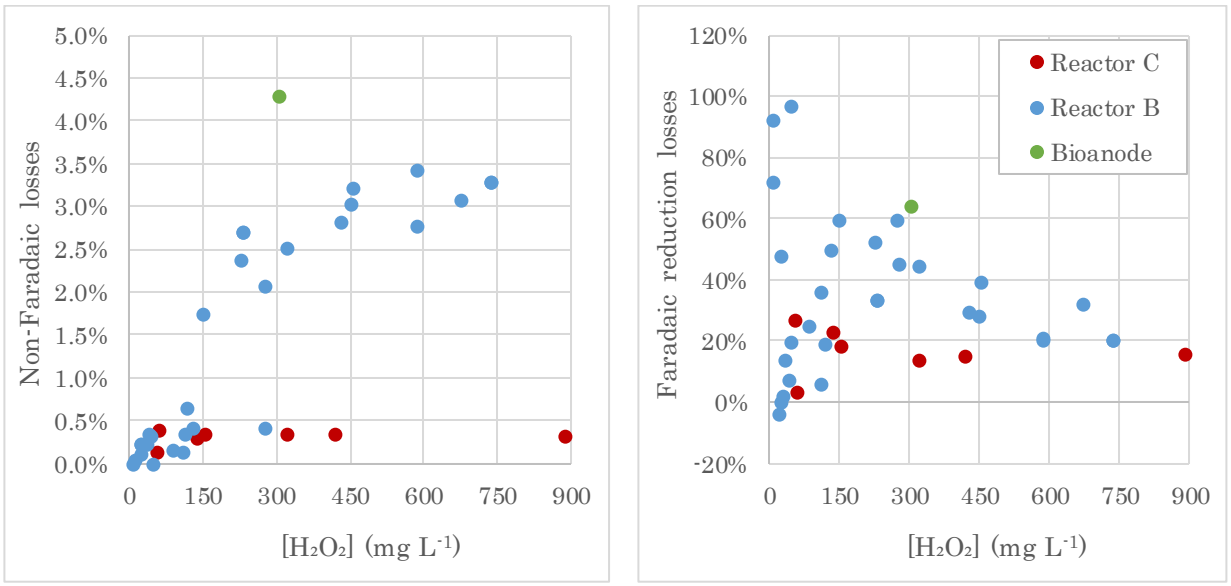

a b

Figure 13 - a: Relationship between modelled (a) non-Faradaic losses and (b) Faradaic losses as a percent of total produced H_2O_2 and effluent H_2O_2 concentration.
Note: Model shown used $k_{decomposition}$=0.23 h^{-1}, the value for decomposition in the bulk fluid and on container walls but not over an unpolarised electrode.

The strong dependence (R^2=0.79, p=7x10^{-11}) of the non-Faradaic losses in Reactor B experiments indicates that accumulation of H_2O_2 in the bulk leads to concomitant bulk losses. This disagrees with the analysis from the unmixed batch reactions, which suggested that Faradaic losses probably dominate any real non-Faradaic decomposition by reducing H_2O_2 before it could diffuse away. It is also notable that experiments carried out in Reactor C both have lower non-Faradaic losses (due to having less dead space and shorter HRT) and that the non-Faradaic losses are inelastic with respect to the effluent H_2O_2 concentration. The bioanode experiment can be seen to be underperforming abiotic experiments. The data for Faradaic losses does not show a clear correlation with concentration. The narrowing spread of the data is most likely due to the fewer number of points at higher concentrations. This shows that Faradaic losses don't depend on effluent concentrations but are controlled by

other factors, which makes sense because Faradaic reduction must act on adsorbed species on the electrode surface. Reactor C can again be seen to outperform other experiments.

To investigate another probable factor affecting Faradaic losses, data from only Reactor C was examined with respect to cathode potential, shown in Figure 14. This figure shows a dependence of Faradaic losses on cathode potential, with a lower potential, higher overpotential cathode causing much greater Faradaic losses. Polarizing the cathode 600 mV below the highest potential testes of -400 mV vs Ag|AgCl (-177 mV vs SHE) led to a fivefold increase in Faradaic losses, while non-Faradaic losses were fairly constant and much smaller in absolute terms. Although a more polarized cathode has more electrostatic repulsion, it also has more thermodynamic potential for Faradaic reduction. Further testing may be able to identify an optimum balance between these opposing factors.

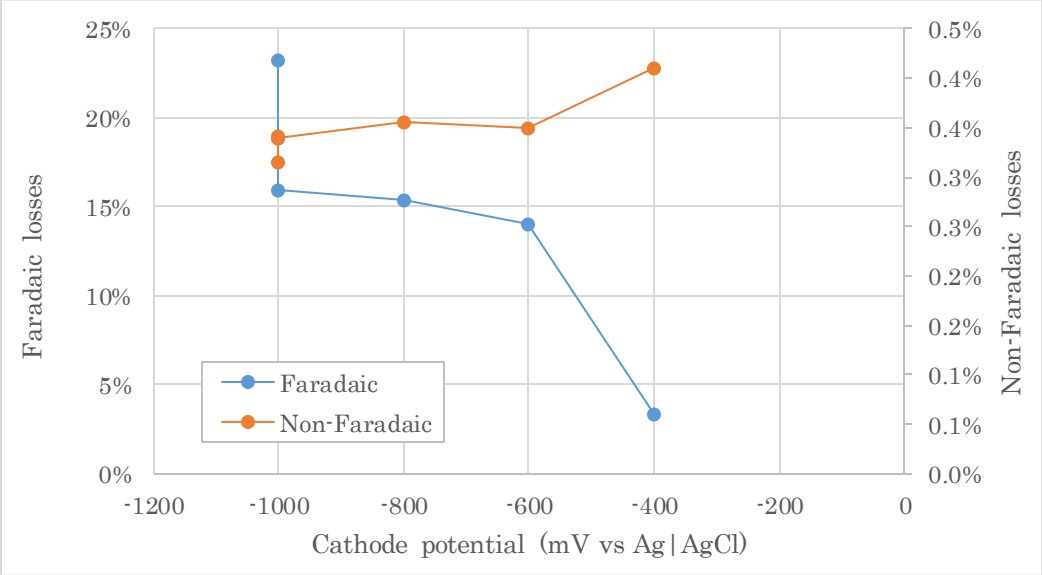

Figure 14 - Effect of cathode potential on model results for Faradaic and non-Faradaic losses in Reactor C

In general high values for Faradaic losses underline the need to control chemical and physical processes on the electrode itself through design aspects such as catalyst pretreatment, fluid shear, electrostatic repulsion, etc. to lower Faradaic losses; non-Faradaic losses are already relatively low and can be addressed with attention to surface area to volume ratio and HRT as shown by Reactor C.

Additionally, it should be noted that the continuous mode modelling appears to hold for most cases due to the better mixing and thus more valid assumptions as compared to the batch analysis. The model did break down once, for a trial using Reactor B, -800 mV vs Ag|AgCl

cathode potential (-577 mV vs SHE) at a 0.6 minute HRT in 100 mM NaCl; This trial had a high CE at 73.2% and was modelled to lose only 0.2% of H_2O_2 non-Faradaically. Still, this loss was high enough to require a negative Faradaic loss to balance the equation, the same as the result in the batch analysis. As these experimental conditions are similar to others tested that did not fail, it cannot be further speculated on but it is recommended in general to validate the mass balance model with further testing.

3.5 Conclusions

The present work has comprehensively examined variables that affect H_2O_2 production in a divided electrolysis cell. Firstly, we confirmed that electrogenerated H_2O_2 is best stored at acidic pH, that excessive aeration promotes decomposition, that stirring does not promote decomposition, and that carbon black catalyzes H_2O_2 decomposition in its virgin state and even more so once functionalized by being subjected to cathodic polarization and H_2O_2. We adopt the first order rate constants of 0.45 h^{-1} for H_2O_2 in contact with functionalized carbon black to make liberal estimates of bulk decomposition and estimate uncatalyzed decomposition to occur at 0.23 h^{-1}.

Secondly we showed that although the batch configurations used by most researchers exhibit declining CE as batch life continues and H_2O_2 concentration increases, this result is not reproduced in continuous mode reactors running equivalent HRTs. In particular, a moderate CE of 60-70% may be maintained across HRT from 1-11 hours, producing H_2O_2 up to 730 mg L^{-1} if current density is maintained below 3 mA cm^{-2} in a neutral electrolyte. We confirm that alkaline electrolyte appears to favour H_2O_2 production, but that since neutral feeds quickly alkalize, pH adjustment may not be necessary, especially at scale. Decreasing cathode potential leading to increased current density is shown to deteriorate CE in most cases due to higher rates of Faradaic reduction. Our mass balance model is the first we know of to attempt to quantify mass flows in a H_2O_2-producing electrochemical cell.

Lastly, we show that the cathodes tested operate at a comparable current density to that produced by bioanodes and that the results produced may be able to be reproduced in a microbial system with some modifications, for example, to control pH to circumneutral.

4 *In situ* oxidation of S(IV) in a single chamber electrolysis cell via cathodic hydrogen peroxide electrogeneration and anodic oxidation

4.1 Overview

A single chamber electrolysis cell equipped with commercially available graphite anode and carbon black-based gas diffusion electrode (GDE) cathode is applied for the oxidation of S(IV) in solutions of sodium sulfite and bisulfite to S(VI) in alkaline (pH=9.5) conditions. The main mechanisms responsible for S(IV) removal are oxidation via cathodically electrogenerated H_2O_2 and direct anodic oxidation on the electrode surface. Due to removal processes at both electrodes, coulombic efficiency (CE) exceeds 100%. The most complete removal obtained was 98.9% at 61.1% CE in a reactor amended with NaCl to improve conductivity, while 86.3% at 79.4% CE was achieved in compact reactor with a 2.1 mm spacing between electrodes. Under lower removal rates, CE up to 200% was observed. It is found that pH and cathode potential do not affect reactor performance under conditions tested.

4.2 Introduction

Sulfur (IV), present variously as sulfur dioxide, sulfite, bisulfite, and metabisulfite, is an important pollutant that may be present in industrial wastewaters and in air emissions. Although it is not acutely harmful in aquatic environments and is not regulated in wastewater effluent in Canada [145], it poses environmental and health threats as a respiratory irritant, smog and acid rain precursor and is set to be subject annual ambient air quality in the low part per billion by 2020 [146], [147]. Fugitive S(IV) from processes like sulfuric acid manufacture may also be captured and recovered to make industrial process more economical.

Oxidation of S(IV) by diatomic oxygen has been studied in the context of atmospheric science [148]-[151] (as it is the most important oxidant of S(IV) in the troposphere [152]), emissions scrubbing [153], [154], and oxygen scavenging for corrosion control in boilers [155], but these require expensive catalysts or high temperatures to have fast enough kinetics to be useful. Hydrogen peroxide (H_2O_2) is a much better oxidant, is environmentally-friendly, and is widely used across many industrial sectors [139]. It has been studied previously, namely for chemisorption in emissions scrubbing [156]-[160], in studies in acid solutions pertinent to atmospheric sciences [161]-[166], and direct [167], [168] or mediated [169] oxidation on an

anode surfaces, especially for the hybrid sulfur (Westinghouse) cycle for hydrogen generation [170].

The majority of industrially used H_2O_2 is synthesized and concentrated offsite and transported to its point of use, incurring costs for delivery and storage, but promising options exist for H_2O_2 production via electrogeneration in fuel or electrolysis cells [13]. Electrogenerated H_2O_2 currently enjoys some use in the pulp and paper industry [13] but there remains a huge and growing market for H_2O_2 [141] that electrogeneration may be able to meet the needs of for certain users and applications.

Electrogeneration of H_2O_2 has been studied heavily in both chemical electrolysis systems [15]-[32] and H_2O_2-producing microbial electrochemical cells (MECs) and microbial fuel cells (MFCs) [33]-[42]. Although a work by Yamanaka et al. [16], [22] has produced concentrated streams up to 7% directly, the majority of work uses less harsh and expensive conditions and produces appreciable but dilute amounts of H_2O_2, typically a few hundred to a few thousand mg L^{-1}, with the maximum reviewed of 9.67 g L^{-1} [35]. These systems faced challenges in generating high concentrations and maintaining high coulombic efficiency (CE). This tradeoff has also been noted explicitly as the principle challenge in peroxide electrogeneration over a planar cathode such a gas diffusion electrode (the most commonly used and effective type for H_2O_2 electrogeneration) in reviews [106].

One strategy that has been applied to overcome limitations in the efficiency of H_2O_2 production in electrochemical cells has been to combine generation and reaction of H_2O_2 in a single system, using H_2O_2 for an intended reaction before it is consumed by unintended reactions, such as bulk decomposition, anodic oxidation, or cathodic reduction. This *in situ* treatment strategy has been principally investigated in systems what use an advanced oxidation process, either UV [23], electro-Fenton[15], [44]–[47], bioelectro-Fenton [48]–[61], or photoelectro-Fenton[21], [62]–[65]. Only limited work examines direct use of H_2O_2, which does not require additional catalysts or power for UV lamps: for example a Shen at al. [67] into the possibility of coupling anodic and cathodic oxidation to treat dye and Al-Shafei's [66] use of direct oxidation by H_2O_2 in a divided cell for treatment of organosulfur compounds in petroleum. In practice none of these technologies appear to have been scaled-up and commercialized; for example. in the pulp and paper industry, one of the largest H_2O_2 users,

technologies reviewed for the industry do not include *in situ* reaction [14] but instead focus on generation and *ex situ* use.

Though many studies focussed on cathodic removal processes, anodic oxidation may also be used in electrochemical cells in conjunction with H_2O_2 [62]–[64], [66], [67], [138] and carries the possibility of raising coulombic efficiencies to 200% [71]. Direct anodic oxidation of S(IV) specifically has been studied on metallic and carbon-based anodes [171], showing no catalytic activity in concentrated sulfuric acid [170] but working in in dilute acid-alkaline solutions [171] over graphite anodes. Another possible useful anodic oxidation is water electrolysis producing oxygen, which may in turn be applied at the cathode for H_2O_2 synthesis [14] or participate in other reactions. However, as discussed, there are slow kinetics for S(IV) oxidation with O_2, limiting this potential anodic function.

The present work addresses the barriers to uptake of H_2O_2 electrogeneration for pollution control, namely higher operating costs for systems requiring pH control (e.g. Fenton systems), separation of homogenous catalysts, expensive heterogeneous catalysts, and expensive separators. Here, we study the efficacy of a single-chamber H_2O_2 electrogeneration system, treating S(IV) as a model contaminant, using commercially available, unmodified graphite plate and gas diffusion electrodes.

4.3 Materials and methods

4.3.1 Electrolysis cell

A single-chamber electrolysis cell was constructed of polypropylene (McMaster-Carr, USA). The reactor consisted of a bored-out block, leaving a cylindrical space as the reaction chamber (6.35 cm diameter) with the anode completely covering one side and the cathode completely covering the other (projected surface area of 31.7 cm^2 each). Inlet and outlet fittings were installed on opposite sides of the reactor, a hole was drilled in the top to snugly hold a Ag|AgCl reference electrode (MF 2052, BASI, USA) and a 1 mm diameter hole was left in the top to allow pressure equalization. During most testing, a 4.45 cm thick reaction chamber (Reactor A) was used giving an internal volume of 63.0 mL. Viton gaskets (McMaster-Carr, USA) of 2.1 mm thickness were placed between the reaction chamber and the electrodes. A commercially-available gas diffusion electrode (GDE; GDS 2230, AvCarb, USA) was used as a cathode. Its nominal thickness was 275 um and its construction consisted of a carbon paper backing with a carbon black/ polytetrafluoroethylene (PTFE) mesoporous layer. An isomolded

graphite plate was used as an anode (203101, Fuel Cell Earth, USA). Tubing was Norprene or Tygon (size 16, Masterflex, Cole-Parmer, USA) and a digital pump (Masterflex 7523-80, Cole-Parmer, USA) with two pump heads mounted was used to pump influent and effluent synchronously. S(IV) feed was kept in a gastight 1 L glass bottle with an air-filled 1.6 L gas bag (Chemware® Tedlar® PVF Gas Sampling Bag, Saint-Gobain Performance Plastics, France) to minimize volatilization losses of S(IV). Effluent was pumped through filtration cartridges (0.45 followed by 0.20 µm nylon syringe filters, 25 mm diameter, MicroLiter, USA) to remove any particles that might interfere with spectrophotometric analyses and collected in 60 mL syringes (Biocoat, BD, USA) to prevent volatilization of S(IV) in the effluent, or open vials when S(IV)-free feed was being used.

In some trials, mixing was applied by circulation through a secondary peristaltic pump (SVP1, Stenner, USA) attached to the influent and effluent fittings with T-junctions. The recirculation rate applied was 25 mL min^{-1}, equivalent to 0.40 reactor volumes per minute in Reactor A.

Additional tests investigating the effect of using a higher surface area to volume ratio reactor used a modified reactor, Reactor B. This reactor omitted the HDPE reaction chamber and used only a Viton gasket as the reaction chamber; this required moving the inlet and outlet to the HDPE end plate behind the anode and drilling holes to allow circulation as well as using an HDPE plastic mesh as a spacer and turbulence promoter between the electrodes. This gave an internal volume of 10.0 mL.

A second modified reactor, Reactor C, was constructed to isolate cathodic and anodic reactions by using a dual chamber design with a separator. Reactor C also provided another data point alongside Reactors A and B to study surface area to volume ratio when its separator was removed, leaving a larger volume reaction chamber. Reactor C consisted of two of the 4.45 cm thick reaction chambers used in the initial reactor with a cation exchange membrane (CEM; CMI 7000, Membranes International Inc., USA) separating anode and cathode chambers, with all other specifications identical.

Figure 15 below shows the construction of each reactor and the full experimental setup.

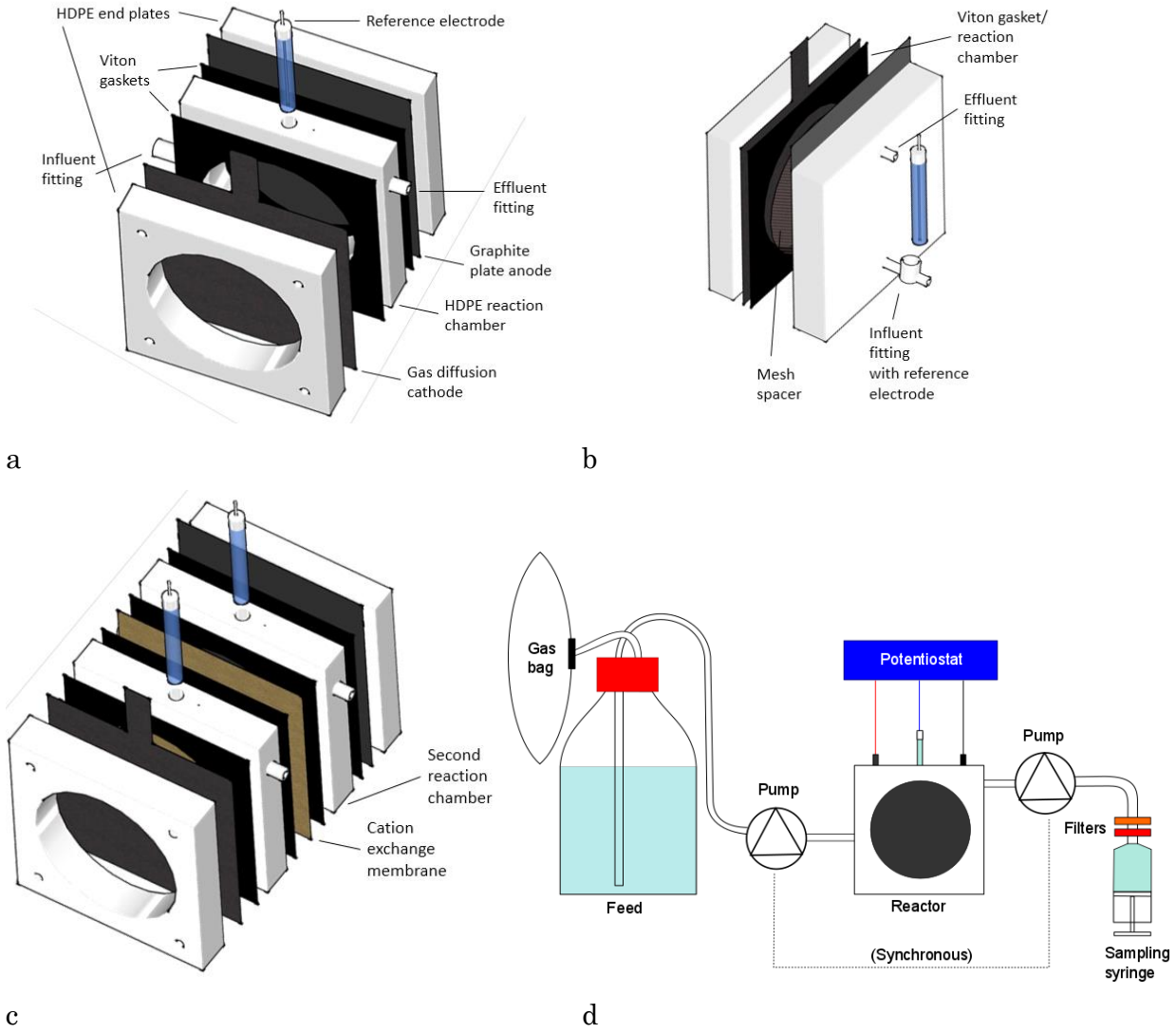

Figure 15 - Reactor construction and experimental setup. A, B, and C show Reactors A. B and C, respectively; D shows the experimental setup.
Note: An open vial kept on ice and out of direct light was used instead of the shown syringe during initial control tests, as described in Section 4.3.2.

A glassy carbon anode (T10-grade, SPI Supplies, USA) was initially tested, but it exhibited significant exfoliation on the face facing the cathode, exhibited unstable performance, and turned electrolyte a dark yellow colour, suspected to be due the formation of graphite oxides. The graphite plate used in all experiments reported here also showed some degree of degradation visible as a yellowing of fluid and presence of graphite particles in the bottom of the reactor, but exhibited stable performance nonetheless.

4.3.2 Reactor operation, sampling, and data processing

The reactor was operated in continuous mode; at time zero the influent/effluent pump was started and, except for a set of control trials with no electrical input, voltage was applied across the electrodes by the potentiostat and electrical data acquisition started. Reactors were run in continuous mode for at least three HRTs before sampling of the effluent began so that a pseudo-steady state could be achieved. This state was confirmed by observing a steady current in trials which applied electrical power. Once pseudo steady state was achieved, for S(IV)-containing feeds, a syringe was affixed to the effluent line after the filtration cartridges and allowed to fill over a period of time, capturing all the effluent and creating a composite sample. For feeds with no S(IV) where only H_2O_2 concentration was being measured, present, samples were collected in open vials that were refrigerated on a bed of ice and covered from direct light to minimize H_2O_2 decomposition.

No less than four sequential samples (usually five, more added for more variable reactions) were taken for each tested set of reaction conditions. The effluent collected was analyzed for volume, concentration (of S(IV) and total sulfur, or H_2O_2) and pH, and this data was associated with the electrical data logged by the potentiostat over the same period, most importantly the cumulative charge passed over the sampling period. All reactors used a potentiostated cathode; both cathode potential and cell voltage were logged by the potentiosat.

For each effluent sample S(IV) and H_2O_2 concentrations were measured by spectrophotometry in duplicate, at minimum, and averaged to produce a single concentration estimate for each composite sample. In order to analyze a set of reaction conditions across the entire operation time of a reaction testing them, the set of mean concentration values, one for each sample taken, was averaged again to produce one value; the corresponding standard deviation reflecting the spread of the averaged concentrations for each sample is shown as error bars.

4.3.3 Reagents

Electrolyte used as feed for the reactor was prepared using sodium sulfite (ACS grade, Sigma, USA) or sodium bisulfite (ACS grade, EM Science, Germany) as a source of S(IV). Purity was verified using both ion chromatography (IC) and redox titration.

pH and conductivity adjustment of S(IV) solutions were carried out in a magnetically-stirred beaker with continuous monitoring by pH and/or conductivity probes. pH adjustment was carried out using hydrochloric acid (37%wt, ACS grade, Sigma-Aldrich, USA) or sodium hydroxide (5 M solution prepared from solid pellets; technical grade, Anachemia, Canada). Conductivity was adjusted using food-grade sodium chloride (Iodized table salt, Windsor Salt Company, Canada). S(IV) concentration validation was carried out via IC and spectrophotometry afterward to compensate for solution volume change and any S(IV) removal.

All electrolytes were prepared in deionized water generated at the University of Waterloo (verified to be >1 μS cm^{-1}).

4.3.4 Analytical methods

4.3.4.1 Reagent validation

Firstly ion chromatography (IC) was done using a Dionex ICS 1100 system equipped with a Dionex AS-DV autosampler and a suppressed conductivity detector. The following operating specifications were used: analytical column: Dionex IonPac AS4A-SC Analytical (4 x 250mm), guard column: Dionex IonPac AG4A-SC Guard (4 x 50mm), eluent: 1.8 mM Na_2CO_3/ 1.7 mM $NaHCO_3$, flow rate: 2.0 mL min^{-1}, temperature: ambient (~25°C), suppressor: Dionex Anion Self-Regenerating Suppressor (Dionex ASRS 300 4mm) with Autosuppression Recycle Mode, applied current: 32 mA, sample injection volume: 25 μL. The setup used cannot distinguish S(IV) from S(VI), so its sulfate (S(VI)) standard was used to represent total sulfur. This was verified by processing standardized sulfite and sulfate samples through the machine. Secondly, redox titration via the Ripper method [172], which can distinguish S(IV) from S(VI), was done. Iodine solution was prepared from resublimated iodine (ACS grade, Sigma-Aldrich, USA) as titrant, sulfuric acid (95-98%, ACS grade, BDH, USA) was used to acidify samples, and a 10%wt solution of food-grade tapioca starch was used as a colour indicator for presence of excess iodine.

4.3.4.2 Experimental measurement

H_2O_2 concentration was determined spectrophotometrically (Genesys 10S UV-Vis, Thermo Scientific, USA) using the vanadate method developed by Nogueira et al. [142]. A calibration curve was prepared using nominal 35%wt H_2O_2 (technical grade, BDH, USA) standardized

against oven-dried potassium permanganate (ACS grade, EMD, Germany). The calibration curve had an R^2 of 1.00.

S(IV) concentrations were determined spectrophotometrically using a method informed by Huss and Eckert [173] and Syty [174] where samples acidified by mixing with three parts by volume 25% sulfuric acid (prepared from 95-98% sulfuric acid, ACS grade, BDH, USA) were measured using absorbance of the SO_2 peak at 277 nm. The calibration curve had an R^2 of 0.99.

Total sulfur (i.e., S(IV)+S(VI)) concentrations were determined by ion chromatography using the setup already described in Section 4.3.4.1. This measurement was taken to account for any S(IV) loss in addition to oxidation to S(VI) (sulfate).

All electrical measurements, including current, anode potential, cell voltage, and cumulative charge passed, were done using a BioLogic VSP potentiostat running EC-Lab (version 10.23) software on a personal computer. Measurements were logged at 10 second increments. In Reactors A and C, the reference electrode (Ag|AgCl; MF 2052, BASI, USA as previously described), was submerged in the centre of the reactor volume, oriented parallel to the planar electrode and with the centre of its junction 9.5 mm away from the electrode surface. Under the highest current tested, the uncompensated cathode potential was kept within 28 mV of the set value. In Reactor B, the small cathode chamber thickness required creating a fitting using a 3-way hose junction which situated the reference electrode junction 66.9 mm from the cathode surface. Uncompensated cathode potential was maintained within 19 mV of the set value.

pH was measured from influent grab samples and effluent composite samples using an benchtop pH meter (Orion Star A111, Thermo Scientific, USA) and probe (10A, Thermo Scientific, USA) calibrated using pH 4, 7, and 10 buffers.

Conductivity was measured from influent grab samples and effluent composite samples using an Oakton Con 11 Series conductivity/TDS/thermometer (USA).

Volumes were measured using a graduated cylinder with 1 mL increments, except for experiments with Reactor C where volumes were much smaller. In these experiments, volume was estimated gravimetrically using an electronic balance (PR5002, Mettler-Toledo, Switzerland).

Coulombic efficiency (CE) was calculated using the following formula, where n is the number of electrons transferred per mole H_2O_2 generated or S(IV) oxidized (2 mol e^- mol $H_2O_2^{-1}$ or S(IV)), F is Faraday's number (96485 C mol e^{-1}), V is the reactor volume (63 mL for Reactor A, 63 mL for each chamber in Reactor B or 128 mL when assembled without separator, 10 mL for Reactor C), C is the concentration change of H_2O_2 or S(IV) (i.e., the effluent H_2O_2 concentration or the difference between influent and effluent S(IV)), and Q is the charge passed through the reactor during operation (C):

$$CE = \frac{n \cdot F \cdot V \cdot C}{Q} \tag{45}$$

For Reactor B, coulombic efficiency is calculated for each half-cell individually.

S(IV) removal rate was computed as negative concentration change/influent concentration. Influent concentration was checked at least before and after testing and an average value was used to report S(IV) removal rate. S(IV) and total sulfur in the feed bottle itself showed no significant concentration change.

4.3.5 Baseline reactor performance

To provide a basis for experimental results, reactors were run to establish two baselines: S(IV) loss in an unpolarized reactor and H_2O_2 production in the absence of S(IV). Baseline experiments used a cathode that had previously been used for S(IV) treatment to provide a similarly functionalized catalyst surface; previous experiments show catalytic activity develops over time as a GDE is polarized in electrolyte (shown in Figure 7 in Chapter 3).

Some S(IV) could be expected to be lost through operation, sampling, and analysis; this was characterized in a worst-case scenario on a reactor with no electrical input and concomitant H_2O_2 layer on the cathode to incur oxidation and prevent volatilization. Baseline experiments for S(IV) loss showed no loss of S(IV) or total sulfur at pH 3.8-9.5 but did show losses of 9-24% at pH 1.5-1.7; from these latter tests correction factors were estimated but data for very low pH (≤1.7) should be regarded with uncertainty nonetheless.

Baseline H_2O_2 production was assessed at pH 9.5 and HRT from 0.1 hours to 1.3 hours; data is shown in Figure 16 compared with experimental data. The maximum CE achieved was 49.2% at 0.1 h HRT (2.1 mM, 74.8 mg L^{-1} H_2O_2 produced), while it decreased to 15.5% at 1.3 h (4.8 mM, 163.3 mg L^{-1} H_2O_2). This performance is comparable but slightly lower to what

was observed by Barros et al, [25] also working in alkaline medium with an unmodified catalyst, who achieved ~60% CE and ~400 mg L^{-1} in their batch at a similar retention time.

4.4 Results and discussion

Full summaries of continuous test results are included in Appendix A.

4.4.1 Comparison of coulombic efficiency with and without *in situ* treatment

The primary research goal of this study was to investigate whether reacting a target compound with H_2O_2 *in situ* can raise the process efficiency over H_2O_2 generation directly. Experiments were undertaken under identical conditions at various HRTs to investigate this question; results are shown below in Figure 16.

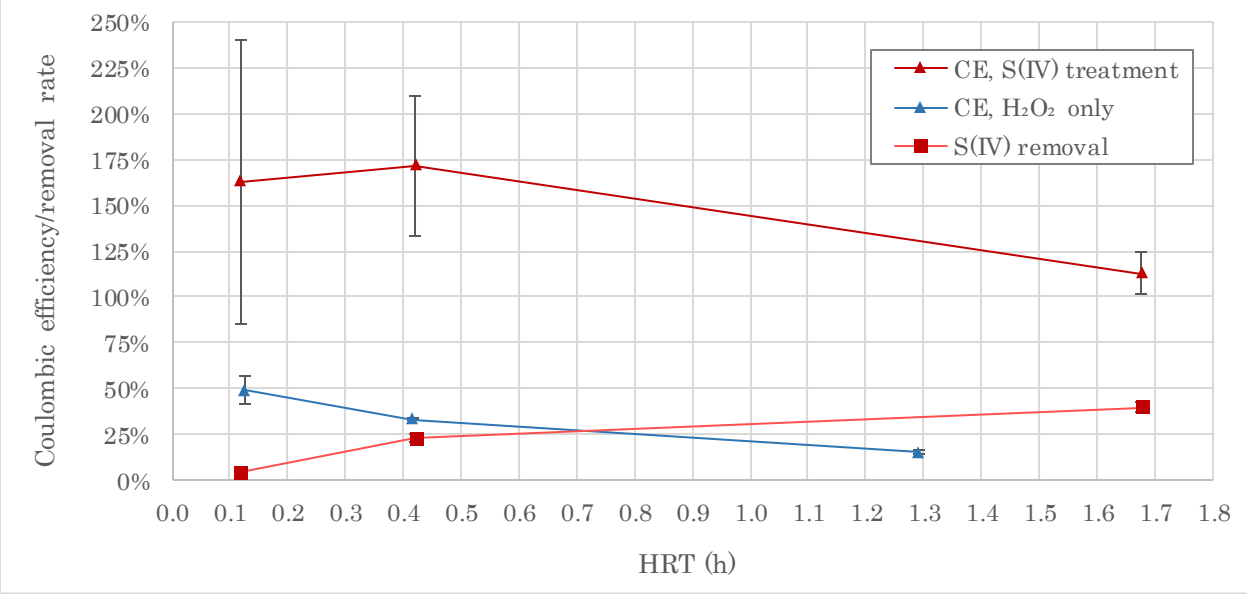

Figure 16 - Comparison of coulombic efficiency achieved in Reactor A with and without S(IV) feed.
Note: S(IV) removal is also shown for trials with S(IV) feed. Reaction conditions were cathode potential of -1000 mV vs Ag|AgCl (-778 mV vs SHE), pH 9.5 feed, and all electrolytes had a conductivity of 27 mS cm^{-1}. 100mM S(IV) (verified at 105-109 mM by IC) was used as feed for the S(IV) trials while NaOH and NaCl were used to prepare feed for the H_2O_2 trial of appropriate pH and conductivity. Despite similar conductivities, current varied throughout all trials from 2.1-3.1 mA cm^{-2} for S(IV) trials (highest at 0.42 h HRT) and from 2.1-3.6 mA cm^{-2} for H_2O_2 trials (highest for 1.29 h HRT)

In trials with and without S(IV) a predictable decrease in CE can be observed as the HRT is prolonged with a concomitant removal rate increase (in the trials with S(IV)). The CE curve for the trials with S(IV) is consistently higher than that of the curve for H_2O_2 production only, 3.3 times more efficient at the lowest HRT and an interpolated 8.1 times more efficient at the highest HRT. Furthermore, CE for the S(IV) trials based on a 2-electron calculation is >100%, signifying that anodic oxidation processes are also taking place in this reactor. These results

demonstrate the large advantages of reacting a target compound with H_2O_2 produced *in situ* as well as coupling anodic and cathodic (via H_2O_2) oxidation processes in a single reactor. The large error bars around the CE values at lower HRT for the S(IV) trials are due to the small removal efficiency resulting in a larger standard error for a given instrument error.

4.4.2 Determination of removal mechanism

In order to determine whether S(IV) removal processes were dominated by either electrode, a divided, dual chamber reactor (Reactor B) was used. Reactor B was operated with and without the cation exchange membrane in place; results are shown in Figure 17 below.

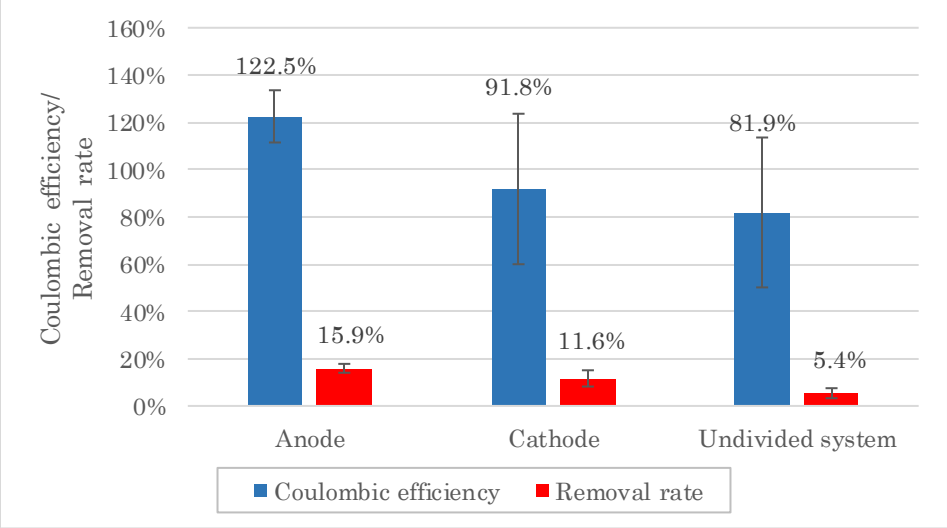

Figure 17 - Coulombic efficiency and removal rate in Reactor B's half cells (first two sets of data) compared with performance in an undivided Reactor B.
Note: Cathode potential was set to -1000 mV vs Ag|AgCl (-778 mV vs SHE) HRT was 0.42 h, influent pH 9.5, and influent S(IV) 100 mM (verified by IC to be 104-110). Anode potential ranged from +1014 to +1107 mV vs Ag|AgCl (+1236 to +1329 mV vs SHE) during the divided cell trials. Current density was similar despite the presence/absence of the CEM between all trials around 3.58-3.61 mA cm^{-2}.

This data shows 37% more removal happens in the anode in this reactor, while both anode and cathode have high efficiencies close to 100%. Thus, anodic oxidation processes play a comparable to H_2O_2 oxidation in this system. The anodic efficiency was measured as >100% suggesting some diffusion across the CEM occurred. Interestingly, in the undivided control system under identical conditions, the reactor performed poorer than either half cells individually. If the half cell processes had no interaction, it would be expected that removal in the control cell would be the average of the two half cells and that CE would be the sum of the half cells. The significantly deteriorated performance may be due to the different mixing conditions in the undivided cell or anodic oxidation of H_2O_2.

The fact that the cathodic oxidation processes can achieve 91.8% efficiency, with no augmentation from anodic processes, should not be overlooked. This may be compared to the 33.2 % CE achieved for H_2O_2 production only under similar conditions as shown in Figure 16. It is known from previous testing (included in Appendix C) that S(IV) oxidation by H_2O_2 is rapid across a broad pH range and without excess reagents; only under very acidic pH <0.5 did any reactions tested not go to completion in less than 1 second. Thus it can be theorized that in the present system, H_2O_2 and S(IV) react as soon as H_2O_2 is produced, either on the electrode surface or in the diffusion boundary layer, before H_2O_2 can be reduced to water and drive CE down as occurs in electrolysis cells for H_2O_2 production only.

4.4.3 Factors affecting reactor performance

In addition to testing potential advantages of introducing a target compound for *in situ* oxidation by electrogenerated H_2O_2, numerous operating parameters were tested to help inform further development of this technology.

4.4.3.1 Mixing

Figure 18 below compares the performance of the unmixed reactor (except by normal feeding) with the same system run with recirculation at 0.40 reactor volumes per minute (equivalent to mixing achieved by operation at 2.52 minute or 0.042 hour HRT). Mixing is seen to enhance removal above HRT around 0.5 hours, suggesting that sufficient mixing already takes place at HRTs below this but slower-flowing reactors can benefit from additional mixing. CE data is variable and suggests a small advantage if anything, which can be attributed to better mass transfer and lower H_2O_2 losses on the electrode. The large error bars around the lowest HRT data for the mixed trials and data point above 200% CE outline make these data inadmissible for analysis, but the tight closure on the last point allows some comparison to be made. These large errors occur in CE calculations by magnifying other errors when small removal rates are used in the denominator.

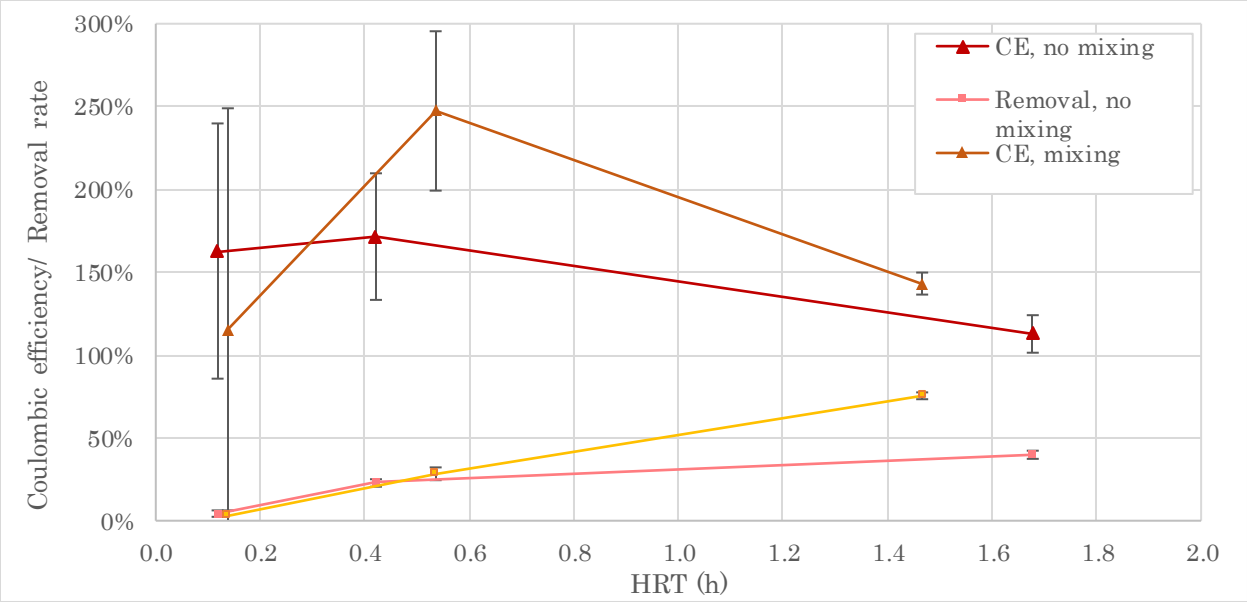

Figure 18 - Effect of mixing on S(IV) removal and CE in Reactor A
Note: Reaction conditions were cathode potential of -1000 mV vs Ag|AgCl (-778 mV vs SHE), pH 9.5 feed, and all electrolytes had a conductivity of 27 mS cm^{-1}. 100mM S(IV) (verified at 105-109 mM by IC) was used as feed for the S(IV) trials while NaOH and NaCl were used to prepare feed for the H_2O_2 trial of appropriate pH and conductivity.

4.4.3.2 Cathode potential

Figure 19 shows results of experiments examining the effect on cathode potential.

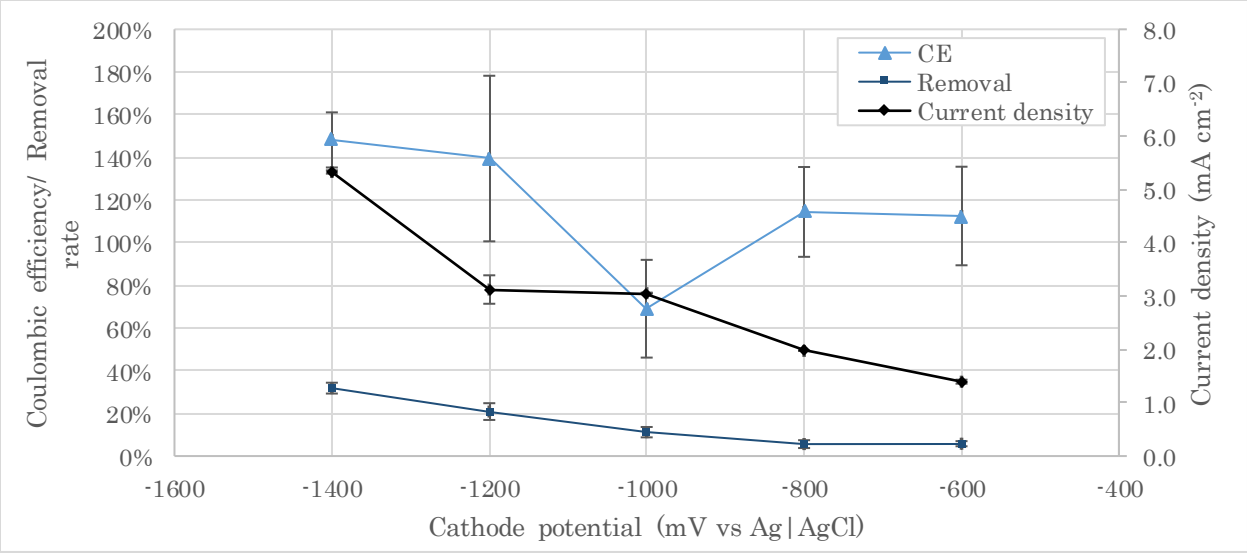

Figure 19 - Effect of cathode potential on S(IV) removal, coulombic efficiency, and current density in Reactor A.
Note: For all trials, influent was ~100 mM S(IV) (91.2-110 mM) at pH 9.5 and the reactor was operated with an HRTs of 0.47 h (+0.09/-0.04).

With increasing polarization, current is predictably seen to increase with concomitant removal rate increase. Interestingly, coulombic efficiency is slightly higher at more polarized potentials (148% versus 113% at the smallest polarization), this may be due to better electrostatic repulsion of ionized H_2O_2 (HO_2^-) in the cathode diffusion boundary layer. This contrasts observations in previous work (Section 3.4.2.3 in Chapter 3) in reactors producing only H_2O_2, higher current tends to lead to higher concentrations of H_2O_2 but lower efficiencies as larger proportions of generated H_2O_2 are reduced to water at the cathode. The generally linear trend in the current curve indicates that the cathode is operating in the linear, ohmic-loss dominated region of its polarization curve (confirmed by cyclic voltammetry shown in Appendix B), suggesting removal rate could be further increased by polarizing the cathode without immediately encountering mass transfer limitations. In practice, increasing cathode potential also drives up anode potential, and when oxidation of the anode itself becomes more favourable than oxidation of the electrolyte, corrosion occurs. Thus, operationally, the optimal cathode potential to be used depends on the choice of anode material as well.

4.4.3.3 pH

Reactor A was tested at pH 1.7, 4.0, and 9.5 using 100 mM S(IV) feed at a cathode potential of -1000 mV vs Ag|AgCl (-778 mV vs SHE) and a 0.4 h HRT. Data (included in Appendix D) did not show any definite trends in coulombic efficiency or removal rate across pH. This could be due to similar pH at the electrode surfaces in all cases due to mass transfer limitations. Independence to pH was also found by other researchers looking at *in situ* electrogeneration of H_2O_2 [21]. Definitively, it can be said that a reactor using an air cathode should not be used at pH below 1.5 to prevent S(IV) loss by volatilization; beyond that the optimal pH choice is probably whatever results from no adjustment of influent wastewater to avoid pH adjustment costs.

4.4.3.4 Surface area to volume ratio

Because the cathodic oxidation reaction is theorized to happen very close to the cathode surface, the effect of maximizing the surface area of the electrode with respect to the reactor volume was studied by changing the reactor volume, i.e., comparing Reactors A (63 mL), B (without separator, 128 mL), and C (10 mL). The result, shown in Figure 20 below, shows a comparable current and coulombic efficiency regardless of size, but a linearly increasing removal rate. Modelling the system with first order kinetics would predict a J-shaped

removal rate curve with an asymptotic approach to 100% removal, the linear shape suggests that the reactor geometry for higher surface-area to volume reactors has additional benefits, for example, turbulence promotion by the plastic mesh spacer. Maximization of surface area to volume and engineering of reactor geometry are present opportunities for improving the reactor without increasing energy input or requiring longer HRT.

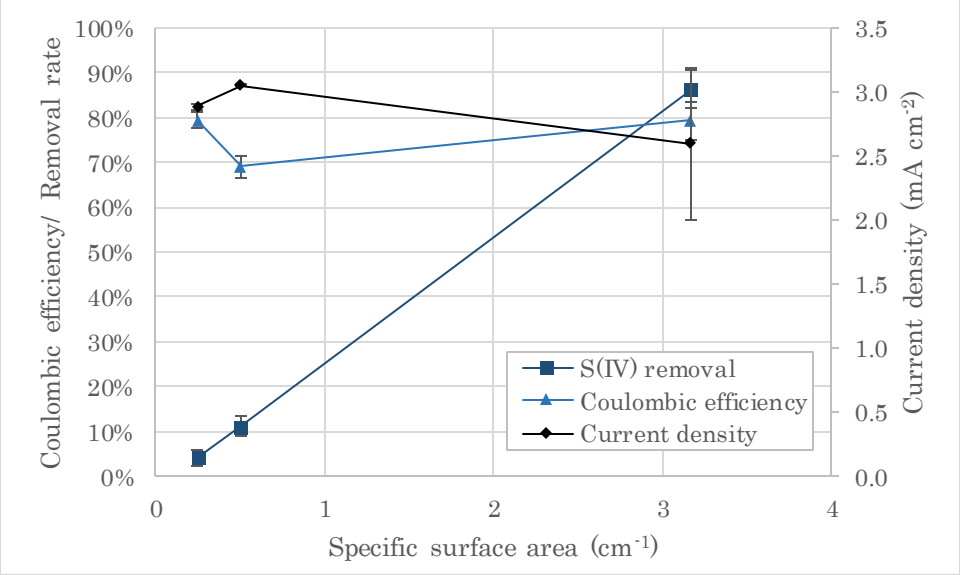

Figure 20 - Effect of surface area to volume ratio on S(IV) removal, coulombic efficiency, and current density in Reactor A.
Note: Experiments are all for an HRT of 0.49 h (+/- 0.06), influent pH of 9.5, and influent S(IV) concentration of 100+/- 6 mM for the two lower Surface area to volume ratio trials, the influent S(IV) for the 3.17 cm^{-1} trial was verified to be 63-75 mM.

4.4.3.5 Influent concentration and conductivity

Trials up to now have all used ~100 mM solutions of S(IV) for feed, which is a relatively high concentration (3200 mg L^{-1}). In order to explore reactor performance at lower concentration, a 10 mM solution was compared with no conductivity or pH adjustment. In Figure 21 below, it can be seen that decreasing the concentration 10 times caused a 5.6 times drop in current density, while a removal actually improved 20 percentage points and Coulombic efficiency dropped 33 percentage points. This suggests that mass transfer was good enough that H_2O_2 had enough S(IV) to react with immediately even in the lower concentration trial. A trial using different reaction conditions and an even lower S(IV) concentration of 2mM achieved similar current and removal as the unadjusted 10 mM trial by prolonging HRT to 1.47 hours and recirculating the reactor at 25 mL min^{-1} (0.4 reactor volumes per minute). Another option for increasing performance without needing to increase costs by increasing HRT (requires

bigger reactor) and mixing (requires more energy) is to increase the solution conductivity. By increasing the 10 mM feed to the same conductivity and pH as the 100 mM feed using NaCl and HCl, higher current density (80% of the 100 m M trial) and a near-perfect removal of 99% were achieved at a decreased but appreciable coulombic efficiency of 61%. The increased conductivity encouraged a greater flux of H_2O_2 off the cathode and the resulting excess led to the good removal and poorer CE.

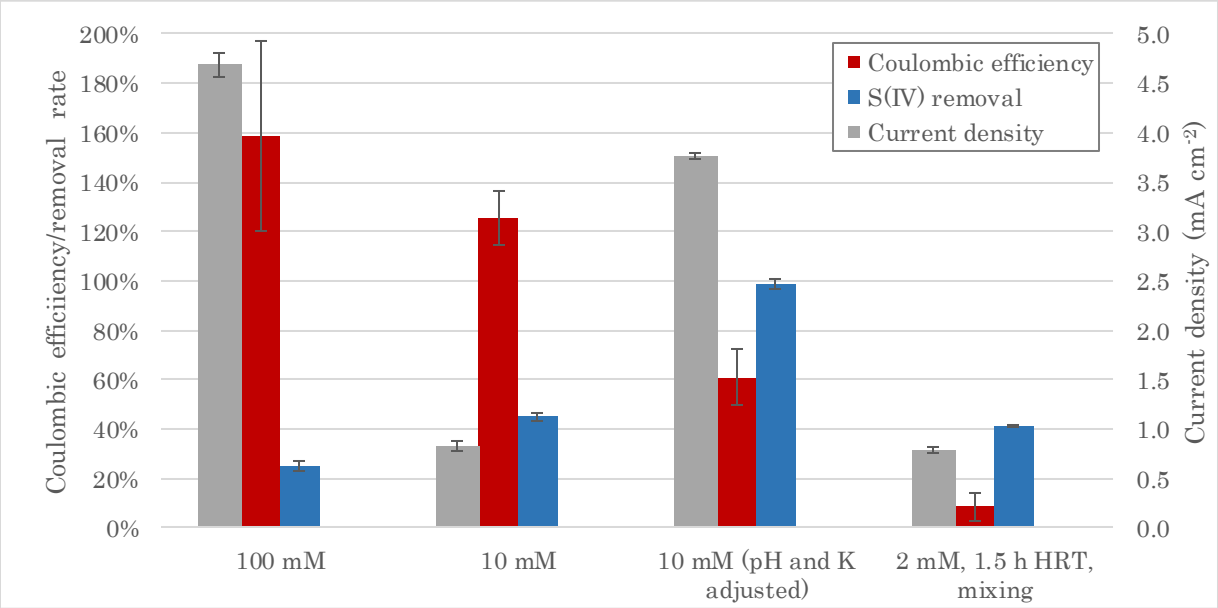

Figure 21 - Effect of influent concentration and conductivity (K) adjustment on ratio on S(IV) removal, coulombic efficiency, and current density in Reactor A.
Note: Experiments all an HRT of 0.40-0.46 h and cathode potential of -1000 mV vs Ag|AgCl (-778 mV vs SHE). The nominal 100 mM trial (actual concentration 113 mM) had a conductivity of 27 mS $cm^{-1}$and a pH of 9.5. The 10 mM (10.1 mM actual) trial with no adjustment had a pH of 8.8. The second (10.1 mM actual) trial was pH adjusted to 9.5 and conductivity adjusted to 27 mS cm^{-1}.

4.5 Conclusion

Coupling H_2O_2 generation and application *in situ* in a single chamber electrolysis cell was demonstrated to be an efficient method of oxidizing S(IV) to S(VI), being 3-8 times more efficient than H_2O_2 production alone and achieving well over 100% efficiency on a 2-electron basis by combining simultaneous anodic and cathodic removal. Oxidation was achieved both by hydrogen peroxide production at the cathode as well as oxidation at the anode, either directly or due to oxygen production, and for S(IV) anodic oxidation may actually be more effective despite poorer thermodynamic potential according to our results. Nonetheless, even the cathodic reaction alone achieved 91.8% efficiency compared to 33.2% for H_2O_2 production alone under similar conditions. The removal rate and coulombic efficiency were not sensitive

to pH. Increasing cathode polarization from -600 mV to -1400 mV vs Ag|AgCl (-378 to -1179 mV vs SHE) increased removal without leading to inefficiency under the conditions tested. Maximizing surface area to volume ratio was shown to increase removal rate linearly without leading to efficiency losses. Lastly, it was demonstrated that changing influent concentration does not have a major effect on removal rate and efficiency due to concomitant conductivity and current changes, but that by increasing conductivity greater removal could be encouraged at the expense of coulombic efficiency. Prolonging HRT and adding more vigorous mixing also prevent ways of increasing removal and sacrificing efficiency.

5 Economic outlook

Although the present work has reviewed research covering many aspects H_2O_2 electrogeneration while contributing to this same body, engineering research is ultimately fruitless if findings cannot be eventually commuted to technology development and deployed to enhance quality of life and protect the environment. Though technical feasibility is well established, the present section will take a brief look at economic viability of H_2O_2 electrogeneration technologies. Though some scholars argue that *in situ* H_2O_2 electrogeneration technologies are both ready for scale-up and economical [71] and others demonstrate significant savings [44], the lack of uptake beyond the paper bleaching industry, which does not apply *in situ* treatment [14], illustrates that despite these claims, significant barriers in research, development, and commercialization exist. The main costs of existing options are materials for electrodes and separators, reagents for pH adjustment and catalysis, and electricity, but this must be also considered in the context of displacing existing, offsite anthraquinone oxidation-driven market and its production, transportation, storage, and handling [109].

5.1 Operating costs

5.1.1 H_2O_2 production only

To begin, the cost traditionally-sourced H_2O_2 must be established. USP Technologies, a major supplier in North America, provides its costs (adjusted to 100% H_2O_2 basis) as USD 1.99 kg^{-1} plus USD 2.87 km^{-1} for freight [77]. Academic studies that quote prices use lower values such as USD 1.5 kg^{-1}, [19], [38], 0.86 kg^{-1} [175] or even as low as USD 0.43-0.55 [59]. Values vary due to regional markets and location of production facilities, but this range will be used to at least estimate the order of magnitude of cost for the null option of purchasing H_2O_2. In order to compare this cost with the figures in kWh kg^{-1} or similar provided by research, a power cost of USD 8.14 $kW^{-1}h^{-1}$ is adopted based on average electricity price in Ontario for 2014-2016 [176]. Table 6 summarizes the costs of commercial H_2O_2, costs determined for the presented work for three points along the frontier of the tradeoff curve presented in Figure 12, and costs taken from studies that report them that were reviewed in Table 3 and Table 4. Costs for the present work estimated that that the applied voltage was double the value of the cathode potential (vs Ag|AgCl; 1.8-2.4 V), real values for cell potential are not available due to improper logging of anode potential. For compatibility, only work focussed on

producing H_2O_2 is shown here, as the diversity of processes and costs for *in situ* systems precludes direct comparison.

Table 6 - H_2O_2 cost comparison

Reference	System	Cost (kWh kg^{-1})
[19], [38], [59], [77], [175]	Commercial	5.30-24.4
Present work	6394 mg L^{-1} at 15.1% CE	25.05
	887.4 mg L^{-1} at 72.5% CE	4.35
	22.4 mg L^{-1} at 99.8%CE	2.84
[38]	Microbial	0.45
[41]		0.87
[37]		0.93
[34]		1.01
[36]		1.1
[35]		3.0
[42]	Non-microbial	2.5
[31]		6.0
[19]		7.45
[25]		8.0
[29]		17
[19]		24.97
[21]		50

This cost comparison indicates not only that the present work produces H_2O_2 at a rate competitive with what is commercially available, but that many others' systems perform similarly. Microbial systems are seen to offer cost savings over chemical systems. The costs quoted are only for electricity, while other substantial costs exist. Nonetheless, proving a

comparable operating cost is a compelling argument for adoption, and cost savings over shipping, storage, and handling required for commercial H_2O_2 may also be factored in.

Even in a system for H_2O_2 production, which has less operating costs than some *in situ* treatment systems, both electrolyte and oxygen are important operating costs that can easily double the cost of electrical power [19]. Luckily, these costs can be avoided by using a GDE with passive O_2 diffusion from air (reviewed in detail in Section 2.4.6.2) and by relying on the intrinsic conductivity of the influent or using a small electrode spacing (discussed in Section 2.4.7).

The present analysis only argues that electrogenerated H_2O_2 may be competitive to consider for operators already needing to pay for H_2O_2. However, as outlined in Section 1.1, the needs of the water/wastewater sector must adapt to meet growing populations and water stress and to do so at scale economically. Thus, the energy cost of treatment, though competitive, may still be prohibitive. Energy cost may be reduced if bioanodes can be engineered that realize the potential for cost reduction they promise, or if other environmental power sources like salinity gradients [38], or sunlight [68] can be leveraged. Li et al. [38] achieved the best reviewed cost of 0.45 kWh kg^{-1} by combining a bioanode with a reverse electrodialysis stack. Additionally, integrating electrochemical systems beyond just at the disinfection step, for example integrating electrochemical treatment with a treatment wetland [42], may displace other more carbon and energy-intensive traditional treatment processes.

5.1.2 *In situ* treatment

In situ treatment may offers additional cost savings by increasing the CE of electrogeneration processes, as demonstrated in Section 4.4.1. Agladze et al. [44] demonstrated successful costs savings with their *in situ* electro-Fenton treatment system which can treat water at USD 0.825 m^{-3} opposed to USD 2.326 m^{-3} that current technology costs. However, *in situ* systems, particular Fenton systems, can incur significant operating costs for their pH and iron requirements, both adjusting for the process and for discharge [47], [104]. Other problems may arise from fouling of GDEs with iron(III) hydroxide [44]. UV systems incur additional power costs for running lamps, though sunlight-powered systems offer cost savings [65]. Despite these drawbacks, EAOPs may still displace more expensive AOPs like ozonation [177].

The system tested in Chapter 4 neglects some of these costs by reacting H_2O_2 directly, however this provides less oxidizing power and does not have favourable kinetics for treatment of all contaminants. When considering the cost of an *in situ* treatment system, the advantages of augmenting H_2O_2's oxidizing power with advanced oxidation must be balanced against other costs. Consideration of the target compound, matrix and interfering compounds, effluent quality standards, and site location may all play into selection of a cost-effective system.

5.2 Capital costs

In addition to the operating costs of an electrochemical system, the capital cost for the reactor itself must be considered, including electrodes, separators, reactor vessel, pumps, power supply and regulation, and other instrumentation. These will be briefly commented on, though a detailed discussion with real dollar value costs will not be explored.

5.2.1 Electrodes

Electrodes may be created inexpensively at scale provided that they contain low amounts or ideally no expensive metals. The majority of the studies reviewed use metal-free electrodes consisting of carbonaceous materials and PTFE, although only a handful use commercially available ones [26], [39], [43] and these are outperformed by others. The present work suggests that commercially available electrodes still deliver H_2O_2 at a competitive cost.

The majority of studies reviewed used an inert counterelectrode as anode, but these materials, such as platinum and DSA, would be unnecessary and prohibitively expensive in a treatment system. The present work suggests the graphite is a viable anode material.

5.2.2 Separators

Although separators may be eliminated in several abiotic designs, allowing significant cost savings, biotic systems will probably always require them to protect ARB from oxidation. In addition to their capital costs, separators incur maintenance costs due to fouling and degradation over time, both of which increase the power required on top of the increased requirement from having a separator at all. Anodic oxidation of H_2O_2, the main concern prompting the use of separators in abiotic systems, may be precluded by using an *in situ* processes that consume H_2O_2 before it may diffuse to the anode, as demonstrated in Chapter 4. Separators have been discussed in detail in Section 2.4.8.

5.2.3 Power supply and regulation

The majority of studies reviewed use a potentiostat or galvanostat to control electrical power. Although this is useful for research, it may not be required for a plant with well-characterized performance and a much less expensive power supply system may be used. In a sufficiently large plant, the electronics themselves may also become negligible compared to other capital and operating costs.

5.3 Conclusion

The H_2O_2 electrogeneration system tested in Chapter 3 produces H_2O_2 at rates competitive with both commercially-available H_2O_2 and results from other studies, around 3-25 kWh kg^{-1}. Furthermore, the design presented in Chapter 4 offers additional savings by removing the cost of a separator and operating at a higher CE, however not all contaminants may be treated by H_2O_2 directly as done here; additional costs for advanced oxidation may be necessary depending on the wastewater. By using commercially-available, metal free electrodes, the tested systems are as low-cost as possible already.

6 Conclusions

Electrogeneration of H_2O_2 is a promising technique to help address growing and changing needs in water and wastewater by providing an environmentally-friendly oxidant on-demand with no requirement for chemical inputs. Despite this, there has not been a wide uptake in H_2O_2 electrogeneration at scale. The present work first sought to optimize cathodic conditions in a divided, continuously-flowing reactor using unmodified, commercially available electrodes to verify conditions suggested by previous work in a context more appropriate to scale-up. Secondly, the strategy of in-situ treatment in an undivided reactor with electrogenerated H_2O_2 with no advanced oxidation was investigated using sulfur(IV) as a model pollutant as a way to overcome limitations exposed in the first part and to further work toward an attractive high-efficiency alternative for industrial adoption.

In the first system focussing on H_2O_2 production only, it was confirmed that alkaline conditions are optimal, which may be facilitated naturally by proton transport limitations creating low pH of 12 or higher from neutral feed. Because high pH also increases decomposition, yields were not as high as possible. Yields could also be decreased by prolonging HRT past 10 hours, below which CE was constant around 60-70%, or by using excessive cathode overpotentials resulting in higher currents but also greater Faradaic reduction losses. Yields could be effectively increased by maximizing surface area to volume ratio in the reactor, which reduced the losses in bulk but made electrode surface processes more significant to reactor performance. These competing factors limit the performance achievable in the H_2O_2 production system, creating a tradeoff curve between coulombic efficiency (CE) and effluent H_2O_2 concentration with extreme points around 7000 mg L^{-1} at ~0% CE and 20 mg L^{-1} at ~100% CE. A microbial system was also operated to demonstrate the compatibility of biogenic current density with the abiotic H_2O_2-producing cathodes studied. A model for mass flows within the reactor has been applied for the first time and results point to a need to control HRT to manage non-Faradaic losses and control cathode potential to manage Faradaic losses.

In the second system focussing on *in situ* S(IV) oxidation with electrogenerated H_2O_2, it was shown that CE gains of 3-8 times can be realized over H_2O_2 production only. Importantly, CE may be improved both by better use of cathodically generated H_2O_2 and by direct anodic oxidation, which was over 30% more important in the reactor tested. Removal could be enhanced by enriching influent with NaCl electrolyte, mixing the reactor during long HRTs

above 0.5 hours, and by increasing surface area to volume ration in the reactor. pH did not have a definite effect on the reaction, though very acidic pH below 1.5 can lead to SO_2 loss through the GDE. This system similarly exhibited a tradeoff, this time between CE and S(IV) removal rate which may not be overcome by using a continuously flowing tank configuration.

Together these findings present clarification of previous work on H_2O_2 electrogeneration in the specific context of continuous reaction over commercially available GDE, a mass balance model for understanding and designing around the competing reactors inherent in an H_2O_2 electrogeneration system, and a proof of concept for *in situ* S(IV) treatment with electrogenerated H_2O_2.

7 Recommendations

Recommendations for future work may be divided into the three chief areas of contribution of the present work, each of which may benefit from further study.

7.1 H_2O_2 electrogeneration

1. Determine the chemical structure of the MPL in the GDE used and how it is altered by use to elucidate catalytic mechanism and determine whether pretreatment may enhance performance
2. Repeat experiments that showed wide error bars and unexplained trends to verify findings and identify remaining knowledge gaps

7.2 Model

1. Improve kinetic constants with repeated trials, cleaner feeds and vessels to reduce catalysis by contaminants
2. Validate conditions (mixing, current density, pH, etc.) in which mass balance model may be applied without violating assumptions
3. Add a spatial dimension to the model to include a diffusion boundary layer to better estimate processes close to electrodes

7.3 *In situ* treatment

1. Verify the anodic oxidation mechanism
2. Determine which applications are strategic for *in situ* treatment with no advanced oxidation based on susceptibility to H_2O_2 attack and priority level for treatment innovation
3. Repeat experiments with more precise measurements in order to address wide error bars and excessive values for CE

8 References

[1] World Water Assessment Programme, 'UN World Water Development Report 4 - Background Information Brief', United Nations, Perugia, Italy, 2012.

[2] A. M. Klasing, *Make it safe: Canada's obligation to end the First Nations water crisis*. Human Rights Watch, 2016.

[3] S. J. Masten, S. H. Davies, and S. P. McElmurry, 'Flint Water Crisis: What Happened and Why?', *J. - Am. Water Works Assoc.*, vol. 108, pp. 22–34, Dec. 2016.

[4] M. Raghav, S. Eden, K. Mitchell, and B. Witte, 'Contaminants of emerging concern in water', University of Arizona Water Resources Research Centre, 2013.

[5] BASE Energy, Inc., 'Energy Baseline Study for Municipal Wastewater Treatment Plants', Pacific Gas & Electric Company, 2006.

[6] P. R. Gogate and A. B. Pandit, 'A review of imperative technologies for wastewater treatment I: oxidation technologies at ambient conditions', *Adv. Environ. Res.*, vol. 8, no. 3, pp. 501–551, Mar. 2004.

[7] P. R. Gogate and A. B. Pandit, 'A review of imperative technologies for wastewater treatment II: hybrid methods', *Adv. Environ. Res.*, vol. 8, no. 3, pp. 553–597, Mar. 2004.

[8] C. Y. Gomec, 'High-rate anaerobic treatment of domestic wastewater at ambient operating temperatures: A review on benefits and drawbacks', *J. Environ. Sci. Health Part A Tox. Hazard. Subst. Environ. Eng.*, vol. 45, no. 10, pp. 1169–1184, Aug. 2010.

[9] Y. J. Chan, M. F. Chong, C. L. Law, and D. G. Hassell, 'A review on anaerobic–aerobic treatment of industrial and municipal wastewater', *Chem. Eng. J.*, vol. 155, no. 1, pp. 1–18, Dec. 2009.

[10] H. Ozgun, R. K. Dereli, M. E. Ersahin, C. Kinaci, H. Spanjers, and J. B. van Lier, 'A review of anaerobic membrane bioreactors for municipal wastewater treatment: Integration options, limitations and expectations', *Sep. Purif. Technol.*, vol. 118, pp. 89–104, Oct. 2013.

[11] B. E. Logan and K. Rabaey, 'Conversion of Wastes into Bioelectricity and Chemicals by Using Microbial Electrochemical Technologies', *Science*, vol. 337, no. 6095, pp. 686–690, Aug. 2012.

[12] A. Matilainen and M. Sillanpää, 'Removal of natural organic matter from drinking water by advanced oxidation processes', *Chemosphere*, vol. 80, no. 4, pp. 351–365, Jun. 2010.

[13] J. M. Campos-Martin, G. Blanco-Brieva, and J. L. G. Fierro, 'Hydrogen peroxide synthesis: an outlook beyond the anthraquinone process', *Angew. Chem. Int. Ed Engl.*, vol. 45, no. 42, pp. 6962–6984, Oct. 2006.

[14] P. C. Foller and R. T. Bombard, 'Processes for the production of mixtures of caustic soda and hydrogen peroxide via the reduction of oxygen', *J. Appl. Electrochem.*, vol. 25, no. 7, pp. 613–627, Jul. 1995.

[15] W. R. P. Barros, R. M. Reis, R. S. Rocha, and M. R. V. Lanza, 'Electrogeneration of hydrogen peroxide in acidic medium using gas diffusion electrodes modified with cobalt (II) phthalocyanine', *Electrochimica Acta*, vol. 104, pp. 12–18, Aug. 2013.

[16] I. Yamanaka, T. Onizawa, S. Takenaka, and K. Otsuka, 'Direct and Continuous Production of Hydrogen Peroxide with 93 % Selectivity Using a Fuel-Cell System', *Angew. Chem. Int. Ed.*, vol. 42, no. 31, pp. 3653–3655, Aug. 2003.

[17] A. D. Pozzo, L. D. Palma, C. Merli, and E. Petrucci, 'An experimental comparison of a graphite electrode and a gas diffusion electrode for the cathodic production of hydrogen peroxide', *J. Appl. Electrochem.*, vol. 35, no. 4, pp. 413–419, Apr. 2005.

[18] C. H. Choi, H. C. Kwon, S. Yook, H. Shin, H. Kim, and M. Choi, 'Hydrogen Peroxide Synthesis via Enhanced Two-Electron Oxygen Reduction Pathway on Carbon-Coated Pt Surface', *J. Phys. Chem. C*, vol. 118, no. 51, pp. 30063–30070, Dec. 2014.

[19] G. R. Agladze, 'Comparative study of hydrogen peroxide electro-generation on gas-diffusion electrodes in undivided and membrane cells', *J. Appl. Electrochem.*, vol. 37, no. 3, pp. 375–383, 2007.

[20] K. Otsuka and I. Yamanaka, 'One step synthesis of hydrogen peroxide through fuel cell reaction', *Electrochimica Acta*, vol. 35, no. 2, pp. 319–322, Feb. 1990.

[21] C. Badellino, C. A. Rodrigues, and R. Bertazzoli, 'Oxidation of pesticides by in situ electrogenerated hydrogen peroxide: Study for the degradation of 2,4-dichlorophenoxyacetic acid', *J. Hazard. Mater.*, vol. 137, no. 2, pp. 856–864, Sep. 2006.

[22] I. Yamanaka, T. Onisawa, T. Hashimoto, and T. Murayama, 'A Fuel-Cell Reactor for the Direct Synthesis of Hydrogen Peroxide Alkaline Solutions from H2 and O_2', *ChemSusChem*, vol. 4, no. 4, pp. 494–501, Apr. 2011.

[23] J. M. Barazesh, T. Hennebel, J. T. Jasper, and D. L. Sedlak, 'Modular Advanced Oxidation Process Enabled by Cathodic Hydrogen Peroxide Production', *Environ. Sci. Technol.*, vol. 49, no. 12, pp. 7391–7399, Jun. 2015.

[24] E. Lobyntseva, T. Kallio, N. Alexeyeva, K. Tammeveski, and K. Kontturi, 'Electrochemical synthesis of hydrogen peroxide: Rotating disk electrode and fuel cell studies', *Electrochimica Acta*, vol. 52, no. 25, pp. 7262–7269, Sep. 2007.

[25] W. R. P. Barros, T. Ereno, A. C. Tavares, and M. R. V. Lanza, 'In Situ Electrochemical Generation of Hydrogen Peroxide in Alkaline Aqueous Solution by using an Unmodified Gas Diffusion Electrode', *ChemElectroChem*, vol. 2, no. 5, pp. 714–719, May 2015.

[26] M. Panizza and G. Cerisola, 'Electrochemical generation of H_2O_2 in low ionic strength media on gas diffusion cathode fed with air', *Electrochimica Acta*, vol. 54, no. 2, pp. 876–878, Dec. 2008.

[27] Z. Qiang, J.-H. Chang, and C.-P. Huang, 'Electrochemical generation of hydrogen peroxide from dissolved oxygen in acidic solutions', *Water Res.*, vol. 36, no. 1, pp. 85–94, Jan. 2002.

[28] J. C. Forti, R. S. Rocha, M. R. V. Lanza, and R. Bertazzoli, 'Electrochemical synthesis of hydrogen peroxide on oxygen-fed graphite/PTFE electrodes modified by 2-ethylanthraquinone', *J. Electroanal. Chem.*, vol. 601, no. 1–2, pp. 63–67, Mar. 2007.

[29] R. M. Reis *et al.*, 'Use of Gas Diffusion Electrode for the In Situ Generation of Hydrogen Peroxide in an Electrochemical Flow-By Reactor', *Ind. Eng. Chem. Res.*, vol. 51, no. 2, pp. 649–654, Jan. 2012.

[30] Y. Sheng *et al.*, 'Electrogeneration of hydrogen peroxide on a novel highly effective acetylene black-PTFE cathode with PTFE film', *Electrochimica Acta*, vol. 56, no. 24, pp. 8651–8656, Oct. 2011.

[31] R. B. Valim *et al.*, 'Electrogeneration of hydrogen peroxide in gas diffusion electrodes modified with tert-butyl-anthraquinone on carbon black support', *Carbon*, vol. 61, pp. 236–244, Sep. 2013.

[32] J. R. Akse *et al.*, 'In Situ Hydrogen Peroxide Generation for Use as a Disinfectant and as an Oxidant for Water Recovery by Aqueous Phase Catalytic Oxidation', presented at the International Conference On Environmental Systems, 1996.

[33] L. Fu, S.-J. You, F. Yang, M. Gao, X. Fang, and G. Zhang, 'Synthesis of hydrogen peroxide in microbial fuel cell', *J. Chem. Technol. Biotechnol.*, vol. 85, no. 5, pp. 715–719, May 2010.

[34] O. Modin and K. Fukushi, 'Development and testing of bioelectrochemical reactors converting wastewater organics into hydrogen peroxide', *Water Sci. Technol. J. Int. Assoc. Water Pollut. Res.*, vol. 66, no. 4, pp. 831–836, 2012.

[35] O. Modin and K. Fukushi, 'Production of high concentrations of $H2O_2$ in a bioelectrochemical reactor fed with real municipal wastewater', *Environ. Technol.*, vol. 34, no. 17–20, pp. 2737–2742, Oct. 2013.

[36] M. N. Young, M. J. Links, S. C. Popat, B. E. Rittmann, and C. I. Torres, 'Tailoring Microbial Electrochemical Cells for Production of Hydrogen Peroxide at High Concentrations and Efficiencies', *ChemSusChem*, vol. 9, no. 23, pp. 3345–3352, Dec. 2016.

[37] R. A. Rozendal, E. Leone, J. Keller, and K. Rabaey, 'Efficient hydrogen peroxide generation from organic matter in a bioelectrochemical system', *Electrochem. Commun.*, vol. 11, no. 9, pp. 1752–1755, Sep. 2009.

[38] X. Li, I. Angelidaki, and Y. Zhang, 'Salinity-gradient energy driven microbial electrosynthesis of hydrogen peroxide', *J. Power Sources*, vol. 341, pp. 357–365, Feb. 2017.

[39] J. Sim, J. An, E. Elbeshbishy, H. Ryu, and H.-S. Lee, 'Characterization and optimization of cathodic conditions for $H2O_2$ synthesis in microbial electrochemical cells', *Bioresour. Technol.*, vol. 195, pp. 31–36, Nov. 2015.

[40] J. Chen, N. Li, and L. Zhao, 'Three-dimensional electrode microbial fuel cell for hydrogen peroxide synthesis coupled to wastewater treatment', *J. Power Sources*, vol. 254, pp. 316–322, May 2014.

[41] D. Ki, S. C. Popat, B. E. Rittmann, and C. I. Torres, '$H2O_2$ Production in Microbial Electrochemical Cells Fed with Primary Sludge', *Environ. Sci. Technol.*, vol. 51, no. 11, pp. 6139–6145, Jun. 2017.

[42] J. B. A. Arends, S. Van Denhouwe, W. Verstraete, N. Boon, and K. Rabaey, 'Enhanced disinfection of wastewater by combining wetland treatment with bioelectrochemical $H2O_2$ production', *Bioresour. Technol.*, vol. 155, pp. 352–358, Mar. 2014.

[43] J. J. Sim, 'Investigation of Microbial Electrochemical Cell (MEC) as a Sustainable Alternative for Synthesizing Hydrogen Peroxide ($H2O_2$)', Jan. 2015.

[44] G. R. Agladze, G. S. Tsurtsumia, B.-I. Jung, J.-S. Kim, and G. Gorelishvili, 'Comparative study of chemical and electrochemical Fenton treatment of organic pollutants in wastewater', *J. Appl. Electrochem.*, vol. 37, no. 9, pp. 985–990, Jul. 2007.

[45] M. Panizza and G. Cerisola, 'Electro-Fenton degradation of synthetic dyes', *Water Res.*, vol. 43, no. 2, pp. 339–344, Feb. 2009.

[46] Y. Wang, Y. Liu, X. Li, F. Zeng, and H. Liu, 'A highly-ordered porous carbon material based cathode for energy-efficient electro-Fenton process', *Sep. Purif. Technol.*, vol. 106, pp. 32–37, Mar. 2013.

[47] H. Luo, C. Li, C. Wu, W. Zheng, and X. Dong, 'Electrochemical degradation of phenol by in situ electro-generated and electro-activated hydrogen peroxide using an improved gas diffusion cathode', *Electrochimica Acta*, vol. 186, pp. 486–493, Dec. 2015.

[48] A. Asghar, A. Salihoudin, A. Aziz Abdul Raman, and W. Mohd Ashri Wan Daud, 'Cathode modification to enhance the performance of in-situ fenton oxidation in microbial fuel cells', *Environ. Prog. Sustain. Energy*, vol. 36, no. 2, pp. 382–393, Mar. 2017.

[49] M. A. F. de Dios, O. Iglesias, E. Bocos, M. Pazos, and M. A. Sanromán, 'Application of benthonic microbial fuel cells and electro-Fenton process to dye decolourisation', *J. Ind. Eng. Chem.*, vol. 20, no. 5, pp. 3754–3760, Sep. 2014.

[50] L. Fu, S.-J. You, G. Zhang, F.-L. Yang, and X. Fang, 'Degradation of azo dyes using in-situ Fenton reaction incorporated into $H2O_2$-producing microbial fuel cell', *Chem. Eng. J.*, vol. 160, no. 1, pp. 164–169, May 2010.

[51] G.-E. Yuan, Y. Li, J. Lv, G. Zhang, and F. Yang, 'Integration of microbial fuel cell and catalytic oxidation reactor with iron phthalocyanine catalyst for Congo red degradation', *Biochem. Eng. J.*, vol. 120, pp. 118–124, Apr. 2017.

[52] B. Zhang, Z. Wang, X. Zhou, C. Shi, H. Guo, and C. Feng, 'Electrochemical decolorization of methyl orange powered by bioelectricity from single-chamber microbial fuel cells', *Bioresour. Technol.*, vol. 181, pp. 360–362, Apr. 2015.

[53] Y. Wang, C. Feng, Y. Li, J. Gao, and C.-P. Yu, 'Enhancement of emerging contaminants removal using Fenton reaction driven by H 2 O 2 -producing microbial fuel cells', *Chem. Eng. J.*, vol. 307, pp. 679–686, Jan. 2017.

[54] X.-Q. Wang, C.-P. Liu, Y. Yuan, and F. Li, 'Arsenite oxidation and removal driven by a bio-electro-Fenton process under neutral pH conditions', *J. Hazard. Mater.*, vol. 275, pp. 200–209, Jun. 2014.

[55] A. Xue, Z.-Z. Shen, B. Zhao, and H.-Z. Zhao, 'Arsenite removal from aqueous solution by a microbial fuel cell?zerovalent iron hybrid process', *J. Hazard. Mater.*, vol. 261, pp. 621–627, Oct. 2013.

[56] L. Liu, Y. Yang, and D. L. Li, 'Accelerated Hexavalent Chromium [Cr (VI)] Reduction with Electrogenerated Hydrogen Peroxide in Microbial Fuel Cells', *Adv. Mater. Res.*, vol. 512–515, pp. 1525–1528, May 2012.

[57] L. Liu, Y. Yuan, F. Li, and C. Feng, 'In-situ Cr(VI) reduction with electrogenerated hydrogen peroxide driven by iron-reducing bacteria', *Bioresour. Technol.*, vol. 102, no. 3, pp. 2468–2473, Feb. 2011.

[58] X.-Y. Yong *et al.*, 'Bio-Electron-Fenton (BEF) process driven by microbial fuel cells for triphenyltin chloride (TPTC) degradation', *J. Hazard. Mater.*, vol. 324, pp. 178–183, Feb. 2017.

[59] X. Zhu and B. E. Logan, 'Using single-chamber microbial fuel cells as renewable power sources of electro-Fenton reactors for organic pollutant treatment', *J. Hazard. Mater.*, vol. 252–253, pp. 198–203, May 2013.

[60] Y. Li, L. Liu, and F. Yang, 'Destruction of tetracycline hydrochloride antibiotics by FeOOH/TiO 2 granular activated carbon as expanded cathode in low-cost MBR/MFC coupled system', *J. Membr. Sci.*, vol. 525, pp. 202–209, Mar. 2017.

[61] N. Birjandi, H. Younesi, A. A. Ghoreyshi, and M. Rahimnejad, 'Electricity generation, ethanol fermentation and enhanced glucose degradation in a bio-electro-Fenton system driven by a microbial fuel cell: Electricity generation, ethanol fermentation and enhanced', *J. Chem. Technol. Biotechnol.*, vol. 91, no. 6, pp. 1868–1876, Jun. 2016.

[62] A. Wang, Y.-Y. Li, and A. L. Estrada, 'Mineralization of antibiotic sulfamethoxazole by photoelectro-Fenton treatment using activated carbon fiber cathode and under UVA irradiation', *Appl. Catal. B Environ.*, vol. 102, no. 3–4, pp. 378–386, Feb. 2011.

[63] Y. B. Xie and X. Z. Li, 'Interactive oxidation of photoelectrocatalysis and electro-Fenton for azo dye degradation using TiO_2–Ti mesh and reticulated vitreous carbon electrodes', *Mater. Chem. Phys.*, vol. 95, no. 1, pp. 39–50, Jan. 2006.

[64] E. Isarain-Chávez *et al.*, 'Mineralization of the drug ß-blocker atenolol by electro-Fenton and photoelectro-Fenton using an air-diffusion cathode for $H2O_2$ electrogeneration combined with a carbon-felt cathode for Fe2+ regeneration', *Appl. Catal. B Environ.*, vol. 96, no. 3–4, pp. 361–369, Jun. 2010.

[65] J. Casado, J. Fornaguera, and M. I. Galán, 'Mineralization of Aromatics in Water by Sunlight-Assisted Electro-Fenton Technology in a Pilot Reactor', *Environ. Sci. Technol.*, vol. 39, no. 6, pp. 1843–1847, Mar. 2005.

[66] E. N. Al-Shafei, 'Process for in-situ electrochemical oxidative generation and conversion of organosulfur compounds', US8871951 B2, 28-Oct-2014.

[67] Z. Shen *et al.*, 'Dual Electrodes Oxidation of Dye Wastewater with Gas Diffusion Cathode', *Environ. Sci. Technol.*, vol. 39, no. 6, pp. 1819–1826, Mar. 2005.

[68] E. Brillas, 'A review on the degradation of organic pollutants in waters by UV photoelectro-Fenton and solar photoelectro-Fenton', *J. Braz. Chem. Soc.*, vol. 25, no. 3, pp. 393–417, Mar. 2014.

[69] S. Parsons, *Advanced Oxidation Processes for Water and Wastewater Treatment*. IWA Publishing, 2004.

[70] J. C. Crittenden, R. R. Trussell, D. W. Hand, K. J. Howe, and G. Tchobanoglous, 'Hydrogen Peroxide/ UV Light Process', in *MWH's Water Treatment: Principles and Design*, 3rd ed., Hoboken, NJ: John Wiley and Sons, 2012, pp. 1455–1472.

[71] D. Pletcher, 'Indirect Oxidations Using Electrogenerated Hydrogen Peroxide.', *Acta Chem. Scand.*, vol. 53, pp. 745–750, 1999.

[72] M. Fagan and J. R. Walton, 'Sulfide and Odor Control for Headworks with $H2O_2$', USP Technologies, Mar. 1999.

[73] M. R. Hoffmann, 'Kinetics and mechanism of oxidation of hydrogen sulfide by hydrogen peroxide in acidic solution', *Environ. Sci. Technol.*, vol. 11, no. 1, pp. 61–66, 1977.

[74] C. N. Satterfield, R. C. Reid, and D. R. Briggs, 'Rate of Oxidation of Hydrogen Sulfide by Hydrogen Peroxide', *J. Am. Chem. Soc.*, vol. 76, no. 15, pp. 3922–3923, Aug. 1954.

[75] E. Vega, M. J. Martin, and R. Gonzalez-Olmos, 'Integration of advanced oxidation processes at mild conditions in wet scrubbers for odourous sulphur compounds treatment', *Chemosphere*, vol. 109, no. Complete, pp. 113–119, 2014.

[76] G. Pfleiderer and H.-J. Riedl, 'Production of hydrogen peroxide', US2158525 A, 16-May-1939.

[77] USP Technologies, 'Cost and Pricing', *USP Technologies*, 2017. [Online]. Available: http://www.h2O2.com/faqs/FaqDetail.aspx?fId=25. [Accessed: 28-Jun-2017].

[78] S. Siahrostami *et al.*, 'Enabling direct $H2O_2$ production through rational electrocatalyst design', *Nat. Mater.*, vol. 12, no. 12, pp. 1137–1143, Nov. 2013.

[79] Arkema Inc., 'Material Safety Data Sheet: Hydrogen Peroxide 70% (All Grades)', 2011. [Online]. Available: http://formosa.msdssoftware.com/imagedir/4c973fddf4f3401e9b0158a2aadc5981.pdf. [Accessed: 07-Jun-2016].

[80] S. Kommineni *et al.*, '3.0 Advanced Oxidation Processes', *Treat. Technol. Remov. Methyl Tert. Butyl Ether MTBE Fron Drink. Water Air Stripping Adv. Oxid. Process Granul. Act. Carbon Sinthetic Resin Sorbents*, vol. 2, pp. 109–208, 2000.

[81] A. J. Bard and L. R. Faulkner, 'Appendix C: Reference Tables', in *Electrochemical Methods: Fundamentals and Applications*, 2nd Edition., Noida, India: John Wiley and Sons, 2004, pp. 808–813.

[82] C. Song and J. Zhang, 'Chapter 2: Electrocatalytic Oxygen Reduction Reaction', in *PEM Fuel Cell Electrocatalysts and Catalyst Layers*, XXI., Springer, 2008, pp. 89–134.

[83] D. Lide, Ed., *CRC Handbook of Chemistry and Physics*, 87th ed. Boca Raton, USA, 2006.

[84] R. Petrucci, W. Harwood, F. G. Herring, and J. Madura, 'Appendix D: Data Tables', in *General Chemistry: Principles and Modern Applications*, 9th ed., Upper Saddle River, NJ: Pearson-Prentice Hall, 2007, pp. A17–A29.

[85] 'Hypochlorous Acid Datasheet', *Chemeo*, 2017. [Online]. Available: https://www.chemeo.com/cid/39-385-2/Hypochlorous%20acid.pdf. [Accessed: 27-Jun-2017].

[86] D. A. Vander Griend, J. S. Golden, and C. A. Arrington, 'Kinetics and Mechanism of Chromate Reduction with Hydrogen Peroxide in Base', *Inorg. Chem.*, vol. 41, no. 26, pp. 7042–7048, Dec. 2002.

[87] I. Sirés, E. Brillas, M. A. Oturan, M. A. Rodrigo, and M. Panizza, 'Electrochemical advanced oxidation processes: today and tomorrow. A review', *Environ. Sci. Pollut. Res.*, vol. 21, no. 14, pp. 8336–8367, Jul. 2014.

[88] C. Comninellis, A. Kapalka, S. Malato, S. A. Parsons, I. Poulios, and D. Mantzavinos, 'Advanced oxidation processes for water treatment: advances and trends for R&D', *J. Chem. Technol. Biotechnol.*, vol. 83, no. 6, pp. 769–776, Jun. 2008.

[89] E. M. Milner, K. Scott, I. M. Head, T. Curtis, and E. H. Yu, 'Evaluation of porous carbon felt as an aerobic biocathode support in terms of hydrogen peroxide', *J. Power Sources*, vol. 356, pp. 459–466, Jun. 2017.

[90] B. E. Logan, 'Exoelectrogenic bacteria that power microbial fuel cells', *Nat. Rev. Microbiol.*, vol. 7, no. 5, pp. 375–381, 2009.

[91] H. Wang and Z. J. Ren, 'A comprehensive review of microbial electrochemical systems as a platform technology', *Biotechnol. Adv.*, vol. 31, no. 8, pp. 1796–1807, Dec. 2013.

[92] J. M. Foley, R. A. Rozendal, C. K. Hertle, P. A. Lant, and K. Rabaey, 'Life Cycle Assessment of High-Rate Anaerobic Treatment, Microbial Fuel Cells, and Microbial Electrolysis Cells', *Environ. Sci. Technol.*, vol. 44, no. 9, pp. 3629–3637, May 2010.

[93] A. Mahadevan, D. A. Gunawardena, and S. Fernando, 'Biochemical and Electrochemical Perspectives of the Anode of a Microbial Fuel Cell', in *Technology and Application of Microbial Fuel Cells*, C.-T. Wang, Ed. InTech, 2014.

[94] B. D. Ratner, A. S. Hoffman, F. J. Schoen, and J. E. Lemons, Eds., '2. Classes of Materials Used in Medicine', in *Biomaterials Science: An Introduction to Materials in Medicine*, San Diego: Academic Press, 2004.

[95] R. Petrucci, W. Harwood, F. G. Herring, and J. Madura, '12-7 Network covalent solids and ionic solids', in *General Chemistry: Principles and Modern Applications*, 9th ed., Upper Saddle River, NJ: Pearson-Prentice Hall, 2007, pp. 497–501.

[96] J. V. Larsen and T. G. Smith, 'Carbon Fiber Structure', White Oak Naval Ordnance Lab, 1971.

[97] J. Gonzalez-Garcia, P. Bonete, E. Exposito, V. Montiel, A. Aldaz, and R. Torregrosa-Maciá, 'Characterization of a carbon felt electrode: structural and physical properties', *J. Mater. Chem.*, vol. 9, no. 2, pp. 419–426, 1999.

[98] C. R. Houska and B. E. Warren, 'X-Ray Study of the Graphitization of Carbon Black', *J. Appl. Phys.*, vol. 25, no. 12, pp. 1503–1509, Dec. 1954.

[99] Z. Chen, D. Higgins, A. Yu, L. Zhang, and J. Zhang, 'A review on non-precious metal electrocatalysts for PEM fuel cells', *Energy Environ. Sci.*, vol. 4, no. 9, pp. 3167–3192, 2011.

[100] I. Morcos and E. Yeager, 'Kinetic studies of the oxygen—peroxide couple on pyrolytic graphite', *Electrochimica Acta*, vol. 15, no. 6, pp. 953–975, Jun. 1970.

[101] R. C. Engstrom and V. A. Strasser, 'Characterization of electrochemically pretreated glassy carbon electrodes', *Anal. Chem.*, vol. 56, no. 2, pp. 136–141, Feb. 1984.

[102] S. M. Senthil Kumar, J. Soler Herrero, S. Irusta, and K. Scott, 'The effect of pretreatment of Vulcan XC-72R carbon on morphology and electrochemical oxygen reduction kinetics of supported Pd nano-particle in acidic electrolyte', *J. Electroanal. Chem.*, vol. 647, no. 2, pp. 211–221, Sep. 2010.

[103] M. H. M. T. Assumpcao *et al.*, 'A comparative study of the electrogeneration of hydrogen peroxide using Vulcan and Printex carbon supports', *Carbon*, vol. 49, no. 8, pp. 2842–2851, Jul. 2011.

[104] W. R. P. Barros, P. C. Franco, J. R. Steter, R. S. Rocha, and M. R. V. Lanza, 'Electro-Fenton degradation of the food dye amaranth using a gas diffusion electrode modified with cobalt (II) phthalocyanine', *J. Electroanal. Chem.*, vol. 722–723, pp. 46–53, May 2014.

[105] E. Guinea *et al.*, 'Degradation of the fluoroquinolone enrofloxacin by electrochemical advanced oxidation processes based on hydrogen peroxide electrogeneration', *Electrochimica Acta*, vol. 55, no. 6, pp. 2101–2115, Feb. 2010.

[106] O. Špalek and J. Balej, 'Porous electrodes for hydrogen peroxide preparation by oxygen reduction. The influence of temperature and pressure applied in preparation of the electrodes on their functional properties', *Collect. Czechoslov. Chem. Commun.*, vol. 46, no. 9, pp. 2052–2059, 1981.

[107] J. Zheng, C. Cheng, J. Zhang, and X. Wu, 'Appropriate mechanical strength of carbon black-decorated loofah sponge as anode material in microbial fuel cells', *Int. J. Hydrog. Energy*, vol. 41, no. 48, pp. 23156–23163, Dec. 2016.

[108] N. Duteanu, B. Erable, S. M. Senthil Kumar, M. M. Ghangrekar, and K. Scott, 'Effect of chemically modified Vulcan XC-72R on the performance of air-breathing cathode in a single-chamber microbial fuel cell', *Bioresour. Technol.*, vol. 101, no. 14, pp. 5250–5255, Jul. 2010.

[109] C. A. Martínez-Huitle, M. A. Rodrigo, I. Sirés, and O. Scialdone, 'Single and Coupled Electrochemical Processes and Reactors for the Abatement of Organic Water Pollutants: A Critical Review', *Chem. Rev.*, vol. 115, no. 24, pp. 13362–13407, Dec. 2015.

[110] G. Rothenberg, 'Chapter 2: The basics of catalysis', in *Catalysis*, Wiley-VCH Verlag GmbH & Co. KGaA, 2008, pp. 39–75.

[111] Z. Yang, H. Nie, X. Chen, X. Chen, and S. Huang, 'Recent progress in doped carbon nanomaterials as effective cathode catalysts for fuel cell oxygen reduction reaction', *J. Power Sources*, vol. 236, pp. 238–249, Aug. 2013.

[112] A. J. Appleby and J. Marie, 'Kinetics of oxygen reduction on carbon materials in alkaline solution', *Electrochimica Acta*, vol. 24, no. 2, pp. 195–202, Feb. 1979.

[113] E. Yeager, 'Dioxygen electrocatalysis: mechanism in relation to catalyst structure', *J. Mol. Catal.*, vol. 38, pp. 5–25, 1986.

[114] F. Wang and S. Hu, 'Studies of electrochemical reduction of dioxygen with RRDE', *Electrochimica Acta*, vol. 51, no. 20, pp. 4228–4235, May 2006.

[115] A. J. Bard and L. R. Faulkner, 'Chapter 2: Potentials and Thermodynamics of Cells', in *Electrochemical Methods: Fundamentals and Applications*, 2nd Edition., Noida, India: John Wiley and Sons, 2004, pp. 44–86.

[116] L. Giorgi, E. Antolini, A. Pozio, and E. Passalacqua, 'Influence of the PTFE content in the diffusion layer of low-Pt loading electrodes for polymer electrolyte fuel cells', *Electrochimica Acta*, vol. 43, no. 24, pp. 3675–3680, Aug. 1998.

[117] L. W. Gosser and J.-A. T. Schwartz, 'Hydrogen peroxide production method using platinum/palladium catalysts', US4832938 A, 23-May-1989.

[118] T. Berzins and L. W. Gosser, 'Electrochemical synthesis of H2 O_2', US5112702 A, 12-May-1992.

[119] H. H. Lee, A.-H. Park, and C. Oloman, 'Stability of hydrogen peroxide in sodium carbonate solutions', *TAPPI J.*, vol. August, 2000.

[120] B. E. Logan, 'Scaling up microbial fuel cells and other bioelectrochemical systems', *Appl. Microbiol. Biotechnol.*, vol. 85, no. 6, pp. 1665–1671, Feb. 2010.

[121] W. H. Leng, W. C. Zhu, J. Ni, Z. Zhang, J. Q. Zhang, and C. N. Cao, 'Photoelectrocatalytic destruction of organics using TiO_2 as photoanode with simultaneous production of $H2O_2$ at the cathode', *Appl. Catal. Gen.*, vol. 300, no. 1, pp. 24–35, Jan. 2006.

[122] T. Xu, 'Ion exchange membranes: State of their development and perspective', *J. Membr. Sci.*, vol. 263, no. 1–2, pp. 1–29, Oct. 2005.

[123] O. Lefebvre *et al.*, 'Conception and optimization of a membrane electrode assembly microbial fuel cell (MEA-MFC) for treatment of domestic wastewater', *Water Sci. Technol.*, vol. 64, no. 7, p. 1527, Sep. 2011.

[124] S. C. Popat, D. Ki, B. E. Rittmann, and C. I. Torres, 'Importance of OH^- Transport from Cathodes in Microbial Fuel Cells', *ChemSusChem*, vol. 5, no. 6, pp. 1071–1079, Jun. 2012.

[125] L. Napoli, J. Franco, H. Fasoli, and A. Sanguinetti, 'Conductivity of Nafion® 117 membrane used in polymer electrolyte fuel cells', *Int. J. Hydrog. Energy*, vol. 39, no. 16, pp. 8656–8660, May 2014.

[126] Membranes International Inc., 'Anion Exchange Membrane', 2016. [Online]. Available: http://www.membranesinternational.com/tech-ami.htm. [Accessed: 15-Jun-2016].

[127] Membranes International Inc., 'Cation Exchange Membrane', 2016. [Online]. Available: http://www.membranesinternational.com/tech-cmi.htm. [Accessed: 15-Jun-2016].

[128] Lenntech BV, 'Water conductivity', *Water Treatment*, 2016. [Online]. Available: http://www.lenntech.com/applications/ultrapure/conductivity/water-conductivity.htm. [Accessed: 15-Jun-2016].

[129] J. Ma, Z. Wang, D. Suor, S. Liu, J. Li, and Z. Wu, 'Temporal variations of cathode performance in air-cathode single-chamber microbial fuel cells with different separators', *J. Power Sources*, vol. 272, pp. 24–33, Dec. 2014.

[130] K. M. V. Bussche, J. T. Corradi, A. R. Oroskar, G. P. Towler, and R. M. Pittman, 'In situ generation of hydrogen peroxide', US7604719 B2, 20-Oct-2009.

[131] US Environmental Protection Agency, 'Membrane Filtration Guidance Manual', US Environmental Protection Agency, Cincinatti, 815-D-03-008, 2003.

[132] E. Abel, 'Über die Selbstzersetzung von Wasserstoffsuperoxyd', *Monatshefte Für Chem. Verwandte Teile Anderer Wiss.*, vol. 83, no. 2, pp. 422–439, Mar. 1952.

[133] F. R. Duke and T. W. Haas, 'The homogeneous base-catalyzed decomposition of hydrogen peroxide', *J. Phys. Chem.*, vol. 65, no. 2, pp. 304–306, 1961.

[134] M. Wekesa and Y. Ni, 'Stabilization of peroxide systems by silicate and calcium carbonate and its application to bleaching of recycled fibres', *Pulp Pap Can.*, vol. 104, no. 12, pp. 85–87, 2003.

[135] E. Neyens and J. Baeyens, 'A review of classic Fenton's peroxidation as an advanced oxidation technique', *J. Hazard. Mater.*, vol. 98, no. 1, pp. 33–50, Mar. 2003.

[136] S. Skounas, C. Methenitis, G. Pneumatikakis, and M. Morcellet, 'Kinetic Studies and Mechanism of Hydrogen Peroxide Catalytic Decomposition by Cu(II) Complexes with Polyelectrolytes Derived from L-Alanine and Glycylglycine', *Bioinorganic Chemistry and Applications*, 2010. [Online]. Available: https://www.hindawi.com/journals/bca/2010/643120/. [Accessed: 13-Jul-2017].

[137] C. M. Lousada, A. J. Johansson, T. Brinck, and M. Jonsson, 'Mechanism of $H2O_2$ Decomposition on Transition Metal Oxide Surfaces', *J. Phys. Chem. C*, vol. 116, no. 17, pp. 9533–9543, May 2012.

[138] J.-S. Do and W.-C. Yeh, 'Paired electrooxidative degradation of phenol with in situ electrogenerated hydrogen peroxide and hypochlorite', *J. Appl. Electrochem.*, vol. 26, no. 6, pp. 673–678, Jun. 1996.

[139] C. W. Jones, *Applications of Hydrogen Peroxide and Derivatives*. Royal Society of Chemistry, 1999.

[140] I. Oller, S. Malato, and J. A. Sánchez-Pérez, 'Combination of Advanced Oxidation Processes and biological treatments for wastewater decontamination—A review', *Sci. Total Environ.*, vol. 409, no. 20, pp. 4141–4166, Sep. 2011.

[141] Global Market Insights, Inc., 'Hydrogen Peroxide Market Size By End-User (Paper & Pulp, Chemical, Waste Water Treatment, Mining), Industry Analysis Report, Regional Outlook (U.S., Canada, Germany, UK, France, Spain, Italy, China, India, Japan, Australia, Indonesia, Malaysia, Brazil, Mexico, South Africa, GCC), Application Growth Potential, Price Trends, Competitive Market Share & Forecast, 2016 – 2024', GMI851, Dec. 2016.

[142] R. F. P. Nogueira, M. C. Oliveira, and W. C. Paterlini, 'Simple and fast spectrophotometric determination of H(2)O(2) in photo-Fenton reactions using metavanadate', *Talanta*, vol. 66, no. 1, pp. 86–91, Mar. 2005.

[143] Solvay SA, 'Hydrogen peroxide handling and storage', 1998.

[144] US Centres for Disease Control, 'Hydrogen peroxide', *NIOSH Pocket Guide to Chemical Hazards*, 2016. [Online]. Available: https://www.cdc.gov/niosh/npg/npgd0335.html. [Accessed: 04-Jul-2017].

[145] 'Wastewater Systems Effluent Regulations, Fisheries Act', *Justice Laws*, 01-Jan-2015. [Online]. Available: http://laws-lois.justice.gc.ca/eng/regulations/SOR-2012-139/FullText.html. [Accessed: 18-Jul-2017].

[146] Environment and Climate Change Canada, 'Air Quality', 14-May-2012. [Online]. Available: https://www.ec.gc.ca/indicateurs-indicators/default.asp?lang=en&n=7DCC2250-1. [Accessed: 18-Jul-2017].

[147] Canadian Council of Ministers of the Environment, 'Sulphur Dioxide', 2014. [Online]. Available: http://www.ccme.ca/en/resources/air/air/sulphur-dioxide.html. [Accessed: 18-Jul-2017].

[148] H. Lu, E. Janin, M. E. Davila, C. M. Pradier, and M. Gothelid, 'Reaction of oxygen and sulphur dioxide with Cu(100)-c(2x2)-Mn surface alloy', *Surf. Sci.*, vol. 408, no. 1–3, pp. 326–334, Jun. 1998.

[149] D. Prasad, A. Rani, P. Madnawat, R. Bhargava, and K. Gupta, 'Kinetics of Surface-Catalyzed Oxidation of Sulfur(iv) by Dioxygen in Aqueous Suspensions of Cobalt(ii) Oxide', *J. Mol. Catal.*, vol. 69, no. 3, pp. 393–405, Nov. 1991.

[150] J. Berglund, S. Fronaeus, and L. Elding, 'Kinetics and Mechanism for Manganese-Catalyzed Oxidation of Sulfur(iv)', *Inorg. Chem.*, vol. 32, no. 21, pp. 4527–4538, Oct. 1993.

[151] B. C. Faust and J. M. Allen, 'Sunlight-initiated partial inhibition of the dissolved iron (III)-catalysed oxidation of S (IV) species by molecular oxygen in aqueous solution', *Atmos. Environ.*, vol. 28, no. 4, pp. 745–748, 1994.

[152] T. A. Staffelbach and G. L. Kok, 'Henry's law constants for aqueous solutions of hydrogen peroxide and hydroxymethyl hydroperoxide', *J. Geophys. Res. Atmospheres*, vol. 98, no. D7, pp. 12713–12717, Jul. 1993.

[153] A. Lancia, D. Musmarra, F. Pepe, and M. Prisciandaro, 'Model of oxygen absorption into calcium sulfite solutions', *Chem. Eng. J.*, vol. 66, no. 2, pp. 123–129.

[154] J. L. Hudson, 'Sulfur Dioxide Oxidation In Scrubber Systems', United States Environmental Protection Agency, 1980.

[155] K. A. Kobe and W. L. Gooding, 'Oxygen Removal from Boiler Feed Water by Sodium Sulfite', *Ind. Eng. Chem.*, vol. 27, no. 3, pp. 331–333, Mar. 1935.

[156] S. Colle, D. Thomas, and J. Vanderschuren, 'Process Simulation of Sulphur Dioxide Abatement with Hydrogen Peroxide Solutions in a Packed Column', *Chem. Eng. Res. Des.*, vol. 83, no. 1, pp. 81–87, Jan. 2005.

[157] S. Colle, J. Vanderschuren, and D. Thomas, 'Pilot-scale validation of the kinetics of SO_2 absorption into sulphuric acid solutions containing hydrogen peroxide', *Chem. Eng. Process. Process Intensif.*, vol. 43, no. 11, pp. 1397–1402, Nov. 2004.

[158] Y. Zhou, X. Zhu, J. Peng, Y. Liu, D. Zhang, and M. Zhang, 'The effect of hydrogen peroxide solution on SO_2 removal in the semidry flue gas desulfurization process', *J. Hazard. Mater.*, vol. 170, no. 1, pp. 436–442, Oct. 2009.

[159] M. Vorbach, R. Marr, and M. Siebenhofer, 'Precipitation of sulfur dioxide from gaseous feed by oxidative chemisorption', *Sep. Sci. Technol.*, vol. 39, no. 4, pp. 879–891, 2004.

[160] D. Thomas, S. Colle, and J. Vanderschuren, 'Kinetics of SO_2 absorption into fairly concentrated sulphuric acid solutions containing hydrogen peroxide', *Chem. Eng. Process. Process Intensif.*, vol. 42, no. 6, pp. 487–494, Jun. 2003.

[161] C. Drexler, H. Elias, B. Fecher, and K. J. Wannowius, 'Kinetic investigation of sulfur(IV) oxidation by peroxo compounds R-OOH in aqueous solution', *Fresenius J. Anal. Chem.*, vol. 340, no. 10, pp. 605–615, Oct. 1991.

[162] L. R. Martin and D. E. Damschen, 'Aqueous oxidation of sulfur dioxide by hydrogen peroxide at low pH', *Atmos. Environ.*, vol. 15, no. 9, pp. 1615–1621, 1981.

[163] J. V. McArdle and M. R. Hoffman, 'Kinetics and mechanism of the oxidation of aquated sulfur dioxide by hydrogen peroxide at low pH', *J. Phys. Chem.*, vol. 87, no. 26, pp. 5425–5429, 1983.

[164] M. A. Vincent, I. J. Palmer, I. H. Hillier, and E. Akhmatskaya, 'Exploration of the mechanism of the oxidation of sulfur dioxide and bisulfite by hydrogen peroxide in water clusters using ab initio methods', *J. Am. Chem. Soc.*, vol. 120, no. 14, pp. 3431–3439, 1998.

[165] J. Turšič, I. Grgić, and B. Podkrajšek, 'Influence of ionic strength on aqueous oxidation of SO_2 catalyzed by manganese', *Atmos. Environ.*, vol. 37, no. 19, pp. 2589–2595, 2003.

[166] H. Elias, U. Gotz, and K. J. Wannowius, 'Kinetics and mechanism of the oxidation of sulfur (IV) by peroxomonosulfuric acid anion', *Atmos. Environ.*, vol. 28, no. 3, pp. 439–448, 1994.

[167] A. J. Appleby and B. Pichon, 'The mechanism of the electrochemical oxidation of sulfur dioxide in sulfuric acid solutions', *J. Electroanal. Chem.*, vol. 95, pp. 59–71, 1979.

[168] J. H. Vélez, J. P. Muena, M. J. Aguirre, G. Ramírez, and F. Herrera, 'Electrochemical oxidation of sulfite in aqueous solution by glassy carbon electrode modified with polymeric Co (II) meso-tetrakis (2-thienyl) porphyrin', *Int. J. Electrochem. Sci.*, vol. 7, no. 4, pp. 3167–3177, 2012.

[169] R. Ojani, J. B. Raoof, and A. Alinezhad, 'Catalytic Oxidation of Sulfite by Ferrocenemonocarboxylic Acid at the Glassy Carbon Electrode. Application to the Catalytic Determination of Sulfite in Real Sample', *Electroanalysis*, vol. 14, no. 17, pp. 1197–12032, 2001.

[170] J. A. O'Brien, J. T. Hinkley, S. W. Donne, and S.-E. Lindquist, 'The electrochemical oxidation of aqueous sulfur dioxide: A critical review of work with respect to the hybrid sulfur cycle', *Electrochimica Acta*, vol. 55, no. 3, pp. 573–591, Jan. 2010.

[171] A. G. Zelinsky and B. Y. Pirogov, 'Electrochemical oxidation of sulfite and sulfur dioxide at a renewable graphite electrode', *Electrochimica Acta*, vol. 231, pp. 371–378, Mar. 2017.

[172] B. Zoecklein, K. Fugelsang, B. Gump, and F. Nury, 'Chapter 20: Laboratory Procedures', in *Wine Anaylsis and Production*, New York: Aspen, 1999, pp. 310–516.

[173] A. Huss and C. A. Eckert, 'Equilibria and ion activities in aqueous sulfur dioxide solutions', *J. Phys. Chem.*, vol. 81, no. 24, pp. 2268–2270, 1977.

[174] A. Syty, 'Determination of sulfur dioxide by ultraviolet absorption spectrometry', *Anal. Chem.*, vol. 45, no. 9, pp. 1744–1747, 1973.

[175] A. Goi, 'Advanced oxidation processes for water purification and soil remediation', Doctoral, Tallinn University of Technology, Tallinn, Estonia, 2005.

[176] Independent Electricity System Operator, 'Price Overview', 2017. [Online]. Available: http://www.ieso.ca/Pages/Power-Data/price.aspx. [Accessed: 21-Feb-2017].

[177] M. Faouzi Elahmadi, N. Bensalah, and A. Gadri, 'Treatment of aqueous wastes contaminated with Congo Red dye by electrochemical oxidation and ozonation processes', *J. Hazard. Mater.*, vol. 168, no. 2, pp. 1163–1169, Sep. 2009.

Appendix A
Summary of experimental data

Table A1 - Summary of Chapter 3 continuous experiment results

										$k_{decomposition}$=0.45 h^{-1}			$k_{decomposition}$=0.23 h^{-1}		
Series	Date	Electrolyte	[Electrolyte]	$E_{cathode}$ (Ag|AgCl)	SA:vol	$[H_2O_2]$ (mg L^{-1})	HRT (min)	Current density (mA cm^{-2})	CE	Faradaic losses (% of current)	Faradaic losses (% of $H2O_2$)	Non-Faradaic losses (% of $H2O_2$)	Faradaic losses (% of current)	Faradaic losses (% of $H2O_2$)	Non-Faradaic losses (% of $H2O_2$)
Initial multivariate	2015-06-03	NaCl	0.1	-1000	3.63	146.5	11.85	1.33	24.2%	36.8%	58.3%	3.4%	37.4%	60.0%	1.8%
	2015-06-05	NaOH	1	-1000	3.63	129.3	2.15	4.71	33.3%	33.1%	49.5%	0.8%	33.2%	49.9%	0.4%
	2015-06-05	NaOH	1	-1000	3.63	84.9	0.58	6.39	59.8%	20.0%	25.0%	0.3%	20.1%	25.2%	0.2%
	2015-06-05	NaOH	1	-1200	3.63	274.3	2.03	9.47	37.1%	31.2%	45.3%	0.8%	31.3%	45.7%	0.4%
pH	2015-07-16	NaOH	1	-1000	3.63	110.3	0.97	3.38	87.9%	5.7%	6.1%	0.7%	5.9%	6.4%	0.3%
	2015-06-08	NaOH	1	-1000	3.63	108.9	0.61	9.97	47.0%	26.4%	35.9%	0.3%	26.5%	36.0%	0.1%
	2015-06-25	NaCl	1	-1000	3.63	8.3	0.45	3.03	15.9%	42.0%	72.6%	0.1%	42.1%	72.6%	0.0%
	2015-06-25	HCl	1	-1000	3.63	4.6	0.39	8.29	3.7%	48.1%	92.9%	0.0%	48.2%	92.9%	0.0%
	2015-07-15	HCl	0.1	-1000	3.63	21.9	0.59	2.73	35.3%	32.3%	47.7%	0.2%	32.3%	47.8%	0.1%
HRT	2015-06-30	NaCl	1	-1000	3.63	45.4	0.40	202.91	1.5%	49.3%	97.1%	0.0%	49.3%	97.1%	0.0%
	2015-07-10	NaCl	0.1	-1000	3.63	672.1	12.31	2.84	50.1%	22.6%	29.3%	6.0%	23.8%	32.2%	3.1%
	2015-07-03	NaCl	0.1	-1000	3.63	734.4	11.19	2.62	65.2%	14.7%	17.2%	6.4%	16.0%	20.3%	3.3%
	2015-07-07	NaCl	0.1	-1000	3.63	585.1	9.52	2.51	63.7%	15.9%	18.8%	5.4%	17.0%	21.5%	2.8%
	2015-07-09	NaCl	0.1	-1000	3.63	115.6	2.14	2.08	67.4%	15.8%	18.7%	1.3%	16.0%	19.3%	0.7%
	2015-07-13	NaCl	0.1	-1000	3.63	42.9	1.11	1.53	66.2%	16.7%	20.0%	0.7%	16.8%	20.3%	0.3%
Cathode potential	2015-07-13	NaCl	0.1	-800	3.63	227.6	11.07	1.10	48.5%	23.7%	31.1%	5.3%	24.7%	33.7%	2.7%
	2015-07-14	NaCl	0.1	-1200	3.63	427.4	10.87	1.94	52.9%	21.4%	27.3%	5.5%	22.5%	30.0%	2.8%
	2015-07-13	NaCl	0.1	-800	3.63	227.6	11.07	1.10	48.5%	23.7%	31.1%	5.3%	24.7%	33.7%	2.7%
	2015-07-15	NaCl	0.1	-1000	3.63	38.9	1.00	1.17	86.2%	6.6%	7.0%	0.7%	6.7%	7.4%	0.4%
	2015-07-16	NaCl	0.1	-800	3.63	20.9	0.61	0.84	104.5%	-3.7%	-3.6%	0.5%	-3.6%	-3.4%	0.2%
	2015-07-16	NaCl	0.1	-900	3.63	22.4	0.61	0.96	99.8%	-0.1%	-0.1%	0.5%	0.0%	0.1%	0.2%
	2015-07-15	NaCl	0.1	-1000	3.63	27.9	0.61	1.25	95.6%	2.0%	2.0%	0.4%	2.1%	2.3%	0.2%
	2015-07-16	NaCl	0.1	-1200	3.63	32.4	0.71	1.59	74.9%	12.4%	14.1%	0.5%	12.5%	14.3%	0.2%

Table A1 - Summary of Chapter 3 continuous experiment results, continued

										$k_{decomposition}$=0.45 h^{-1}			$k_{decomposition}$=0.23 h^{-1}		
Series	Date	Electrolyte	[Electrolyte]	$E_{cathode}$ (Ag|AgCl)	SA:vol	$[H_2O_2]$ (mg L^{-1})	HRT (min)	Current density (mA cm_2)	CE	Faradaic losses (% of current)	Faradaic losses (% of $H2O_2$)	Non-Faradaic losses (% of $H2O_2$)	Faradaic losses (% of current)	Faradaic losses (% of $H2O_2$)	Non-Faradaic losses (% of $H2O_2$)
High surface area:volume ratio	2015-07-24	NaCl	0.1	-1000	10.38	151.4	1.09	1.85	68.2%	15.6%	18.5%	0.7%	15.8%	18.8%	0.3%
	2015-07-27	NaCl	0.1	-1000	10.38	135.5	1.07	1.86	62.2%	18.7%	23.0%	0.6%	18.8%	23.3%	0.3%
	2015-07-27	NaCl	0.1	-1000	10.38	887.4	1.05	10.63	72.5%	13.5%	15.6%	0.7%	13.6%	15.9%	0.3%
	2015-07-27	NaCl	0.1	-800	10.38	417.7	1.09	4.78	73.2%	13.1%	15.1%	0.7%	13.3%	15.4%	0.4%
	2015-07-28	NaCl	0.1	-600	10.38	320.6	1.06	3.67	75.4%	12.0%	13.6%	0.7%	12.1%	14.0%	0.4%
	2015-07-28	NaCl	0.1	-400	10.38	58.4	1.10	0.52	93.6%	2.8%	2.9%	0.8%	3.0%	3.3%	0.4%
	2015-08-03	NaCl	0.1	-600	10.38	53.4	0.52	1.62	57.6%	21.1%	26.7%	0.3%	21.2%	26.9%	0.1%
Bioanode	2015-08-06	KHCO3	0.1	Variable	3.33	302.6	35.59	1.24	19.5%	37.7%	60.4%	8.4%	38.9%	64.5%	4.3%
Conductivity-controlled pH	2015-08-07	NaCl	Adjusted 9.23 mS/cm	-1000	3.63	273.8	14.03	2.09	24.3%	36.6%	57.7%	4.0%	37.2%	59.7%	2.1%
	2015-08-12	NaCl		-1000	3.63	582.8	11.70	2.00	64.9%	14.7%	17.2%	6.7%	16.1%	20.5%	3.4%
	2015-08-10	NaOH		-1000	3.63	453.3	14.58	1.92	42.1%	26.7%	36.3%	6.3%	27.8%	39.4%	3.2%
	2015-08-11	NaOH		-1000	3.63	224.7	13.71	1.44	20.0%	33.6%	50.6%	4.6%	34.4%	52.9%	2.4%
	2015-08-11	NaOH		-1000	3.63	448.5	11.54	1.87	54.3%	20.5%	25.8%	5.9%	21.7%	28.7%	3.0%
	2015-08-12	NaOH		-1000	3.63	320.0	12.42	1.82	36.9%	29.8%	42.5%	4.9%	30.7%	44.9%	2.5%

Table A2 - Summary of Chapter 4 continuous experiment results

Date	Electrolyte	Potential (mV vs Ag|AgCl	Reactor volume (mL)	pH	Conductivity (mS cm^{-1})	Current density (mA cm^{-2})	CE	Removal	Influent pH	Effluent pH	Mixing
2017-04-15	0.1 M sodium sulfite	-1000	63	9.5		2.112	112.7%	2.5%	9.51	7.46	None
2017-04-14	0.1 M sodium sulfite	-1000	63	9.5		3.085	171.5%	2.3%	9.37	8.08	None
2017-04-15	0.1 M sodium sulfite	-1000	63	9.5		2.436	162.8%	1.9%	9.62	9.16	None
2017-04-17	0.1 M sodium sulfite	Open	63	9.5				4.9%			None
2017-04-19	0.1 M sodium sulfite	-1000	63	9.5		3.655	143.1%	2.1%	9.62	6.66	Mixing
2017-04-18	0.1 M sodium sulfite	-1000	63	9.5		2.126	247.3%	3.9%	9.54	8.11	Mixing
2017-04-18	0.1 M sodium sulfite	-1000	63	9.5		2.005	115.5%	3.3%	9.64	8.67	Mixing
2017-04-18	0.1 M sodium sulfite	-1000	63	9.5		0.831	125.7%	2.0%	7.79	6.78	None
2017-04-19	0.1 M sodium sulfite	-1000	63	9.5		0.787	8.8%	1.9%	7.70	3.25	Mixing
2017-04-21	0.1 M sodium sulfite	-1000	63	9.5							
2017-04-21	0.1 M sodium sulfite + HCl	-1000	63	1.7	0.27	3.841	210.9%	2.6%	1.80	1.66	None
2017-04-21	0.1 M sodium sulfite + HCl	Open	63	1.7	0.27			2.2%	1.80	1.77	None
2017-04-21	0.1 M sodium sulfite + NaCl	-1000	63	9.5	0.27	4.687	158.7%	1.4%	9.01	7.97	None
2017-04-22	0.1 M sodium sulfite + NaOH, NaCl	-1000	63	9.78	0.27	3.768	61.1%	0.3%	9.38	5.28	None
2017-04-23	0.1 M sodium sulfite	-600	63	9.5		1.394	112.5%	1.2%	9.65	8.08	None
2017-04-23	0.1 M sodium sulfite	-1400	63	9.5		5.324	148.2%	2.5%	9.58	7.91	None
2017-04-24	0.1 M sodium sulfite	Open	63	9.5							None
2017-04-24	0.1 M sodium sulfite	-1000	63	9.5		3.577	118.1%	2.1%	9.65	7.04	None
2017-04-24	0.1 M sodium sulfite	-1000	63	9.5		3.575	77.1%	2.2%	9.65	12.05	None
2017-05-09	0.1 M sodium sulfite	-1000	128	9.5		4.323	84.7%	2.5%	9.615	8.584	None
2017-05-09	0.1 M sodium sulfite	-1000	128	10.5		2.888	79.5%	1.8%	9.63	8.67	None
2017-04-25	0.1 M sodium sulfite	Open	63	9.5				3.3%	9.57	9.68	None
2017-04-25	0.1 M sodium sulfite	Open	65	9.5				2.7%	9.57	9.62	None
2017-05-11	0.1 M sodium bisulfite/metabisulfite	-1000	63	3.98		3.355	117.2%	4.9%	3.98	2.48	None
2017-05-11	0.1 M sodium bisulfite/metabisulfite	Open	63	3.81				1.6%	3.81	3.67	None
2017-05-12	0.1 M sodium bisulfite/metabisulfite	Open	63	1.5				2.8%	1.30	1.43	None
2017-05-12	0.1 M sodium bisulfite/metabisulfite	-1000	63	1.38		3.590	27.7%	3.7%	1.38	1.47	None
2017-05-13	NaCl + NaOH K=27 mS	-1000	63			2.515	15.5%		9.67	5.74	None
2017-05-13	NaCl + NaOH K=27 mS	-1000	63			2.141	33.2%		9.67	5.20	None
2017-05-13	NaCl + NaOH K=27 mS	-1000	63			3.616	49.2%		9.67	7.46	None
2017-05-16	0.1 M sodium bisulfite/metabisulfite +NaOH	-1200	63			3.122	139.4%	3.9%	9.40	8.07	None
2017-05-16	0.1 M sodium bisulfite/metabisulfite +NaOH	-800	63			1.971	114.4%	1.8%	9.51	8.21	None
2017-05-16	0.1 M sodium bisulfite/metabisulfite +NaOH	-1000	63			3.054	69.0%	2.4%	9.49	8.10	None
2017-05-17	0.1 M sodium bisulfite/metabisulfite +NaOH	-1000	10			2.598	79.4%	4.3%		0.07	None
2017-05-17	0.1 M sodium bisulfite/metabisulfite +NaOH	Open	10					2.6%			None

Appendix B

Supplemental cyclic voltammetry

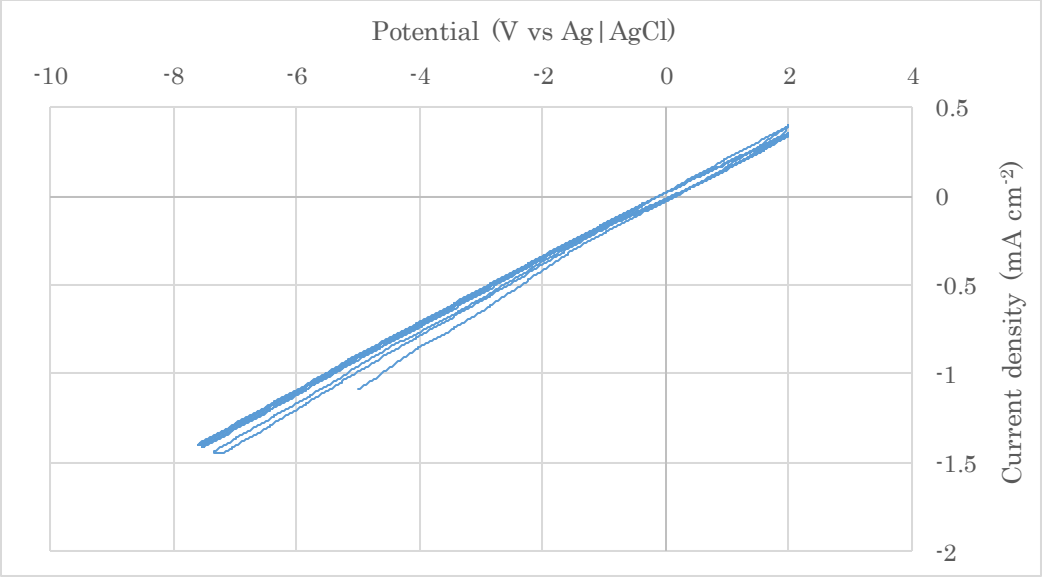

Figure B1 - Cyclic voltammetry of GDE used in Chapter 4 experiments showing linear behaviour across all potentials used in testing as well as under much greater overpotentials.
Note: CV was carried out in Reactor A using DI water as electrolyte. Scan rate was 100 mV S^{-1}, 3 cycles were performed, and signal was logged during the last 50% of each voltage step.

Appendix C

Kinetic quantification of S(IV) oxidation by H_2O_2

C1 Materials and methods

A stopped flow spectrometry apparatus was improvised by using a glass sample cuvette as a reaction vessel and a Genesys 10S UV-Vis (Thermo Scientific, USA) to measure absorbance at 1-second increments. 100 mM Sodium sulphite (ACS grade, Sigma, USA) was used as an S(IV) source, 1 M H_2O_2 was prepared from 35%wt. stock (technical grade, BDH, USA), and sulfuric acid (95-98%, ACS grade, BDH, USA) was used for pH adjustment.

To conduct the stopped flow spectrometry test, 0.5 mL of H_2O_2 was added to 0.5 mL of S(IV) (giving a stoichiometric excess factor of 10) and 3 mL of sulfuric acid solution, adjusted to pH values of 1.0, 2.0, 1.5, 3.15, 10.2 as well as undiluted (pH~=0.1, not measured empirically). Before adding H_2O_2, a baseline measurement was taken at 277 nm for each trial. The vial was inverted twice over ~1 s then inserted into the spectrometer where absorbance was logged at 1 s increments. This procedure is summarized in Figure below.

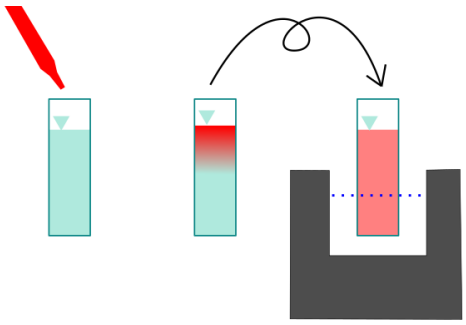

Figure C1 - Schematic of improvised stopped-flow spectrometry apparatus
Note: H_2O_2 is visualized in red and the sample is blue. The gray block represents the spectrometer.

C2 Results

Trials for pH values for all trials using dilute acid showed 100% oxidation within the first second, i.e. no changes were detected once measurement began. Only the concentrated H_2SO_4 trial was orders of magnitude slower. When left overnight, its concentration decreased only 22%. This may be due to the vanishingly small concentration of HO_2^- that might be expected at such pH values.

Appendix D

Effect of pH on S(IV) treatment reactor

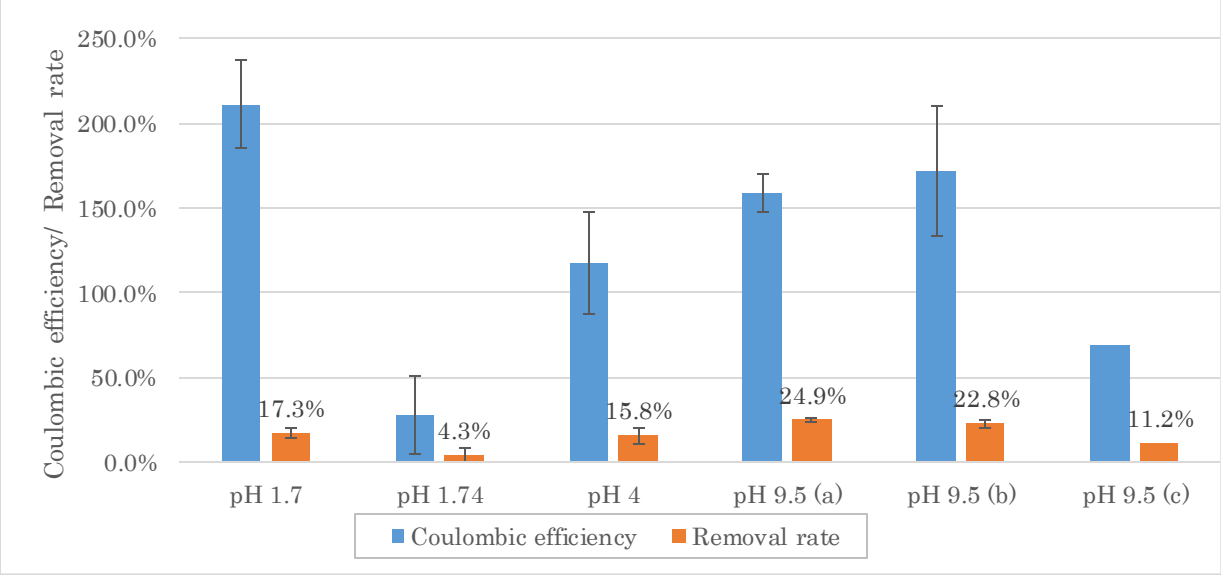

Figure D1 - Effect of pH on S(IV) reactor performance in Reactor A in Chapter 4.
Note: Reaction conditions were cathode potential of -1000 mV vs Ag|AgCl (-778 mV vs SHE) and HRT is 0.40-0.56 min.